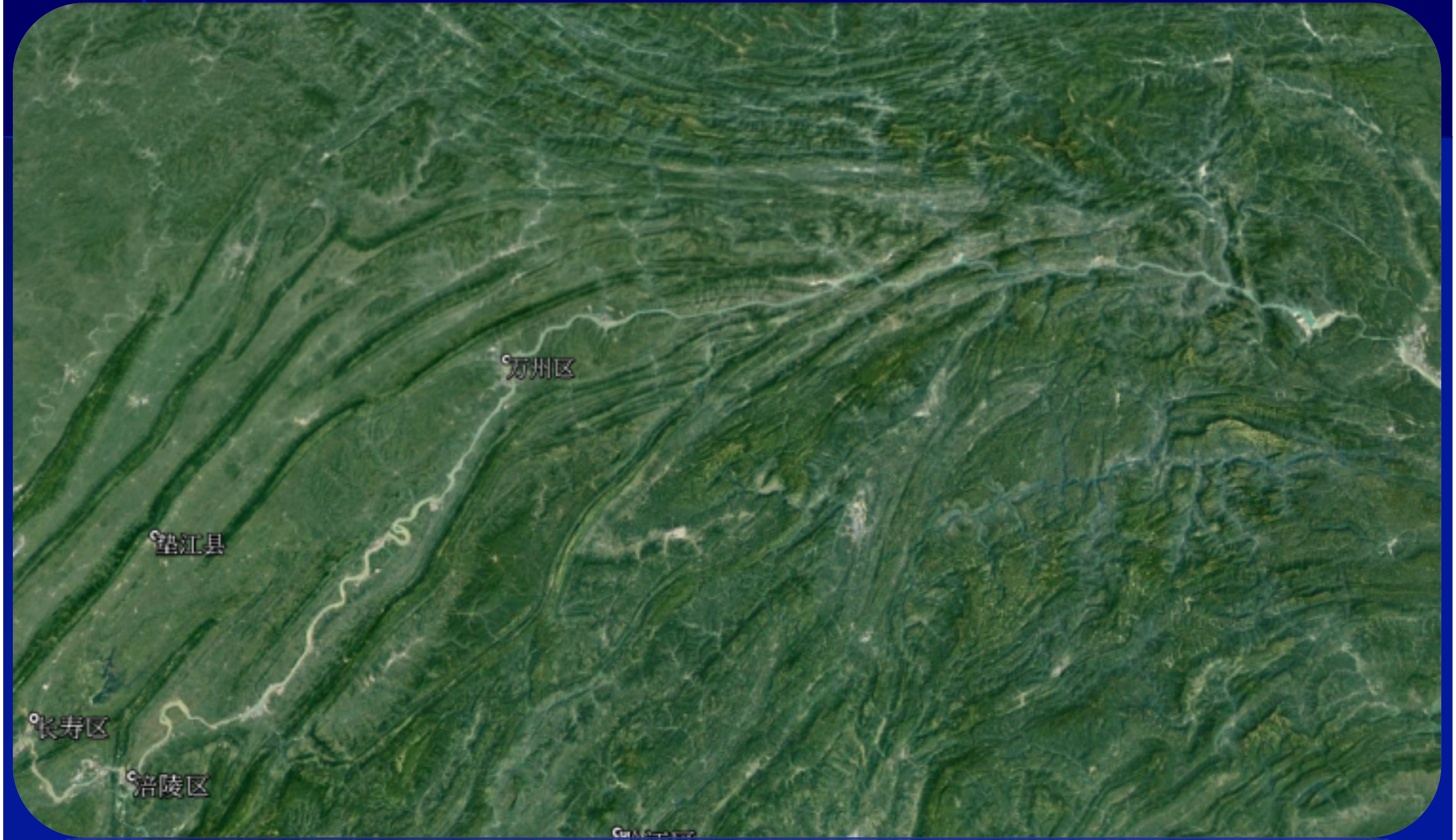
万州区
垫江县
长寿区
涪陵区

瞿塘峡，西起重庆市奉节县的白帝城，东至巫山县的大溪镇，全长仅约8公里。

巫峡，西起重庆市巫山县城东面的大宁河口，东至巴东县官渡口，全长46公里。

西陵峡，西起秭归县香溪口，东止宜昌市南津关，全长约76公里，以险峻闻名于世。“西陵山水天下佳”。

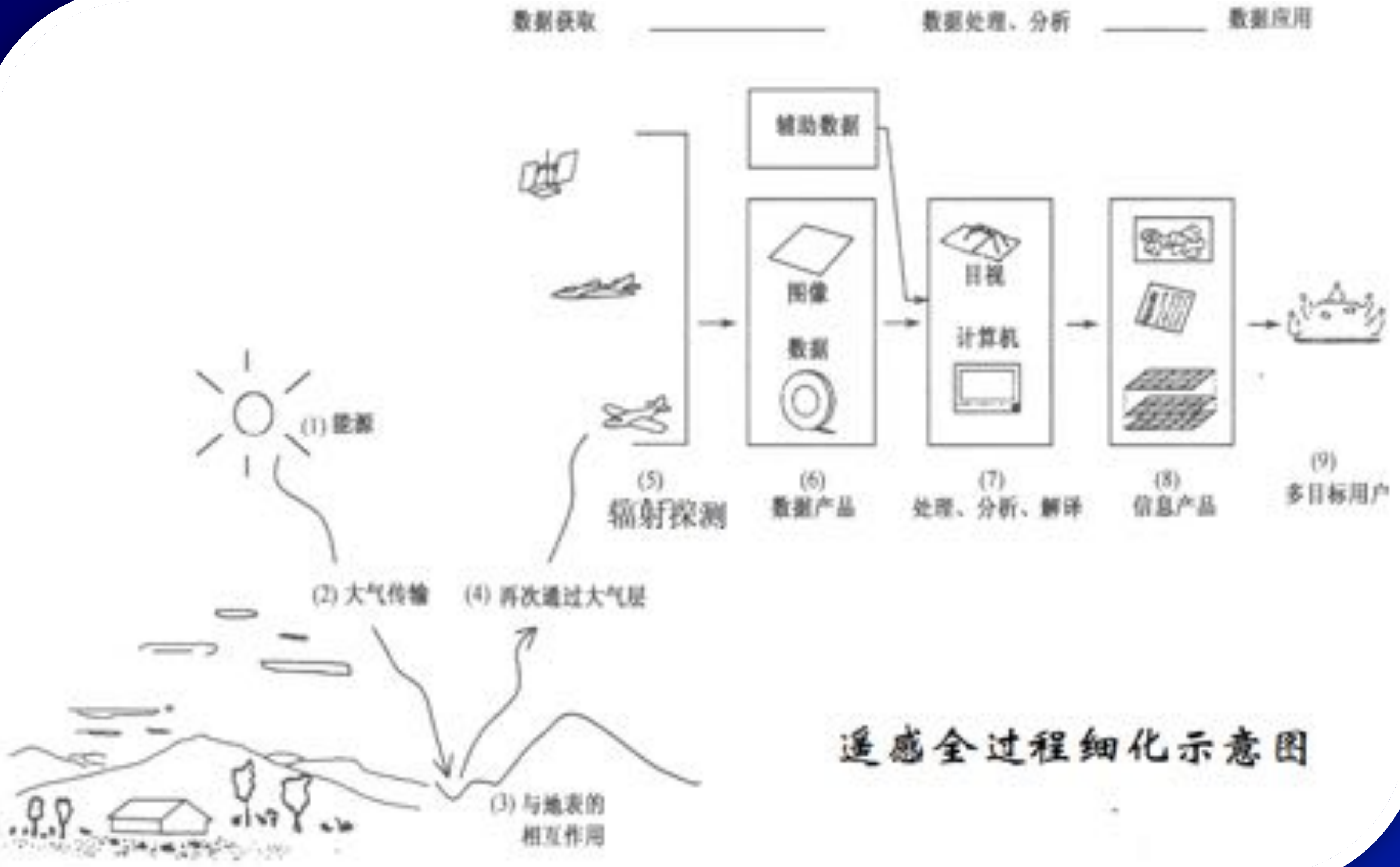
数据获取
数据处理、分析
数据应用
辅助数据
图像
数据
目视
计算机
(1) 能源
(2) 大气传输
(3) 与地表的相互作用
(4) 再次通过大气层
(5) 辐射探测
(6) 数据产品
(7) 处理、分析、解译
(8) 信息产品
(9) 多目标用户

遥感全过程细化示意图

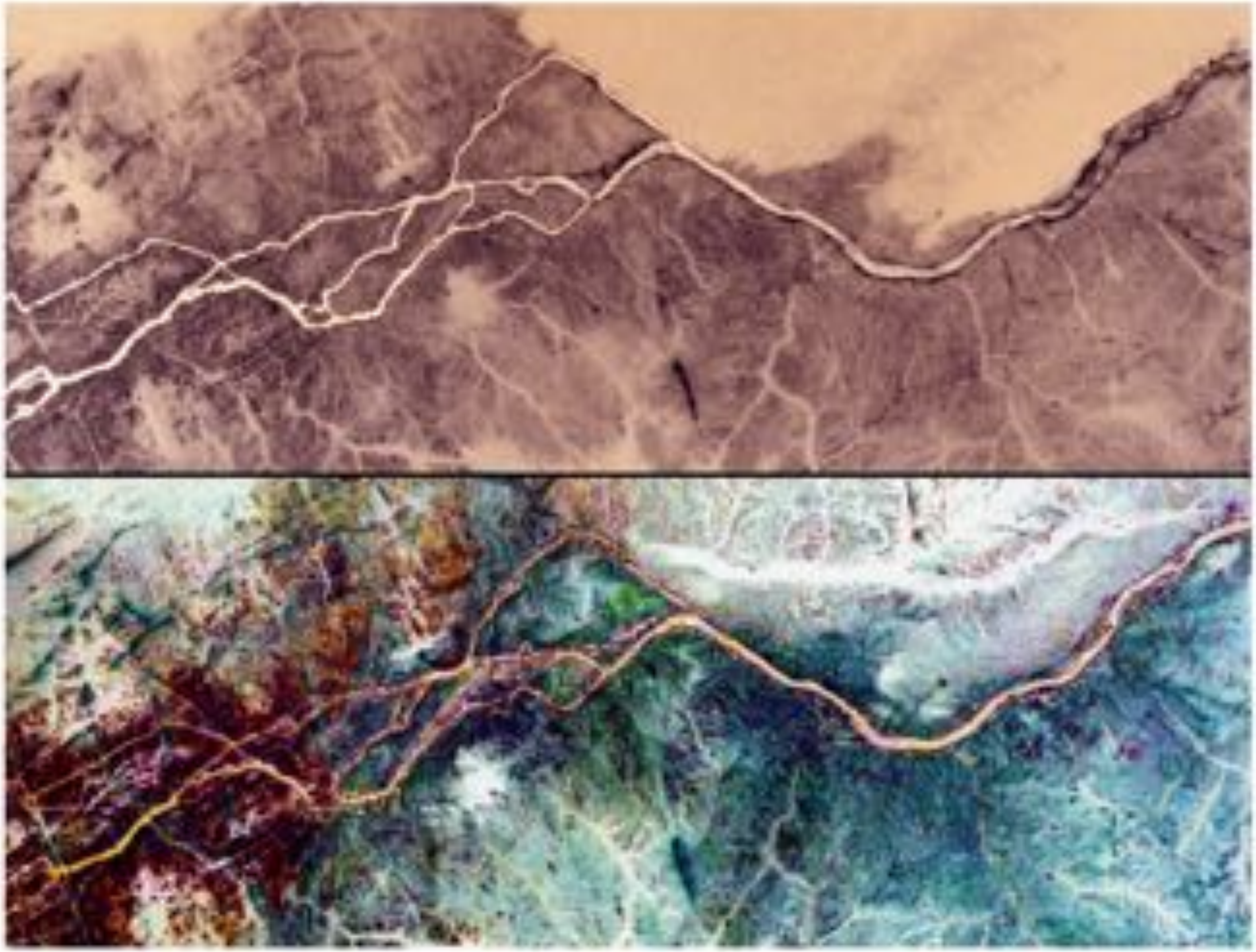

遥感作为一种新型的对地观测系统，它的出现对地球科学各分支的推动是巨大的，遥感是多学科的综合，具有很强的“交叉性”。

它既需要认识电磁波的基本原理，又需要熟悉地球科学及相关学科(空间科学、信息科学、生命科学等)的内容，还融合了数学、计算机科学等多种学科的知识。

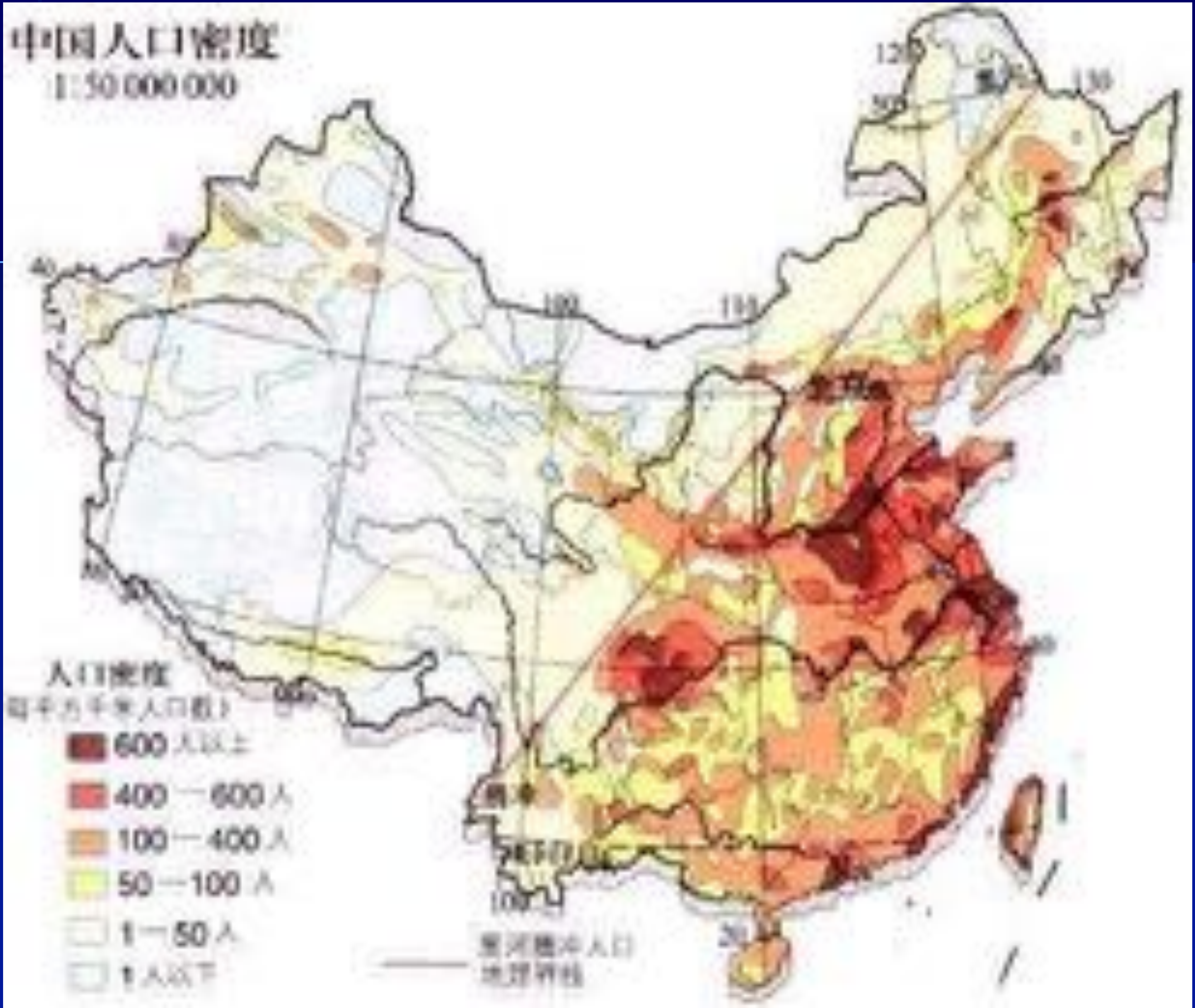
中国人口密度
1:50 000 000
黑河
北京
腾冲
人口密度
（每平方千米人口数）
600 人以上
400 — 600 人
100 — 400 人
50 — 100 人
1 — 50 人
1 人以下
黑河腾冲人口
地理界线
120
130
50
40
100
110
80
90
30
20

胡焕庸线以东地区以43.71%的国土面积养育了94.39%的人口。

李克强发出了“胡焕庸线怎么破”之问：“我国94%的人口居住在东部43%的土地上，但中西部一样也需要城镇化。”

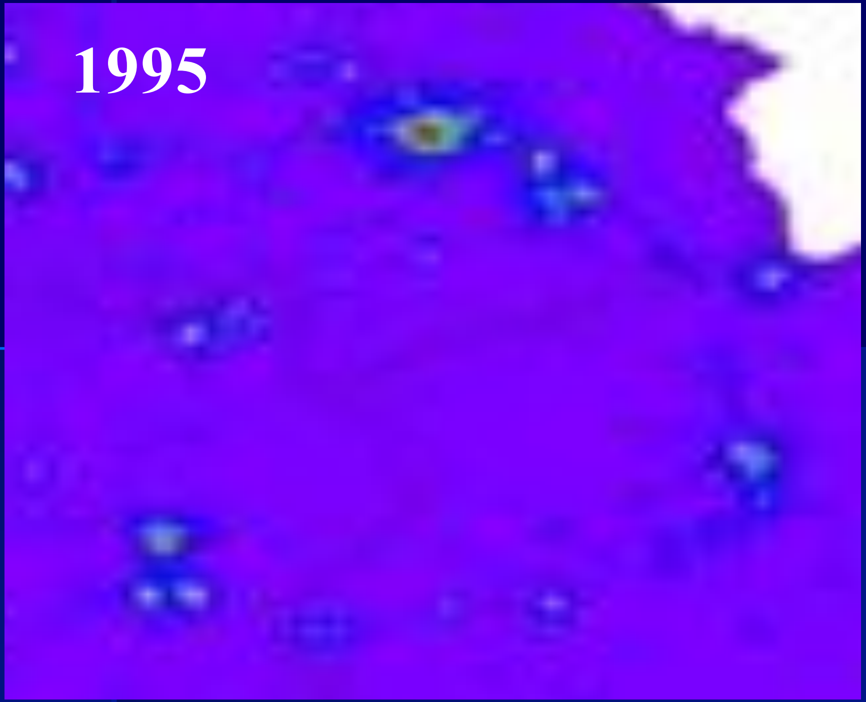
1995

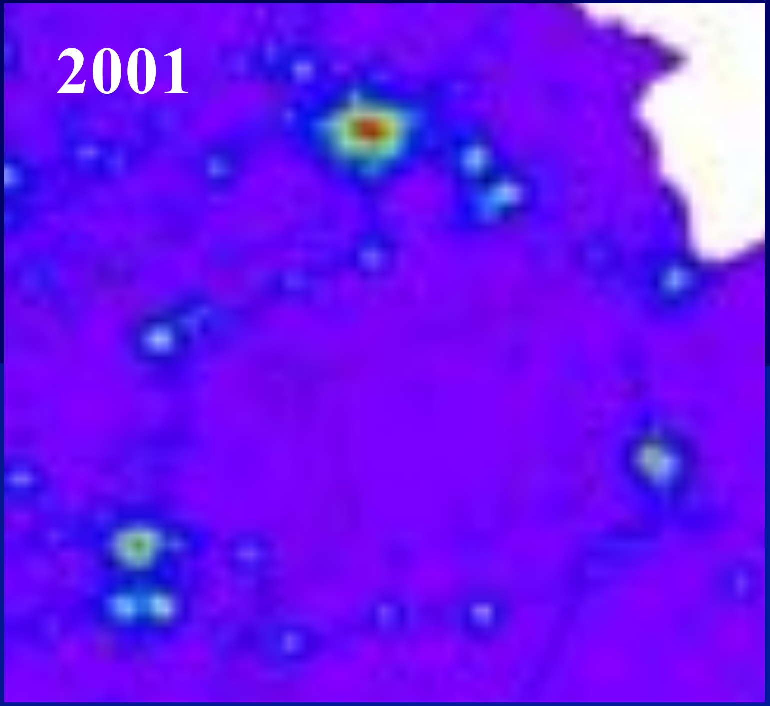
2001

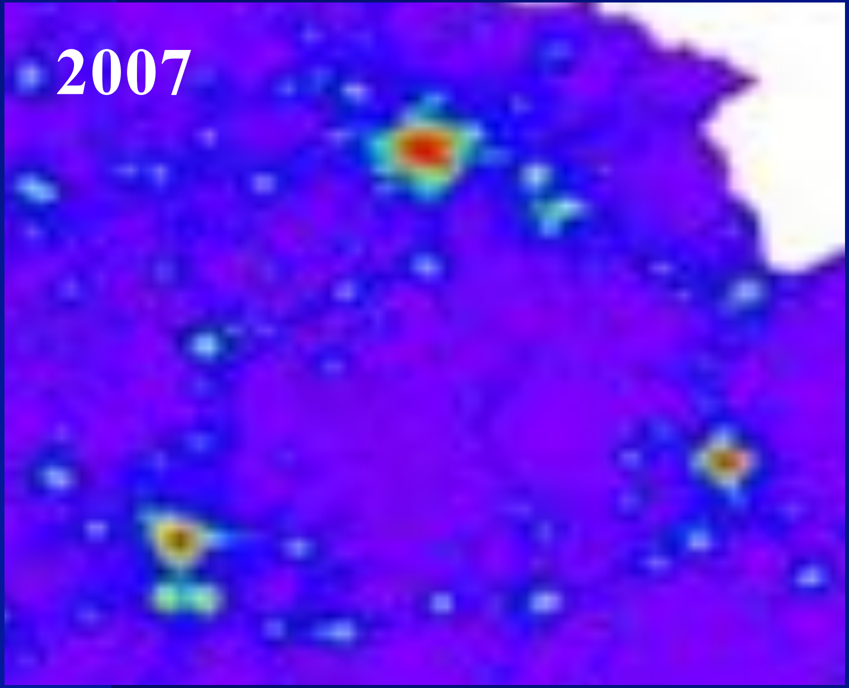
2007

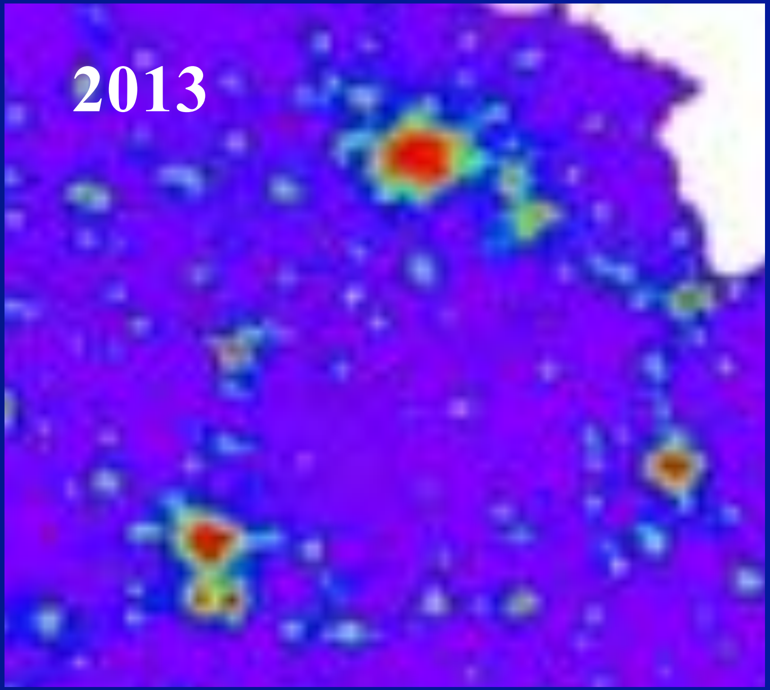
2013


Katia
Irma
Jose


Clouds
Snow
Beijing
Haze
Fog
N
100 km

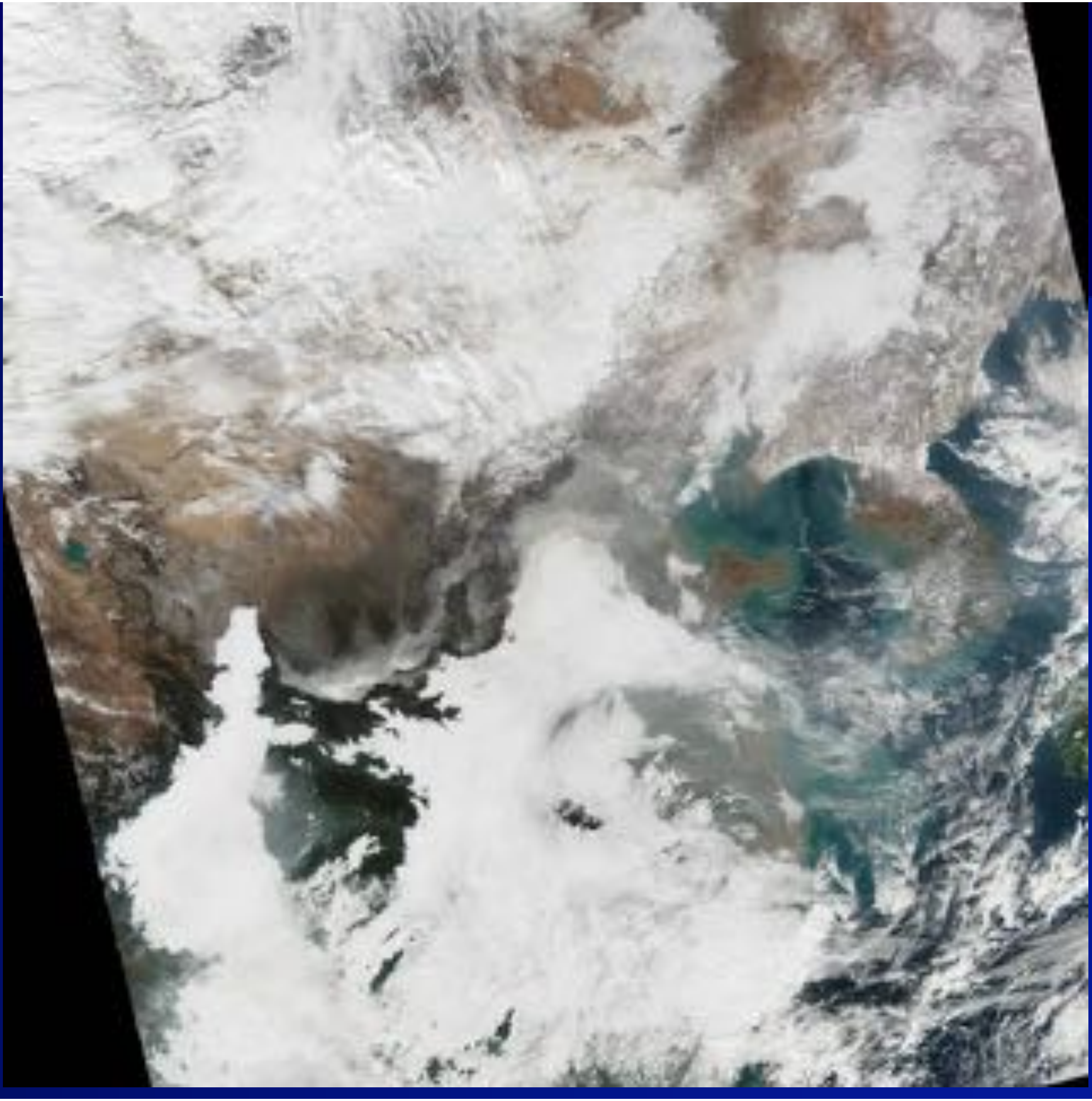

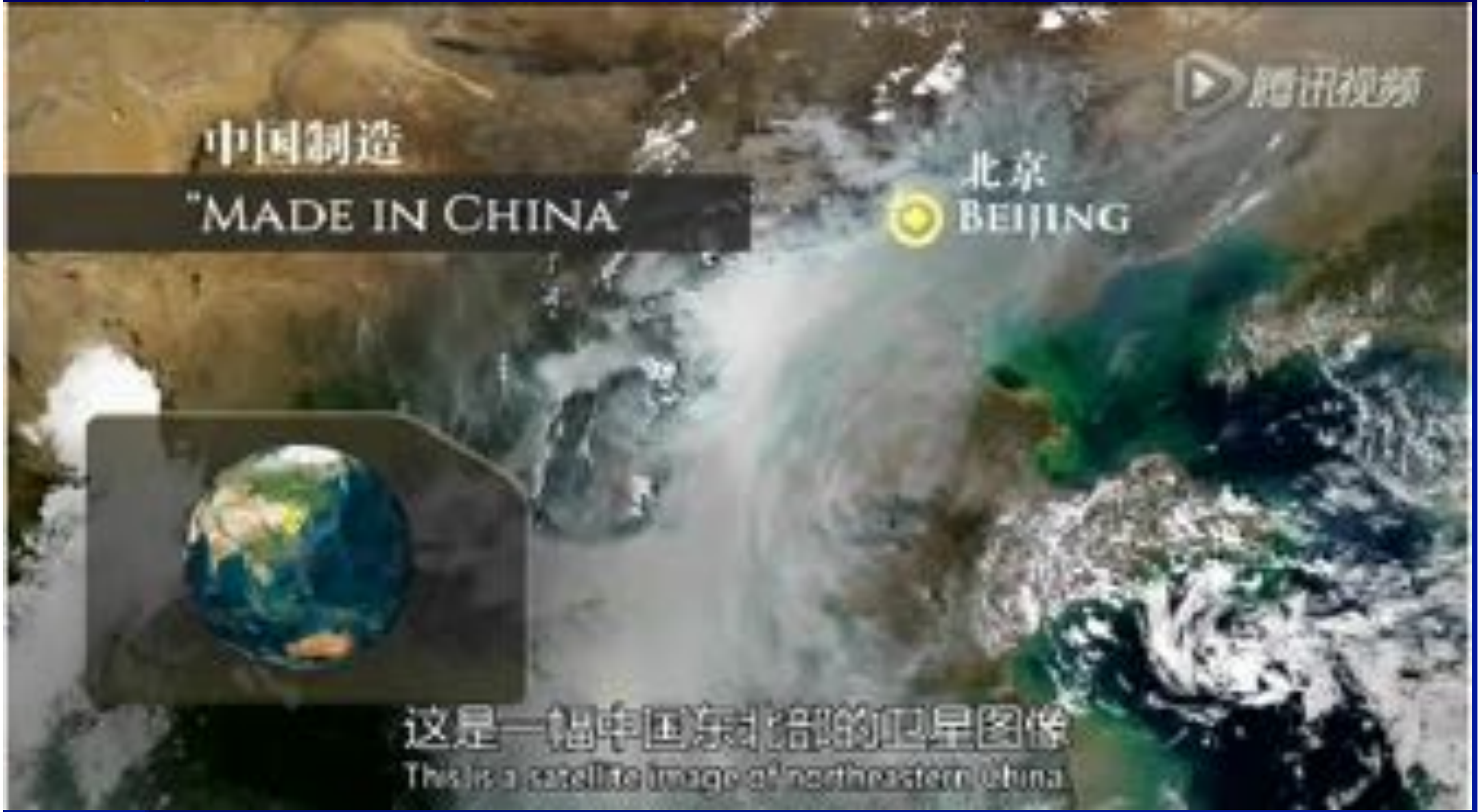

这是一幅中国东北部的卫星图像

This is a satellite image of northeastern China


特克斯县

乾为天，坤为地、震为雷、巽(xùn)为风，坎为水，艮(gèn)为山、离为火、兑为泽

基于ASTER SWIR的MgO反演模型提取基性-超基性岩

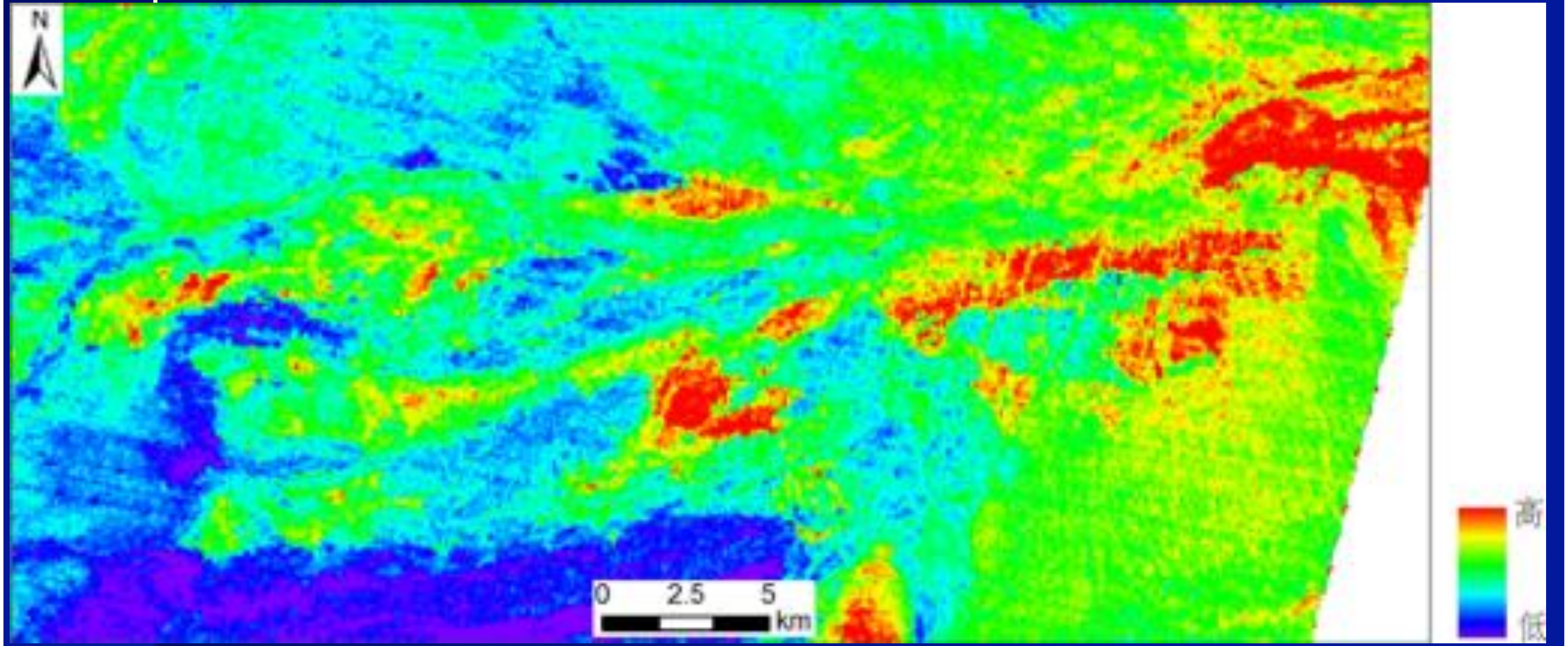

基于ASTER TIR的酸性岩浆岩SiO2反演模型

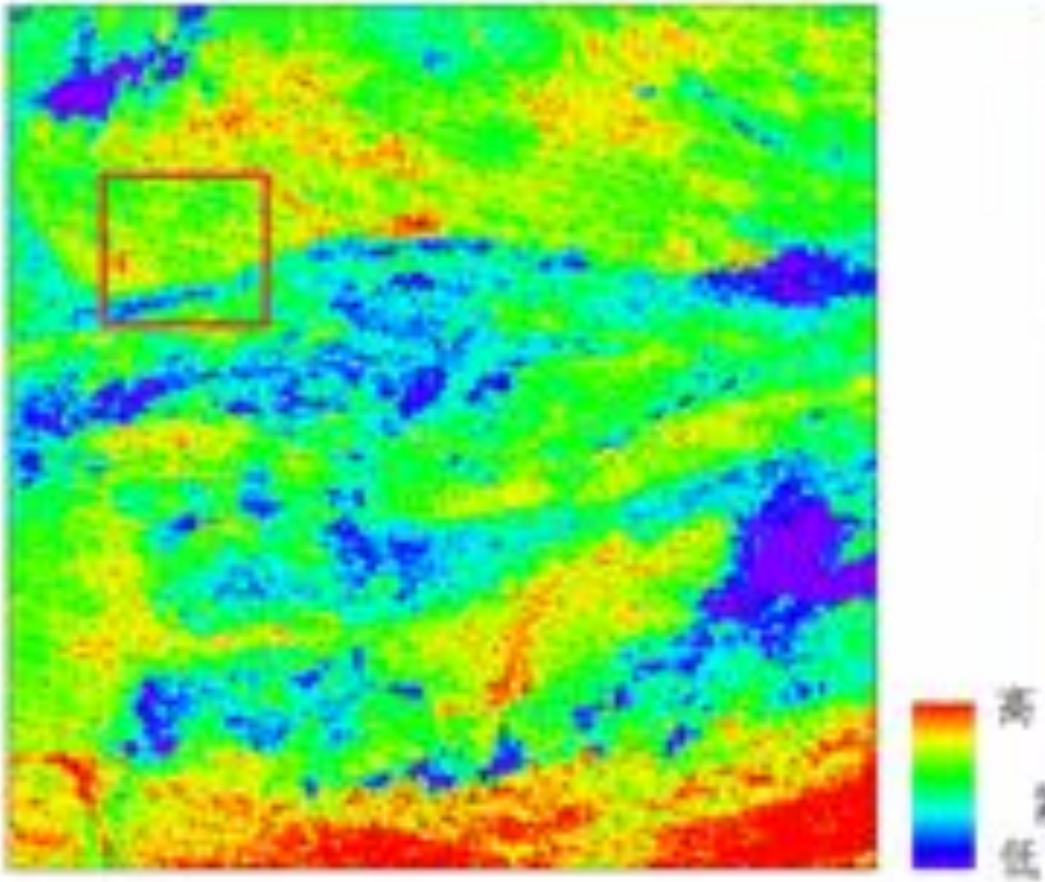

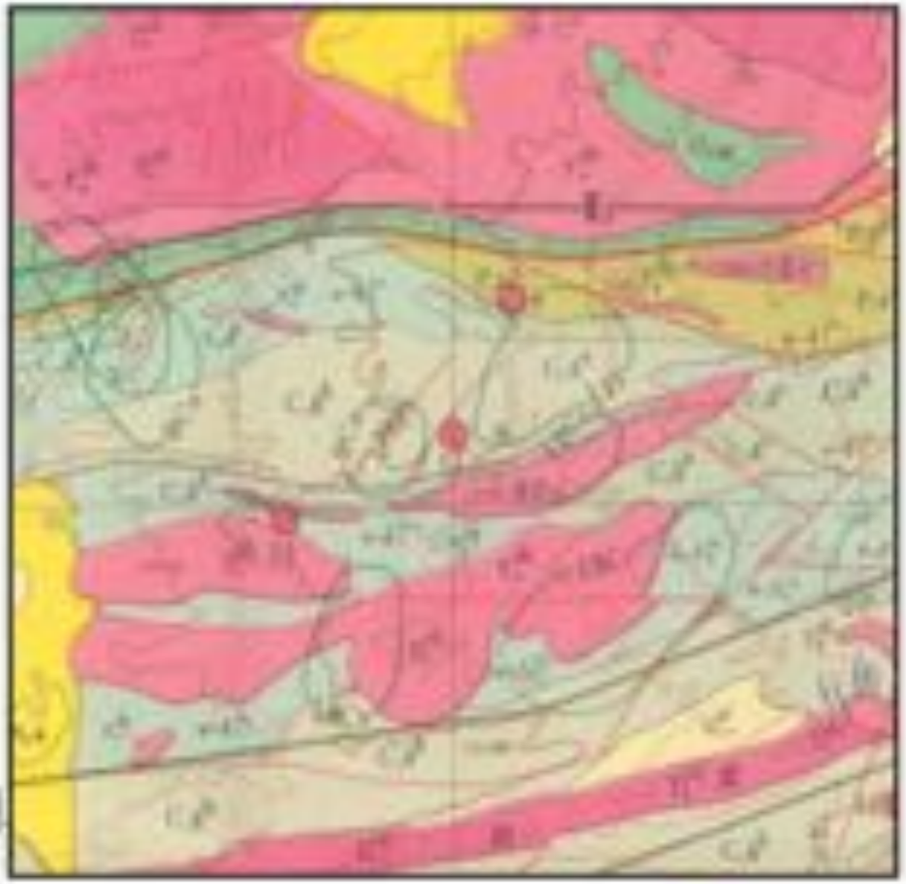

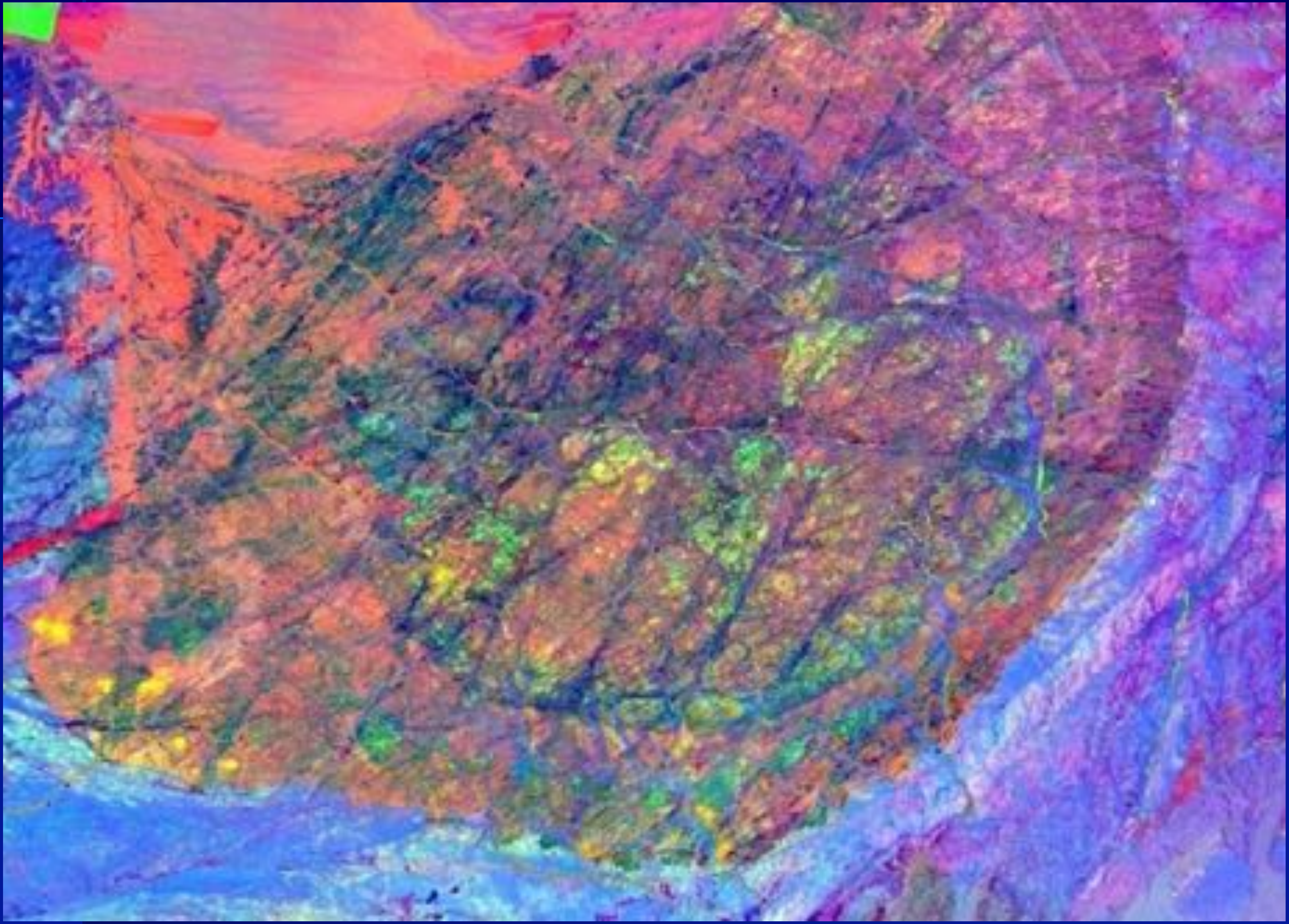

马是被捕食的动物，它的两只眼睛长在头的两侧，看东西立体感很差，虽然其视野可以达到330°，但马的两眼视线重叠的部分只有30°。因此，马会被同一事物惊吓两次。

捕猎动物，两只眼睛都长在前面，两只眼睛的视野重叠，帮助大脑判断物体的远近，为物体的准确定位带来很大帮助。

三维立体解译

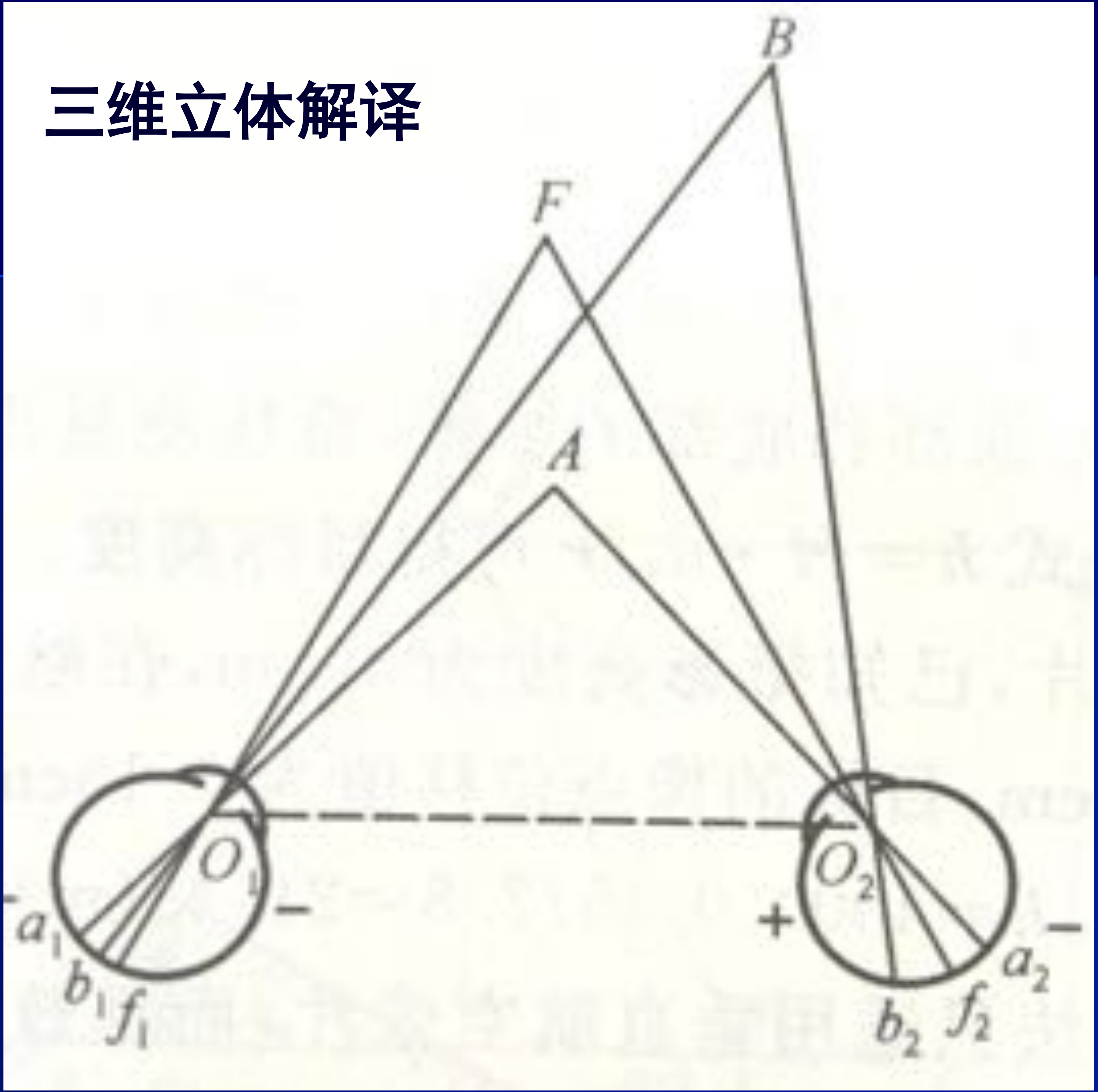

遥感是人的感知器官（眼）视觉分析功能的延长

- 观察距离的扩展：数百—数千公里以至更远；
- 电磁波范围的扩展：所有电磁波段，但主要为可见光、红外、微波；
- 观察方式的扩展：主动方式和被动方式，地面观察和太空观察，瞬时观察和连续观察；
- 认知方式的扩展：生物认知和数据分析。

遥感

可克服现场调查中地形、交通、气候等不利的影响。

显著提高早期识别的准确率和评价精度。

遥感信息的连续性信息可以弥补离散观察的不足。

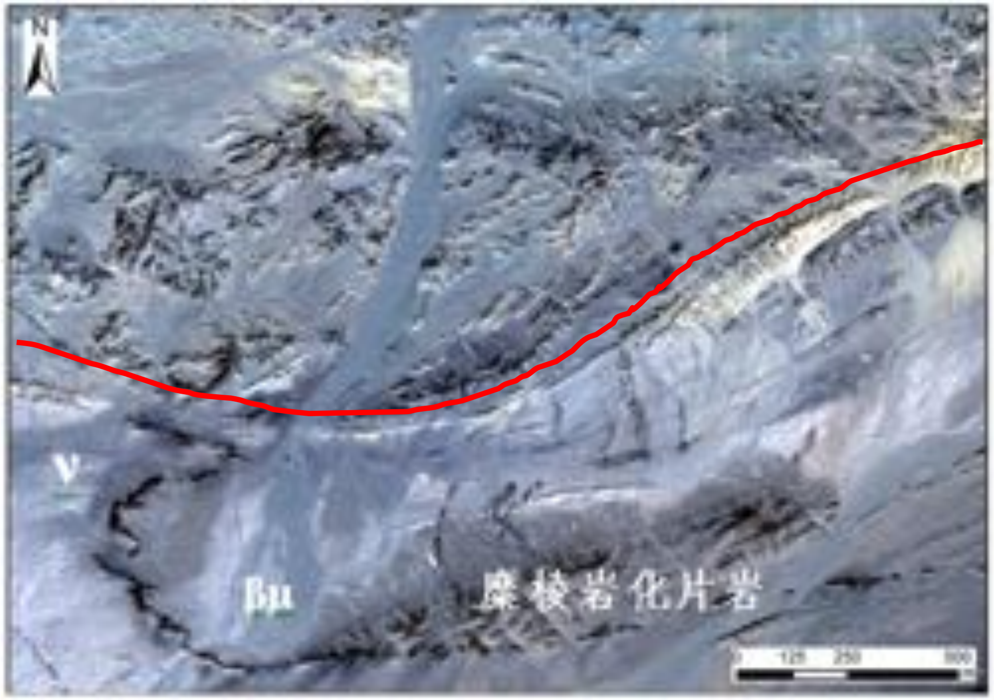

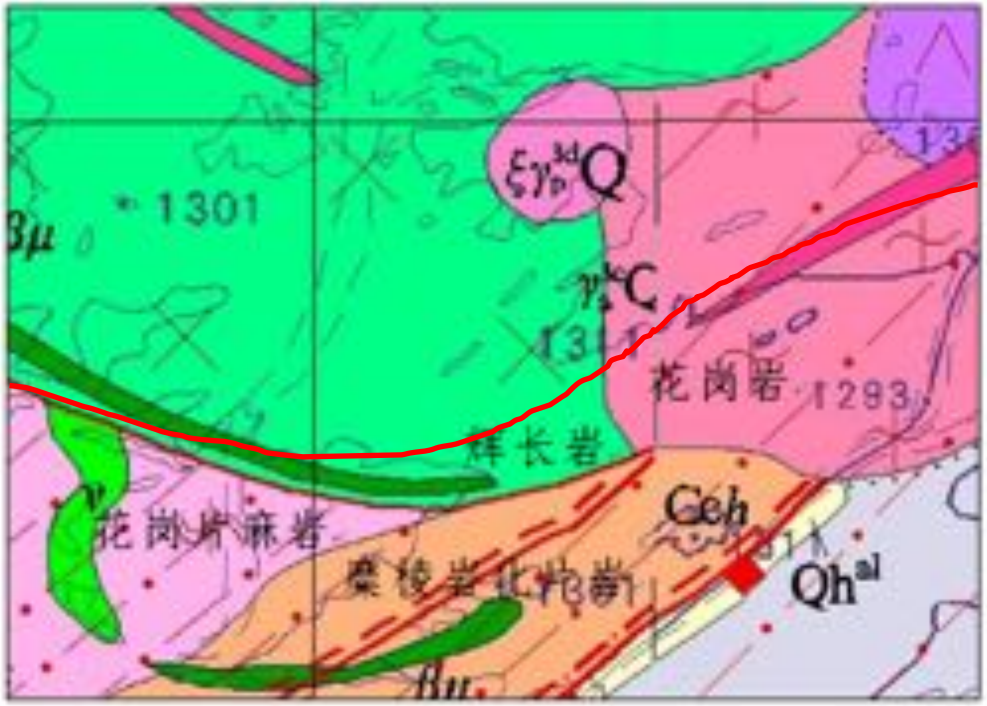

1. 连续的一条岩脉被划分为辉长岩脉与灰绿玢岩脉；
2. 一条弧形断层只表达了西部的一段；
3. 一条北东向展布的地质体被人为的分别划为寒武纪灰色中粒花岗片麻岩、志留纪土黄色似片麻状中粒花岗岩；

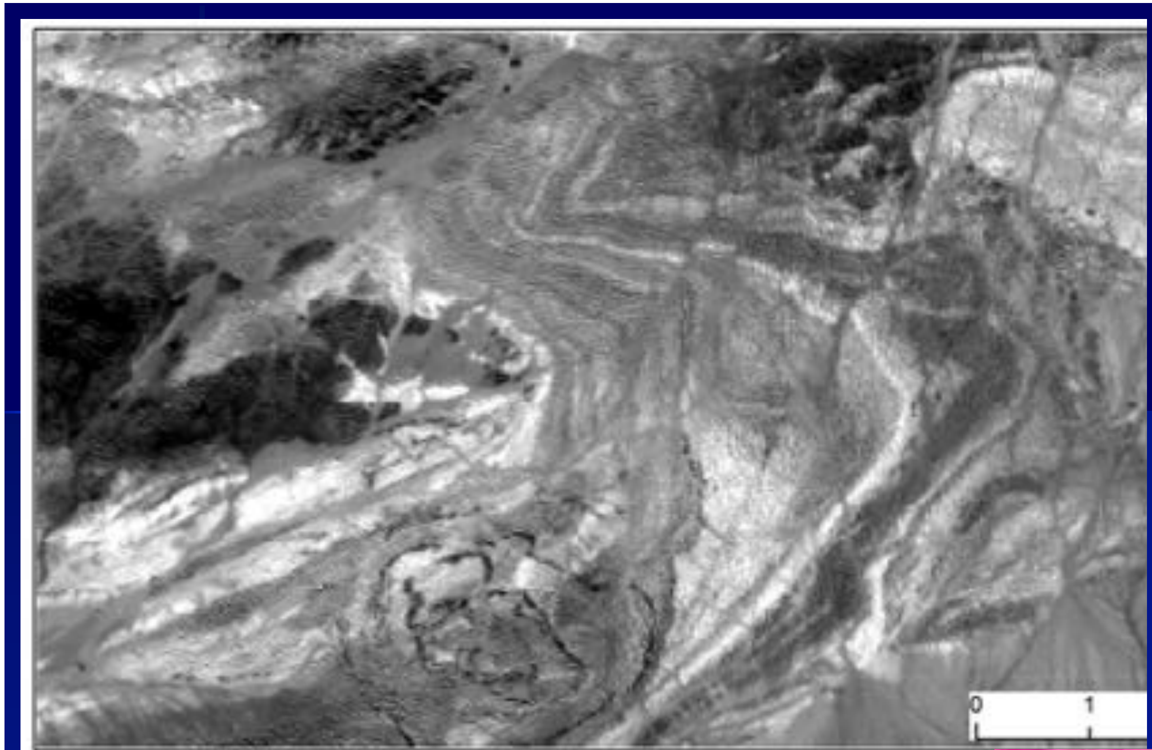
0
1

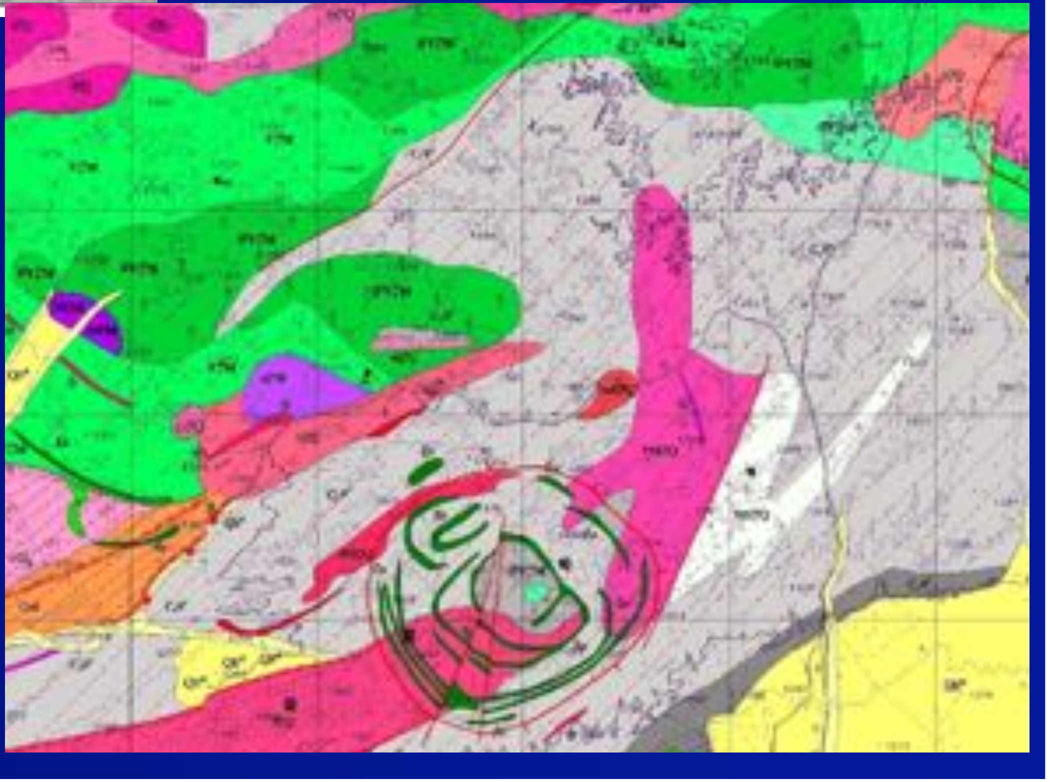

地貌形成过程及动力学

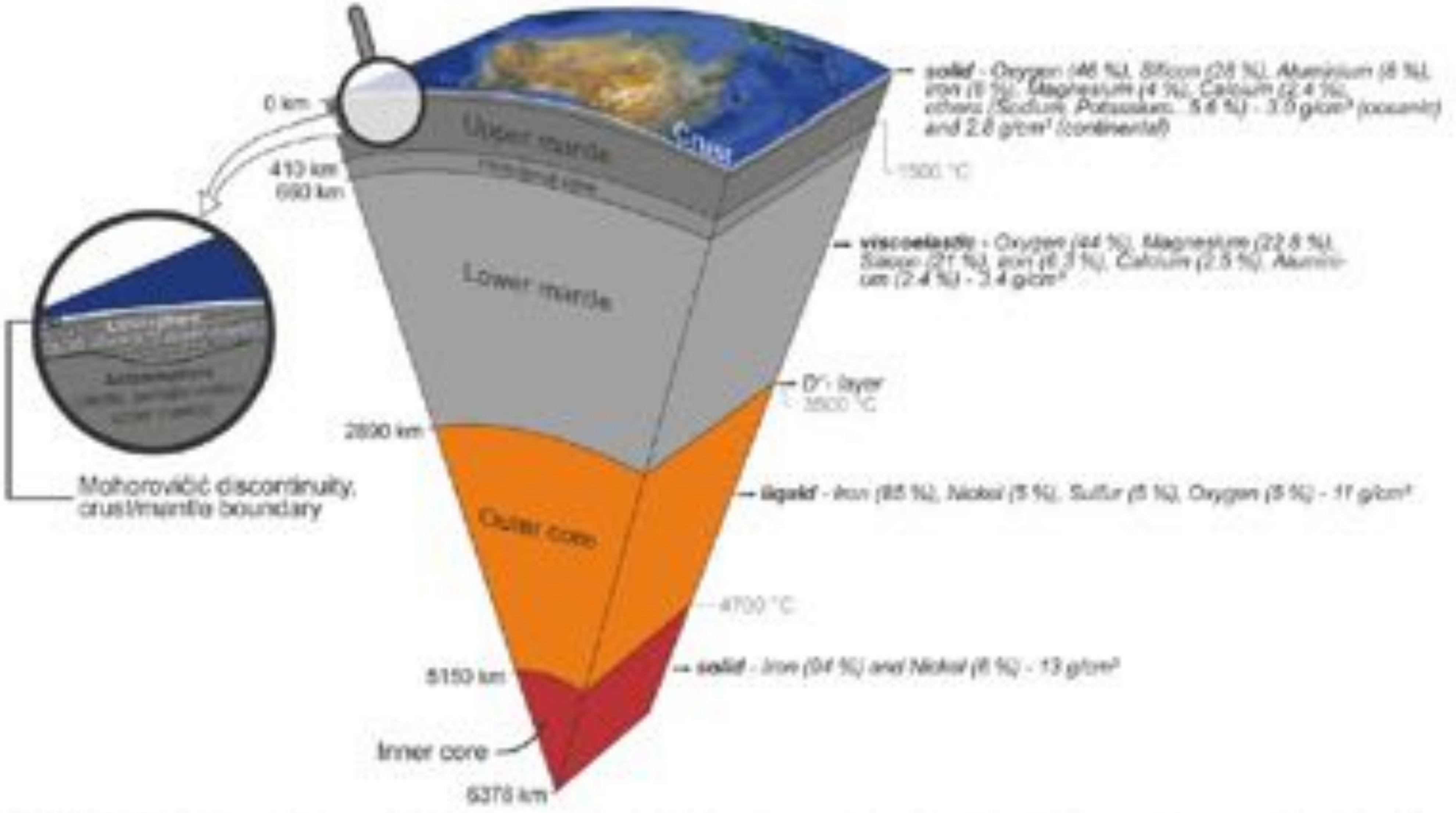
0 km
410 km
660 km
2890 km
5150 km
6378 km
Crust
Upper mantle
Transition zone
Lower mantle
Outer core
Inner core
Mohorovičić discontinuity, crust/mantle boundary
solid - Oxygen (46 %), Silicon (28 %), Aluminium (8 %), Iron (5 %), Magnesium (4 %), Calcium (2.4 %), others (Sodium, Potassium... 5.6 %) - 3.0 g/cm³ (oceanic) and 2.8 g/cm³ (continental)
1500 °C
viscoelastic - Oxygen (44 %), Magnesium (22.8 %), Silicon (21 %), Iron (6.3 %), Calcium (2.5 %), Aluminium (2.4 %) - 3.4 g/cm³
D''- layer
3500 °C
liquid - Iron (85 %), Nickel (5 %), Sulfur (5 %), Oxygen (5 %) - 11 g/cm³
4700 °C
solid - Iron (94 %) and Nickel (6 %) - 13 g/cm³

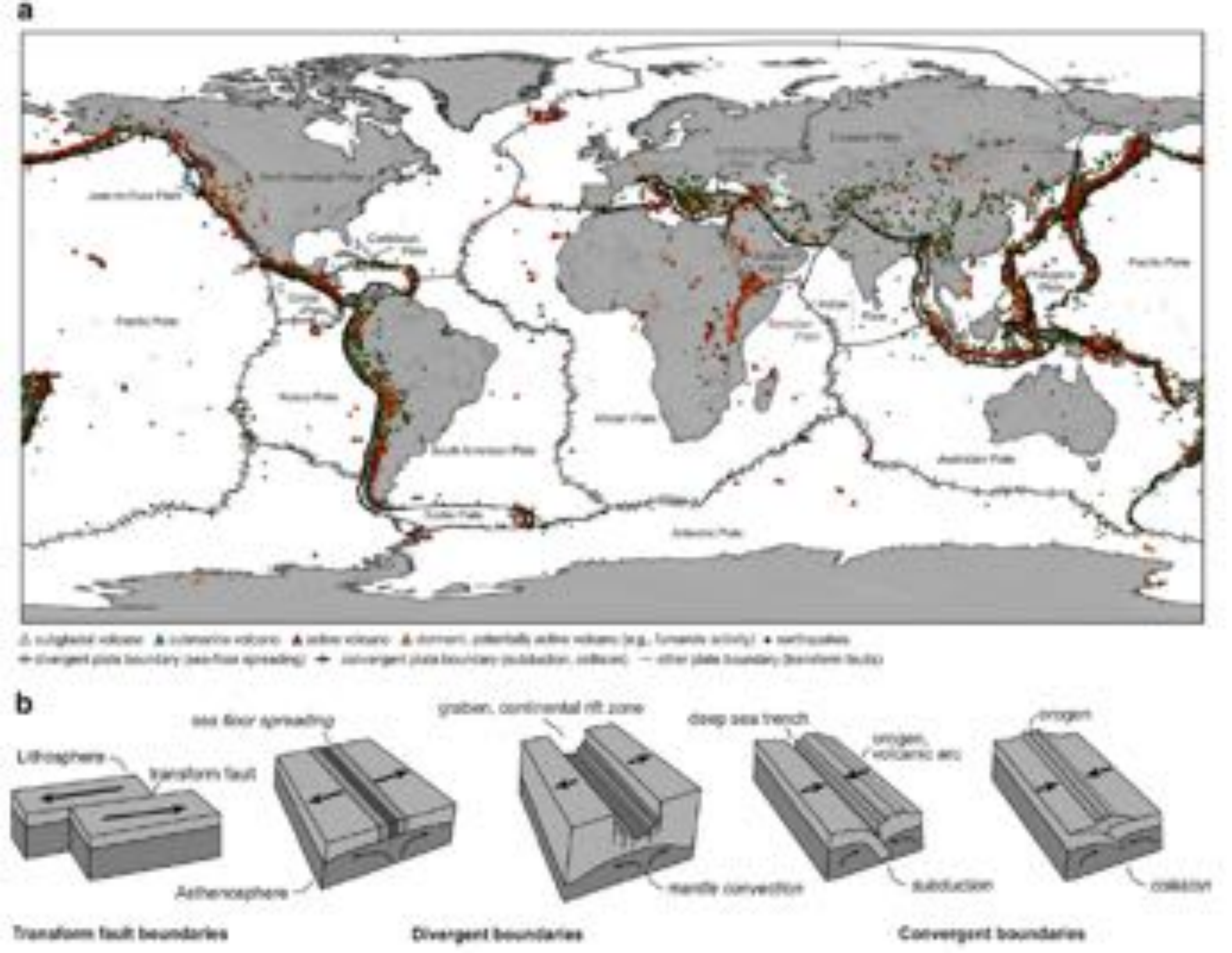
a
△ subglacial volcano ▲ submarine volcano ▲ active volcano ▲ dormant, potentially active volcano (e.g., fumarole activity) • earthquakes
divergent plate boundary (sea-floor spreading) convergent plate boundary (subduction, collision) — other plate boundary (transform faults)
b
Lithosphere
transform fault
Asthenosphere
sea floor spreading
graben, continental rift zone
mantle convection
deep sea trench
orogen, volcanic arc
subduction
orogen
collision
Transform fault boundaries
Divergent boundaries
Convergent boundaries


Image IBCAO
Image U.S. Geological Survey
Data SIO, NOAA, U.S. Navy, NGA, GEBCO
Image Landsat / Copernicus
Google earth
影像拍攝日期：2015/12/14 59° 42′02.12″ 北 21° 30′34.36″ 西 海拔 米 視角海拔高度 2839.35 公里

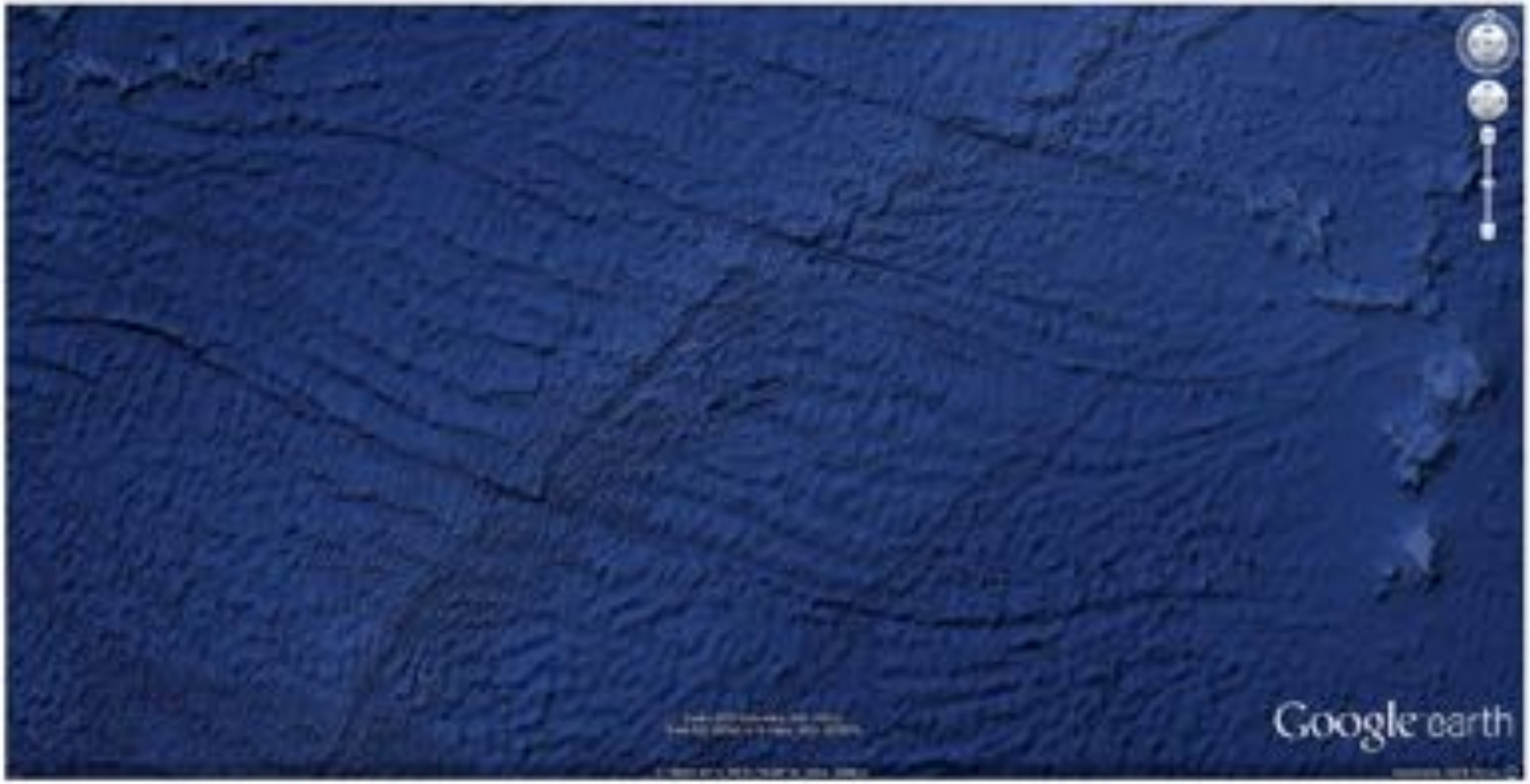
Google earth

a


b
Google earth


Google earth
16° 44'26.32" 北 45° 24'20.26" 东 海拔 1297 米 视角海拔高度 3280.70 公里

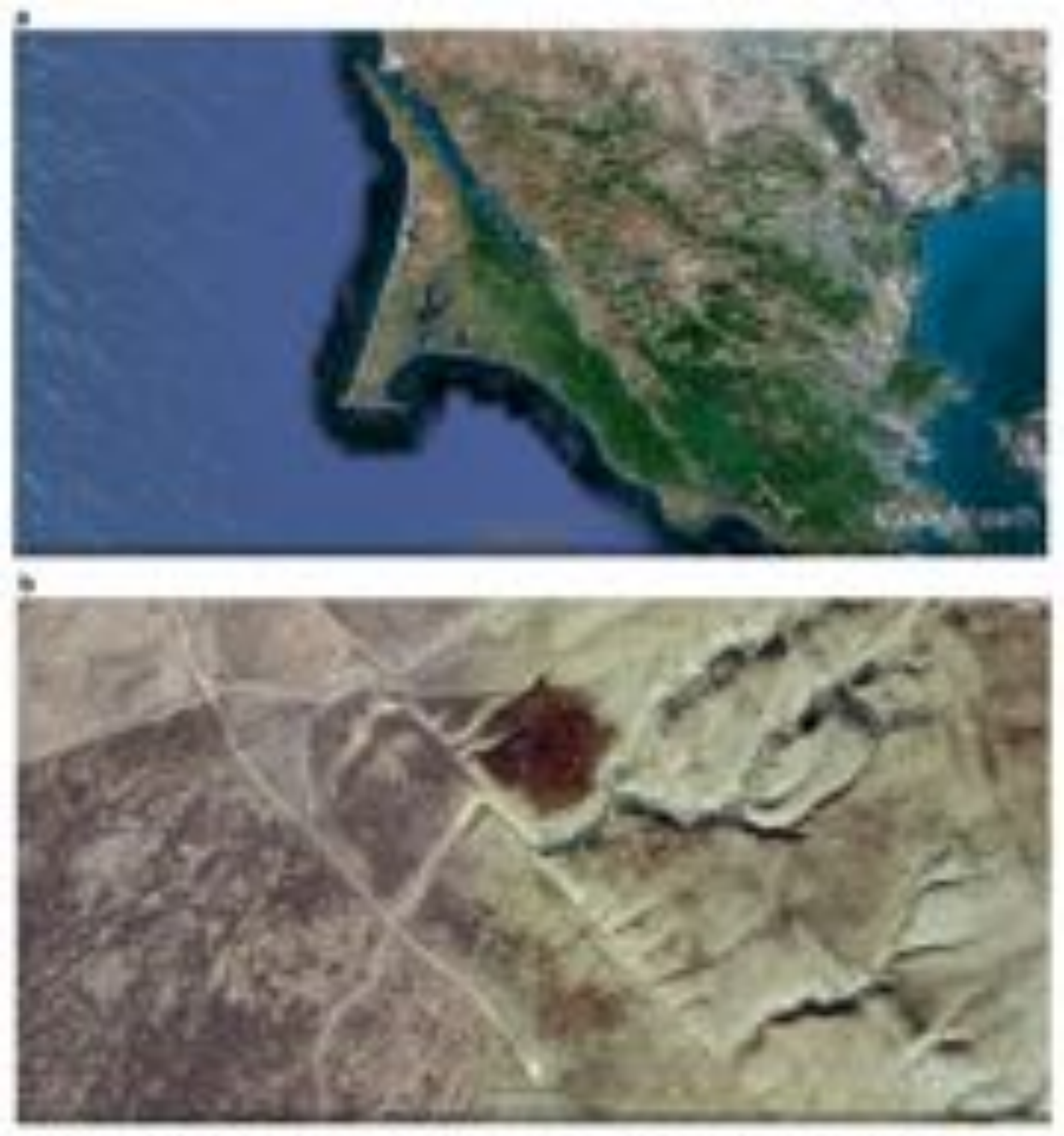
a
Google earth
b


c
Google earth

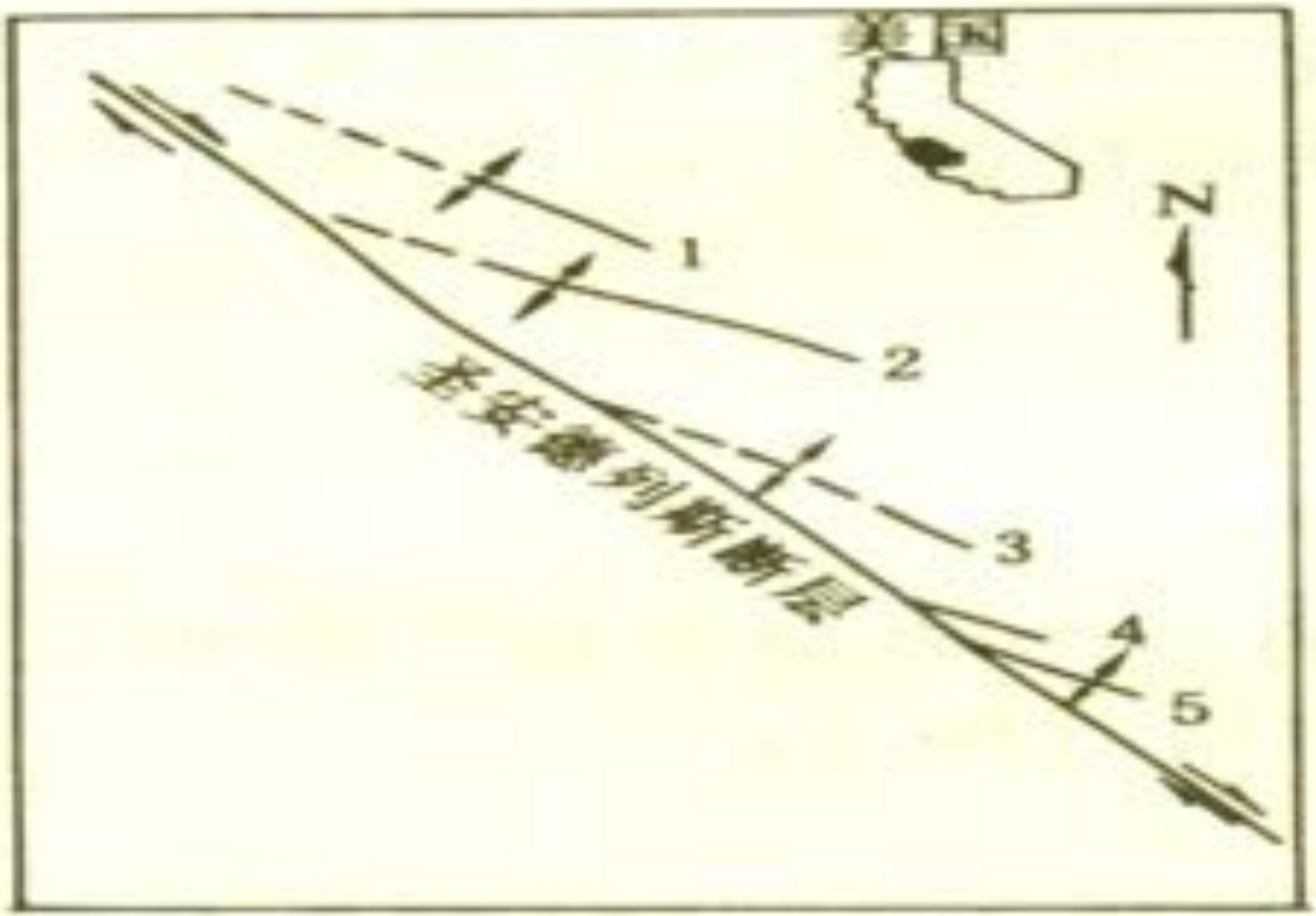

圣安德列斯断层一侧的雁列式褶皱
（据 Moody 等．1956）

Google earth
25° 53'37.17" 北 102° 59'20.00" 东 海拔 2422 米 视角海拔高度 1048.61 公里

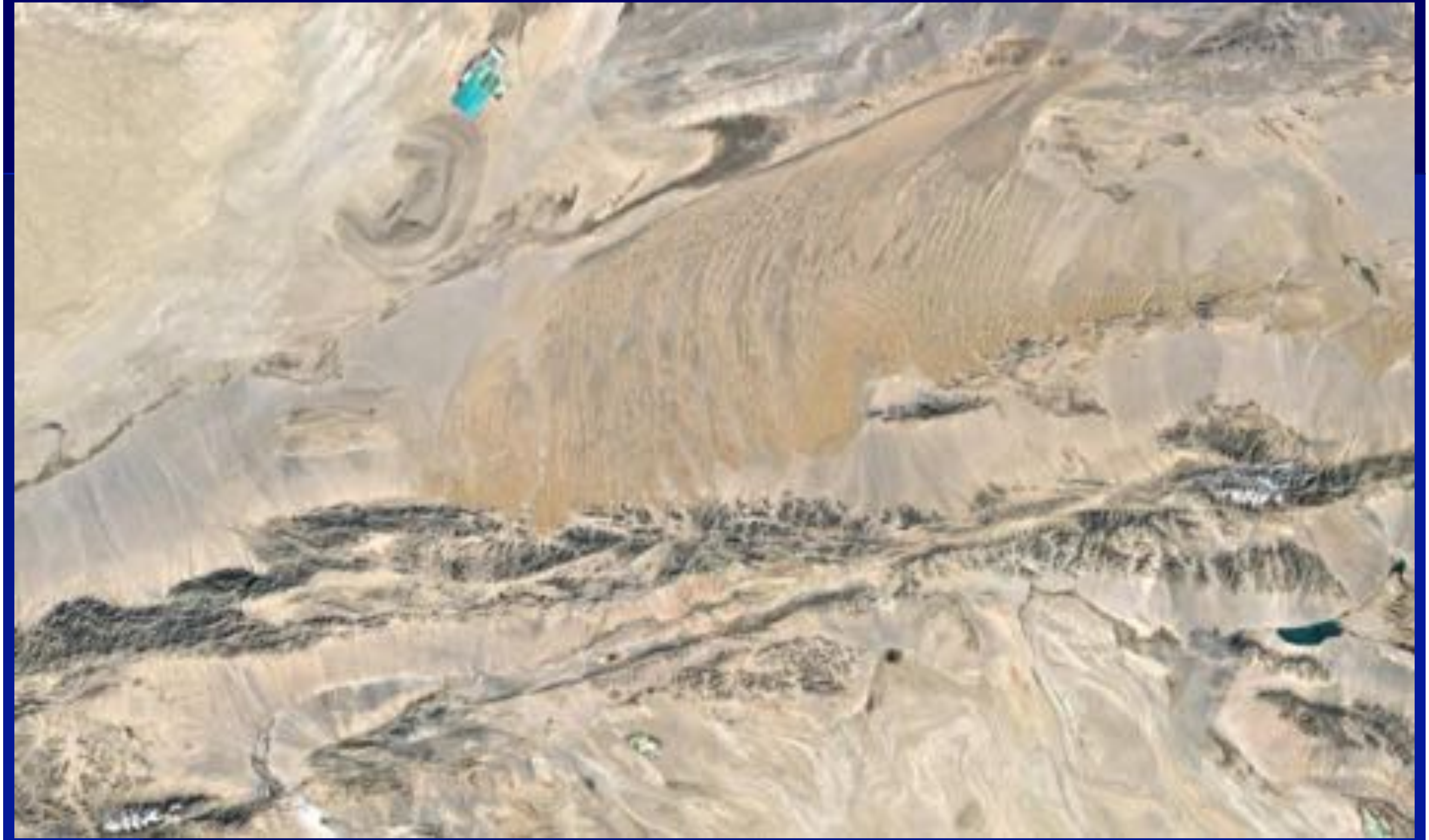

火山地貌

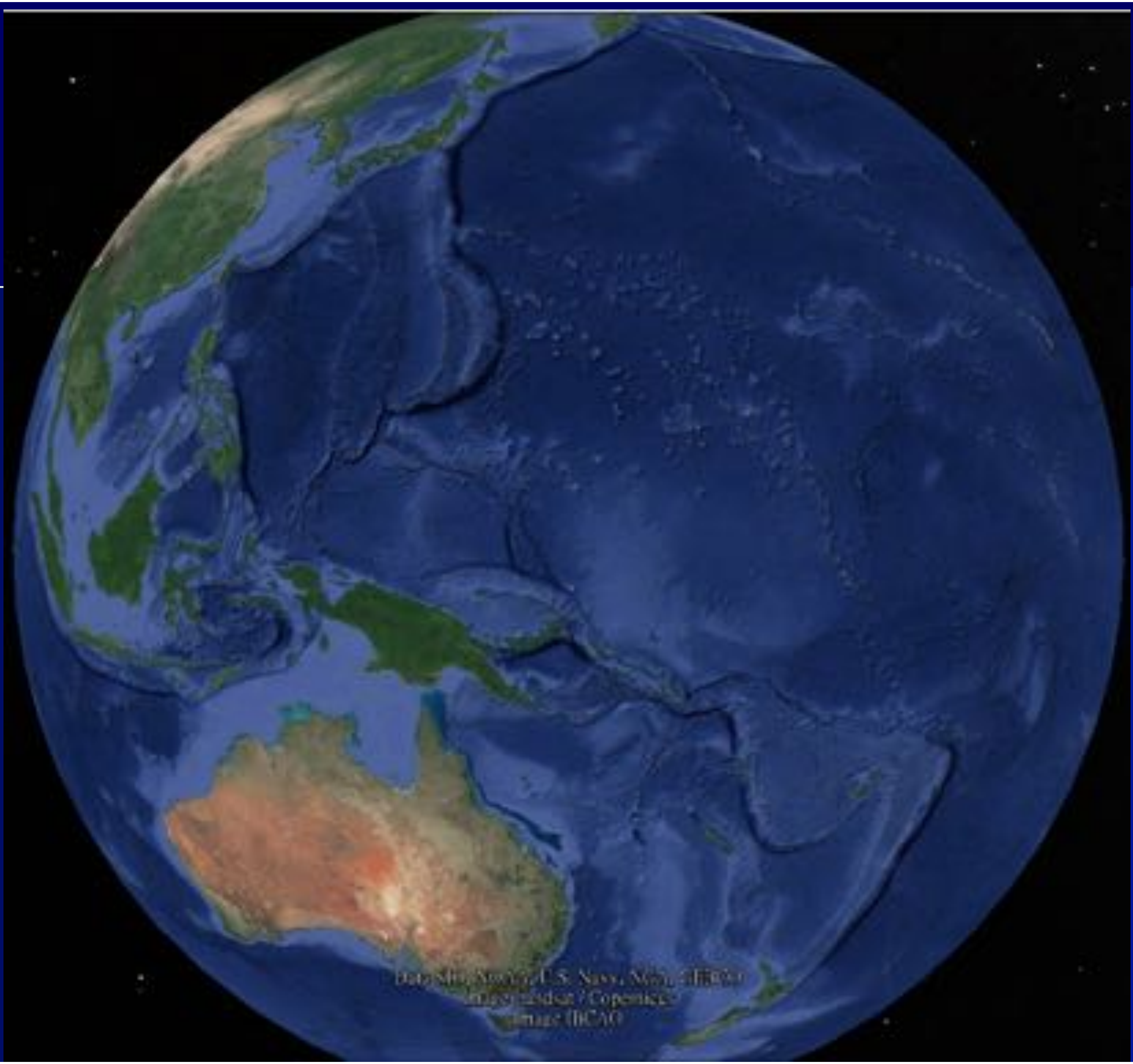
Data SIO, NOAA, U.S. Navy, NGA, GEBCO
Image Landsat / Copernicus
Image IBCAO

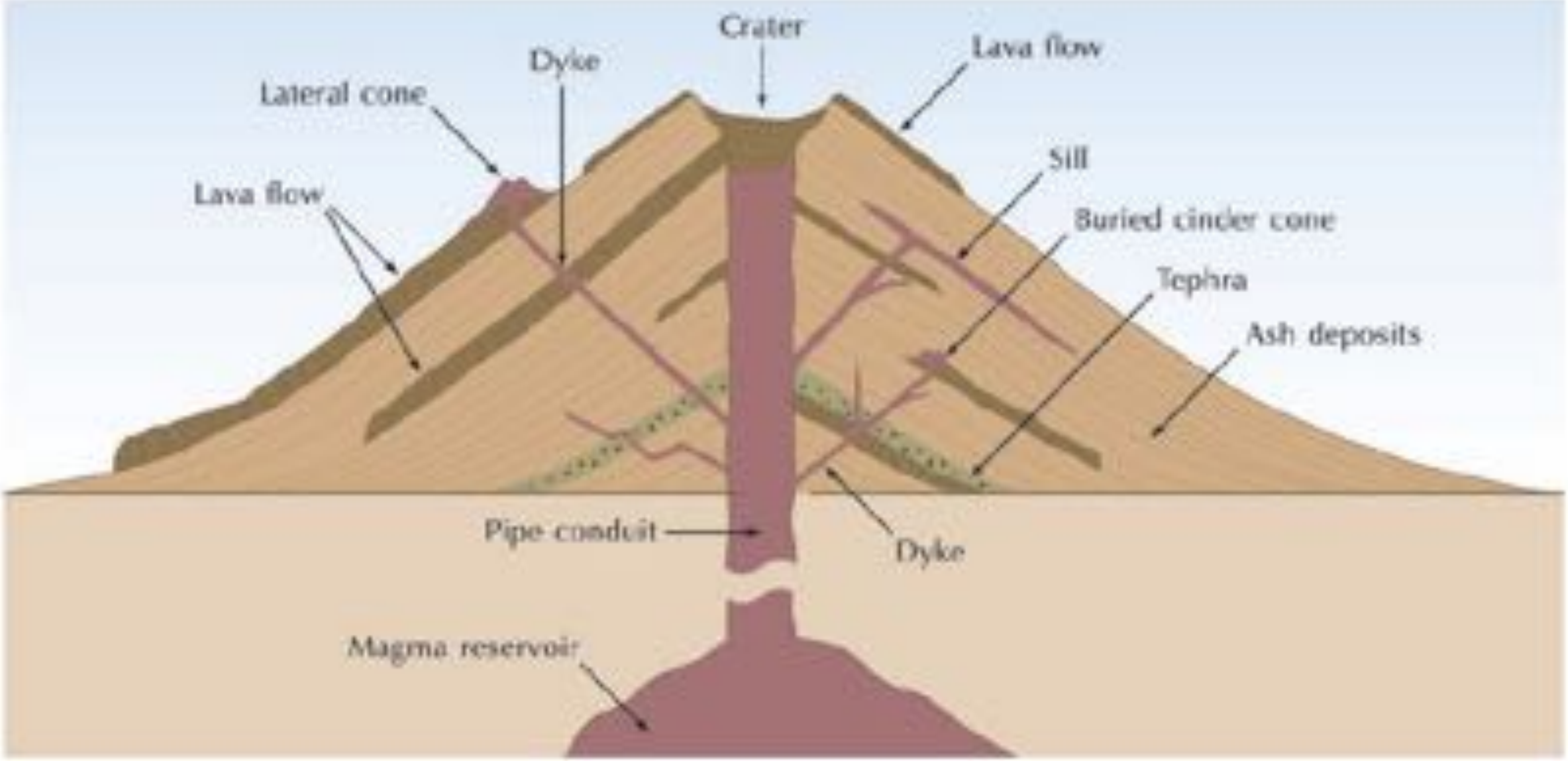
Crater
Dyke
Lava flow
Lateral cone
Sill
Lava flow
Buried cinder cone
Tephra
Ash deposits
Pipe conduit
Dyke
Magma reservoir

Plate 6.4 Novarupta rhyolite tholoid formed in 1912 in the Katmai caldera, Katmai National Park, Alaska USA. (*Photograph by Tony Waltham Geophotos*)


Google earth


多巴湖


Kauai
3.8-5.6
Oahu
2.2-3.3
Molokai
1.3-1.8
Maui
小于1.0
夏威夷
0.8至现在
夏威夷火山岛链
放射性测年资料（百万年）
a
Google earth

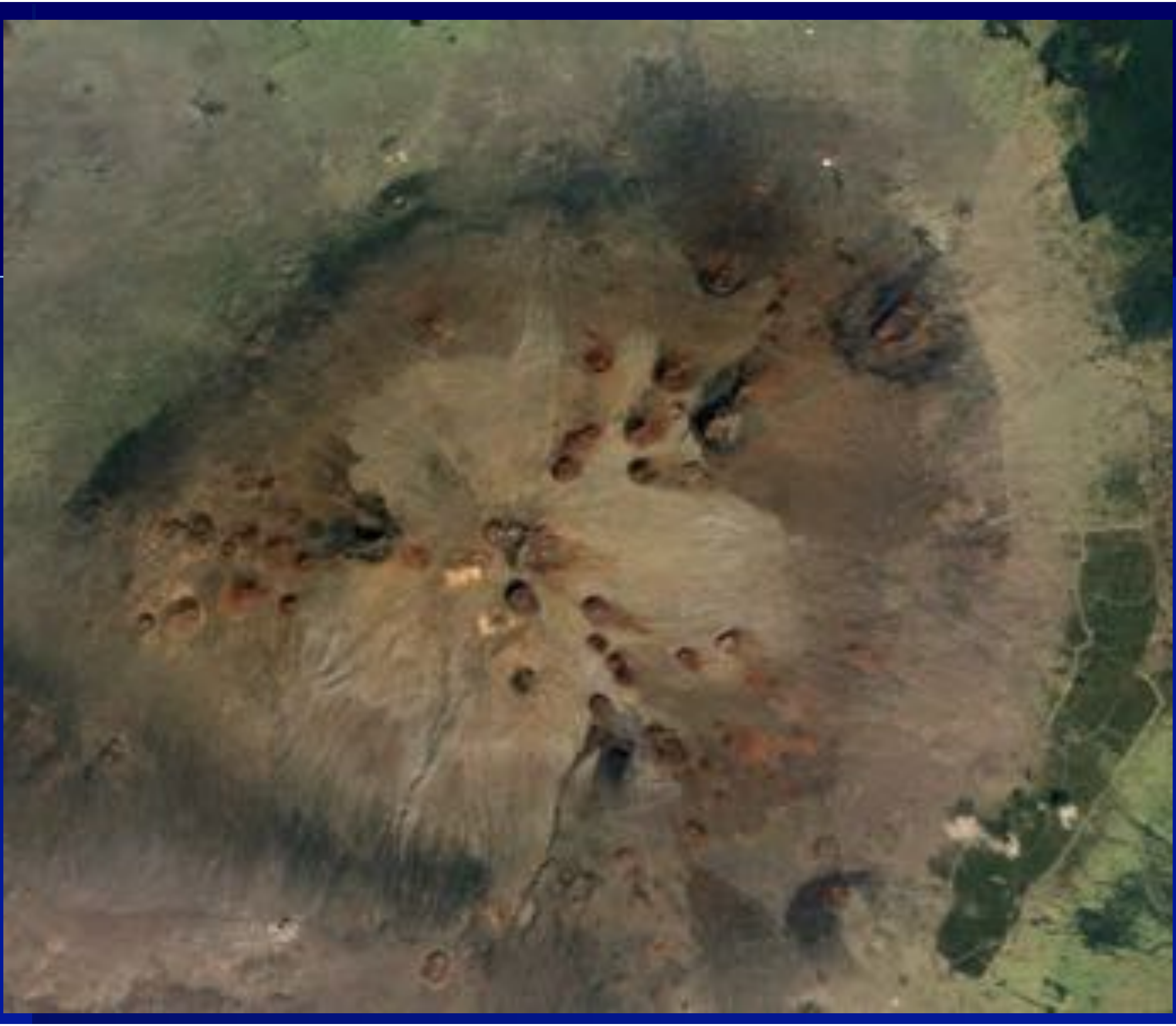


a

b


c


b
Google


Image © 2017 DigitalGlobe
Image © 2017 DigitalGlobe
Google earth

Google


a
b
Google

Fig. 2.10 (a) Vertical basalt columns in southern Iceland, polished by glaciers. (b) The Devil's Postpile, a national monument in the Sierra Nevada of California (USA) showcasing basalt columns of diameters up to 1 m and the height of individual columns

a natural state of destruction due to frost weat

months (Image credit: D. [illegible])

Fig. 2.11 Explosive ash and cinder eruption at the slope of Mt. Batur on Bali, Indonesia (Image credit: D. Kelletat)

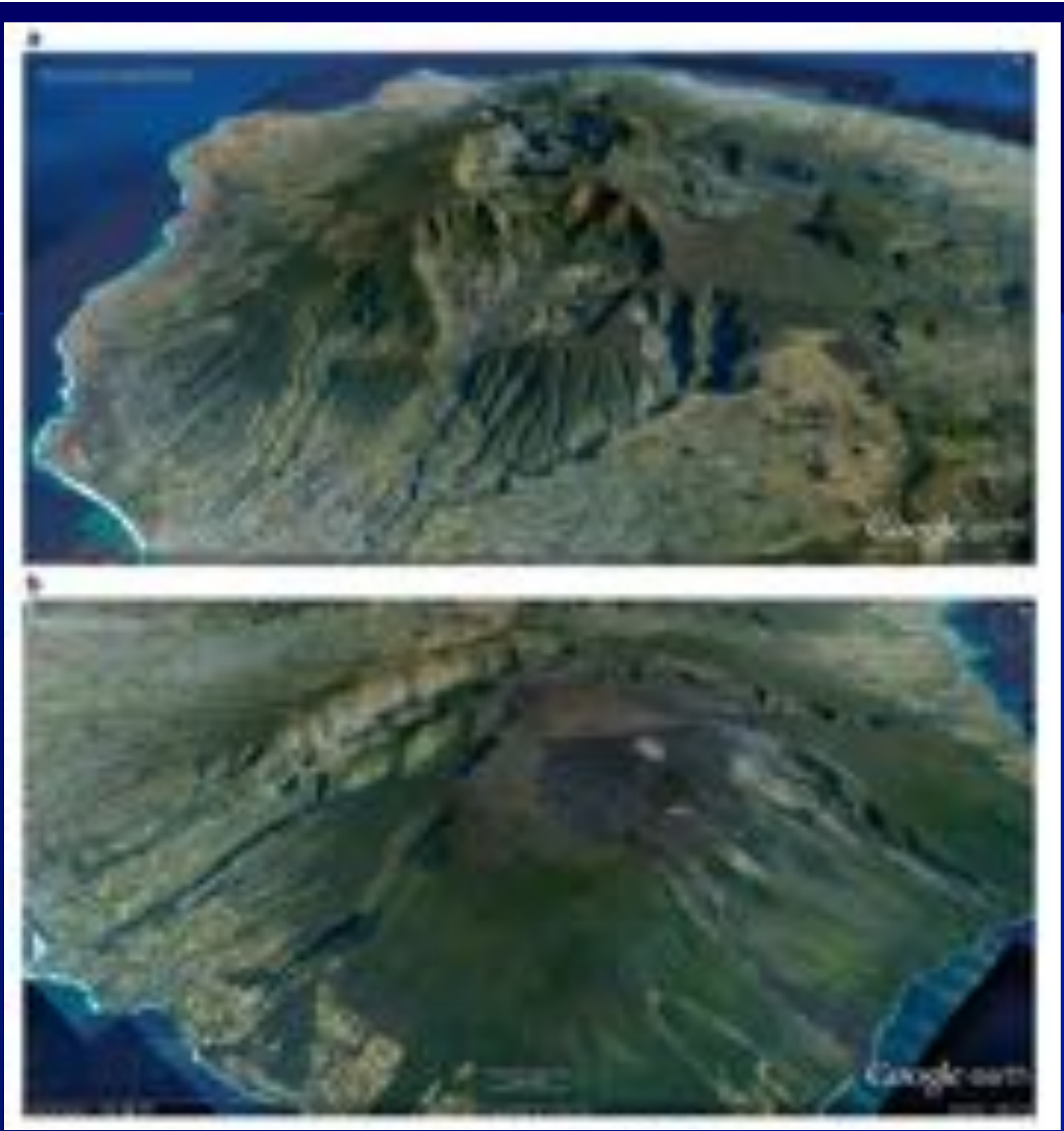
a
b
Google earth
Google earth

长白山


a
b

a

b


a
b
c
Google earth


Google

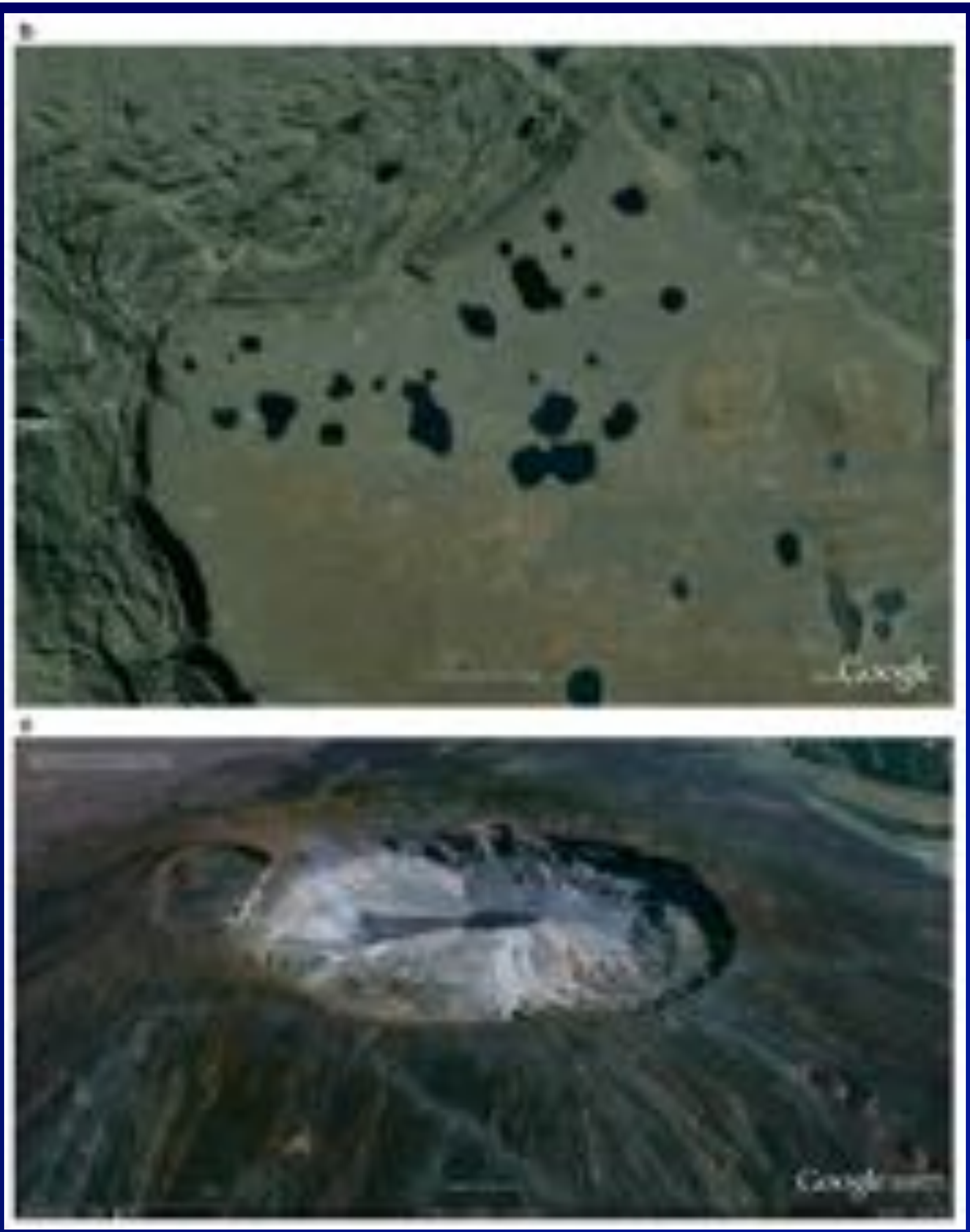
Google
Google earth


a
b


c

a

b

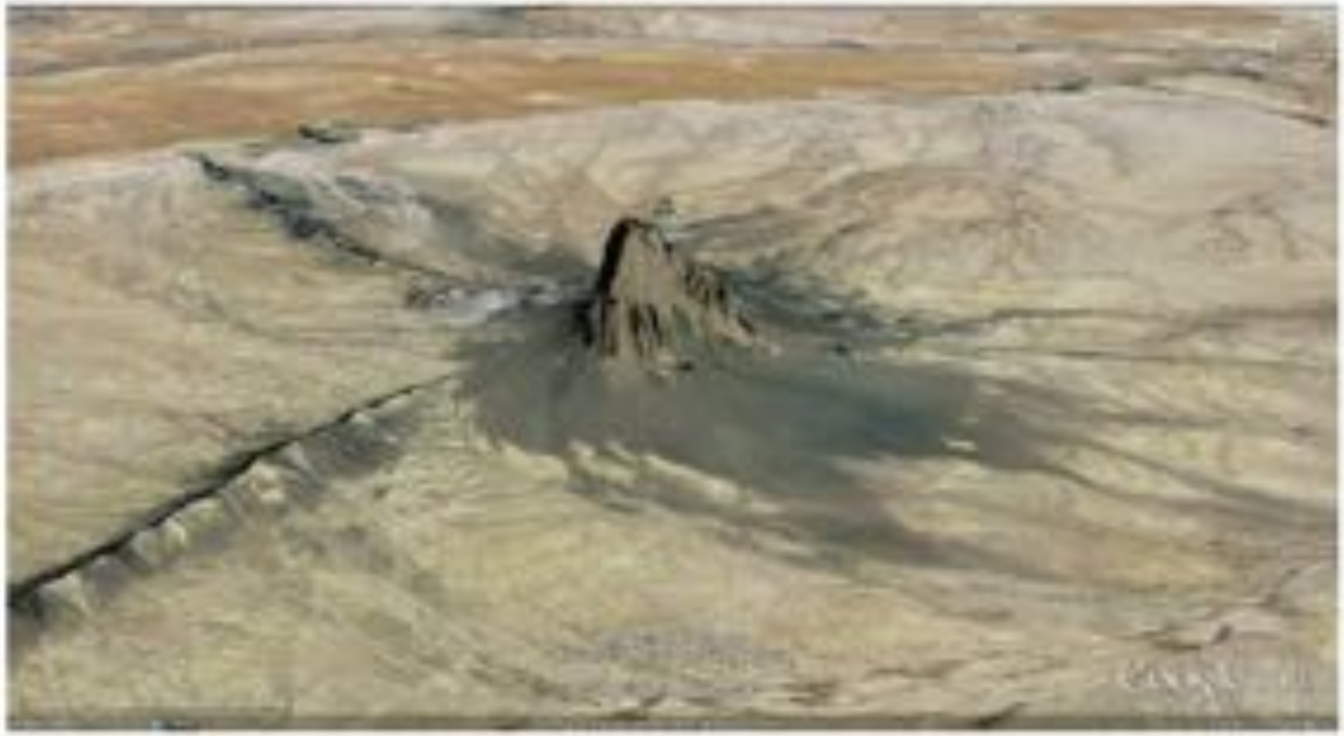

锡林郭勒火山

Google earth

火成岩地貌

Google earth
影像拍摄日期: 2017 5 25 30° 10' 58.75" 北 118° 16' 50.24" 东 海拔 293 米 视角海拔高度 64.55 公里


Google earth
影像拍摄日期：2017/2/12 30°08'42.44" 北 118°11'10.17" 东 海拔 1269 米 视角海拔高度 20.08 公里

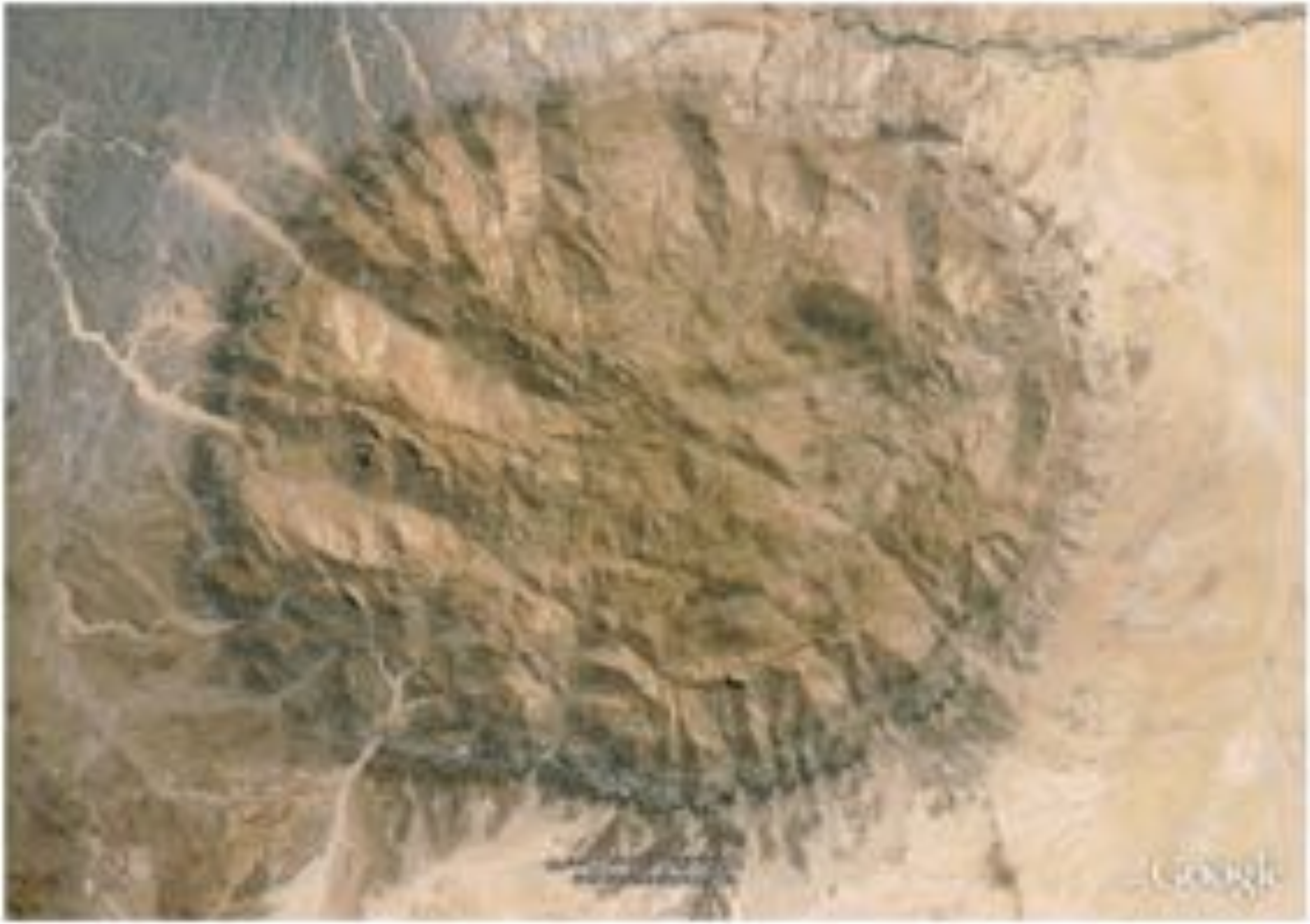
Google


a
Google
b
Google


Google

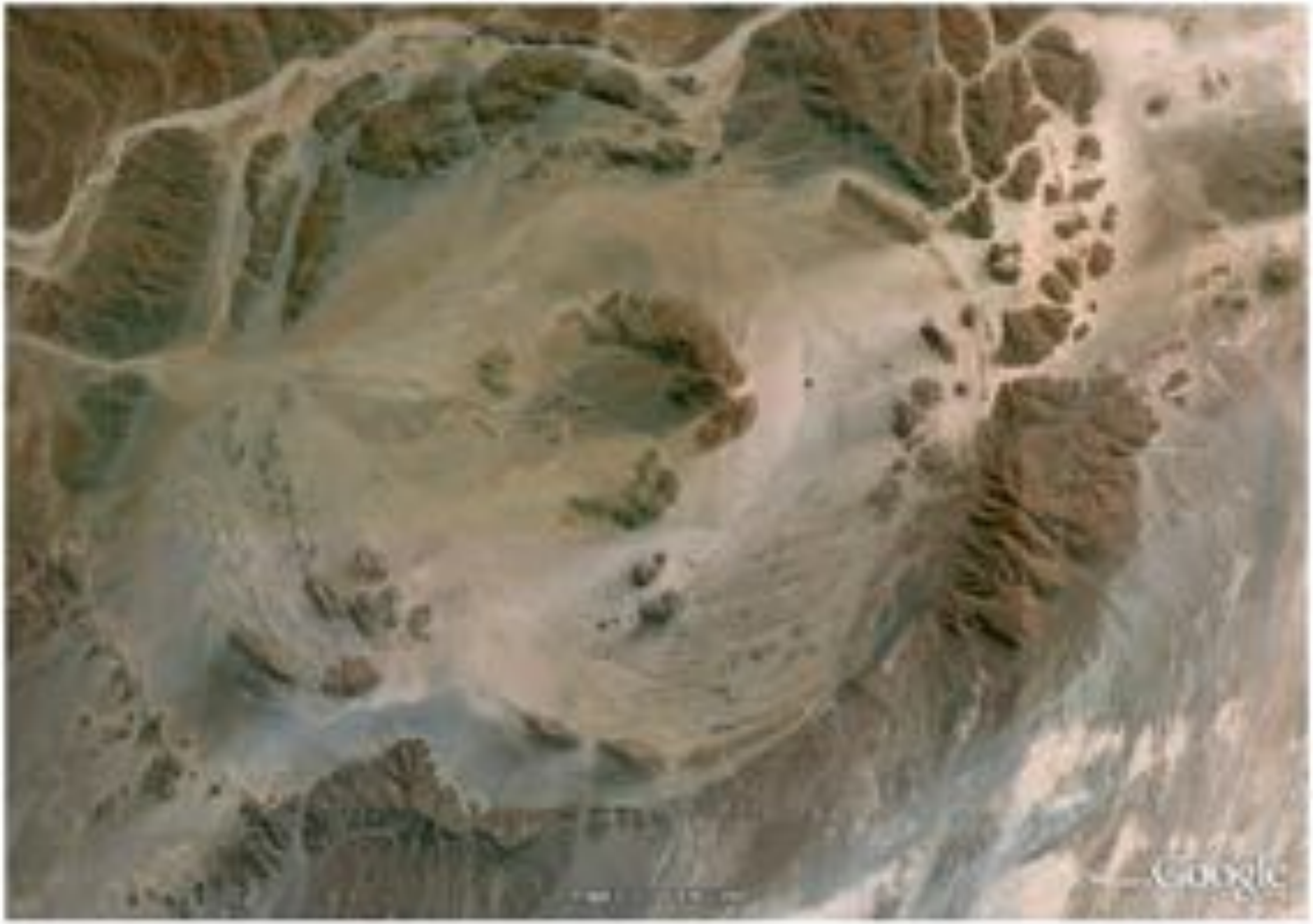
Google


Google earth


Image © 2017 DigitalGlobe
Google earth


b
Google

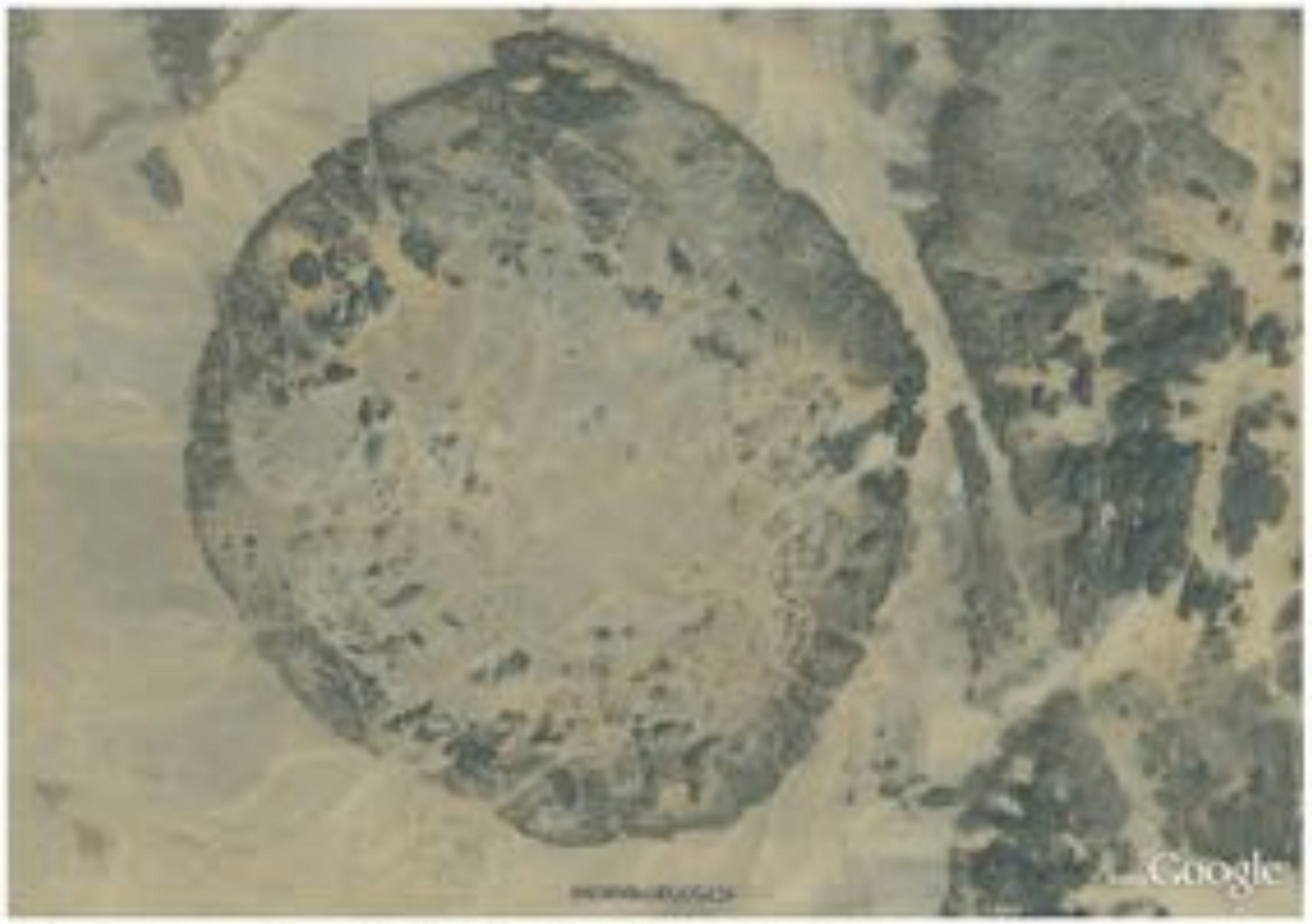
Google

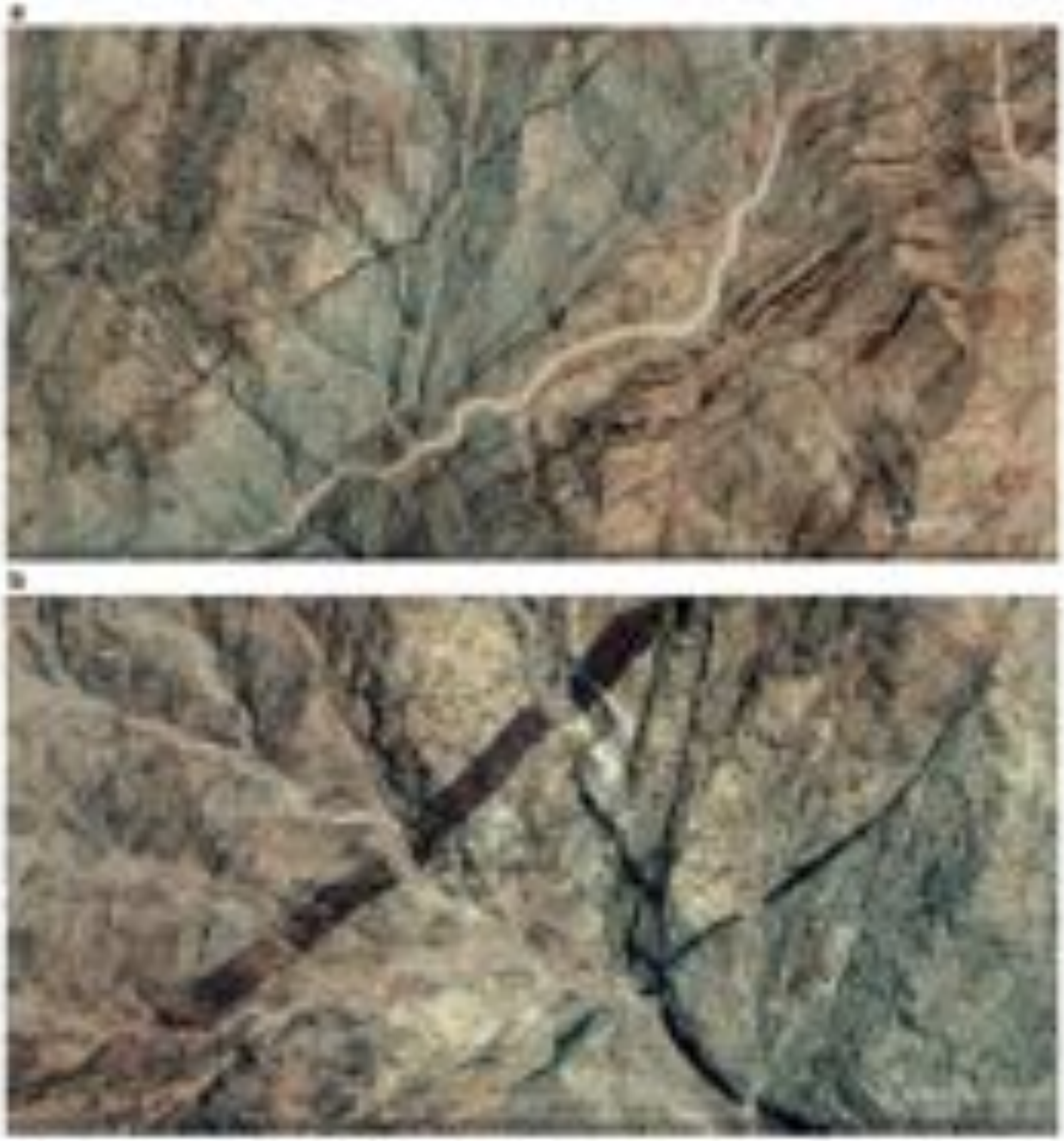
a
b

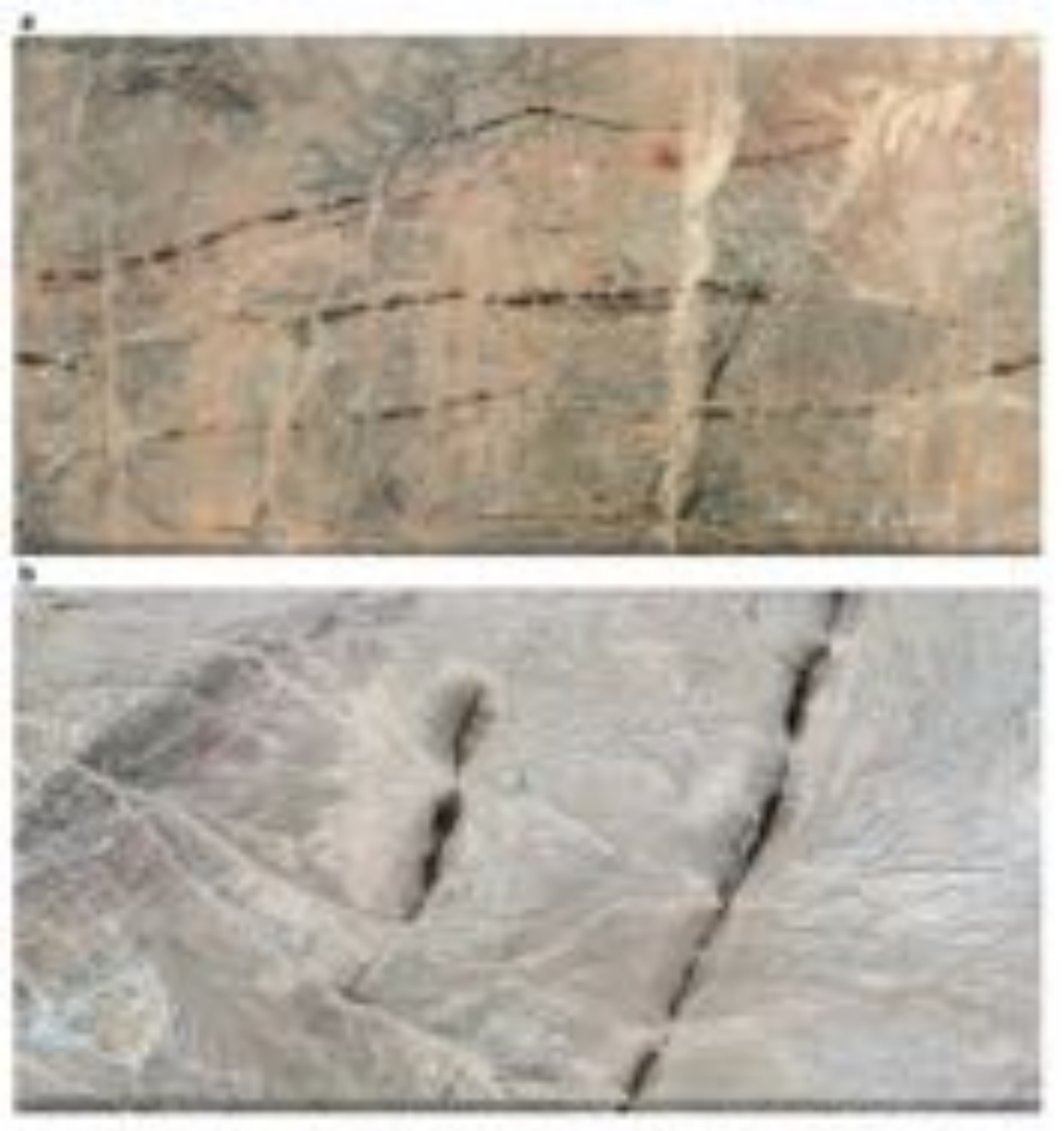
a
b

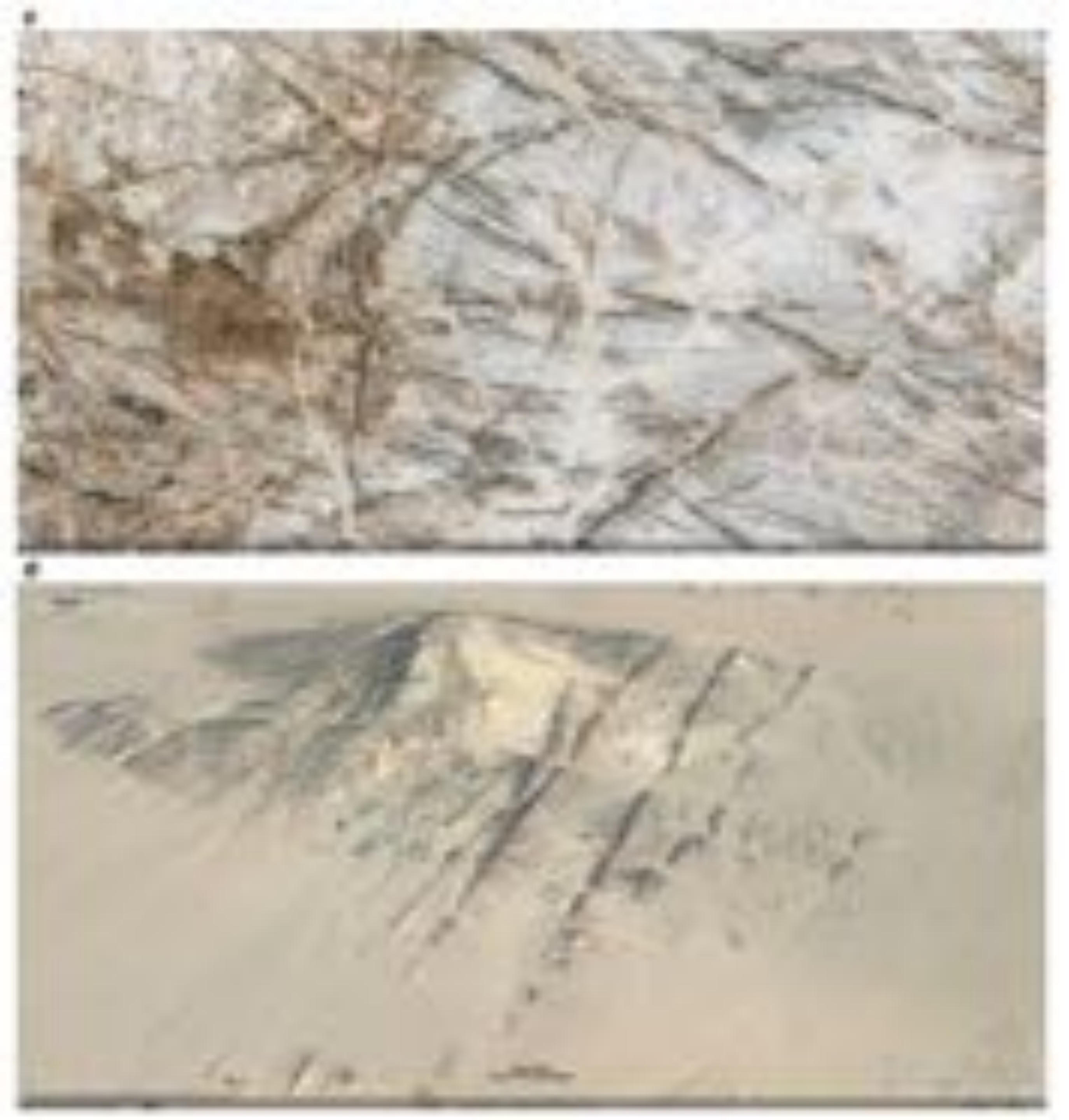

构造地貌

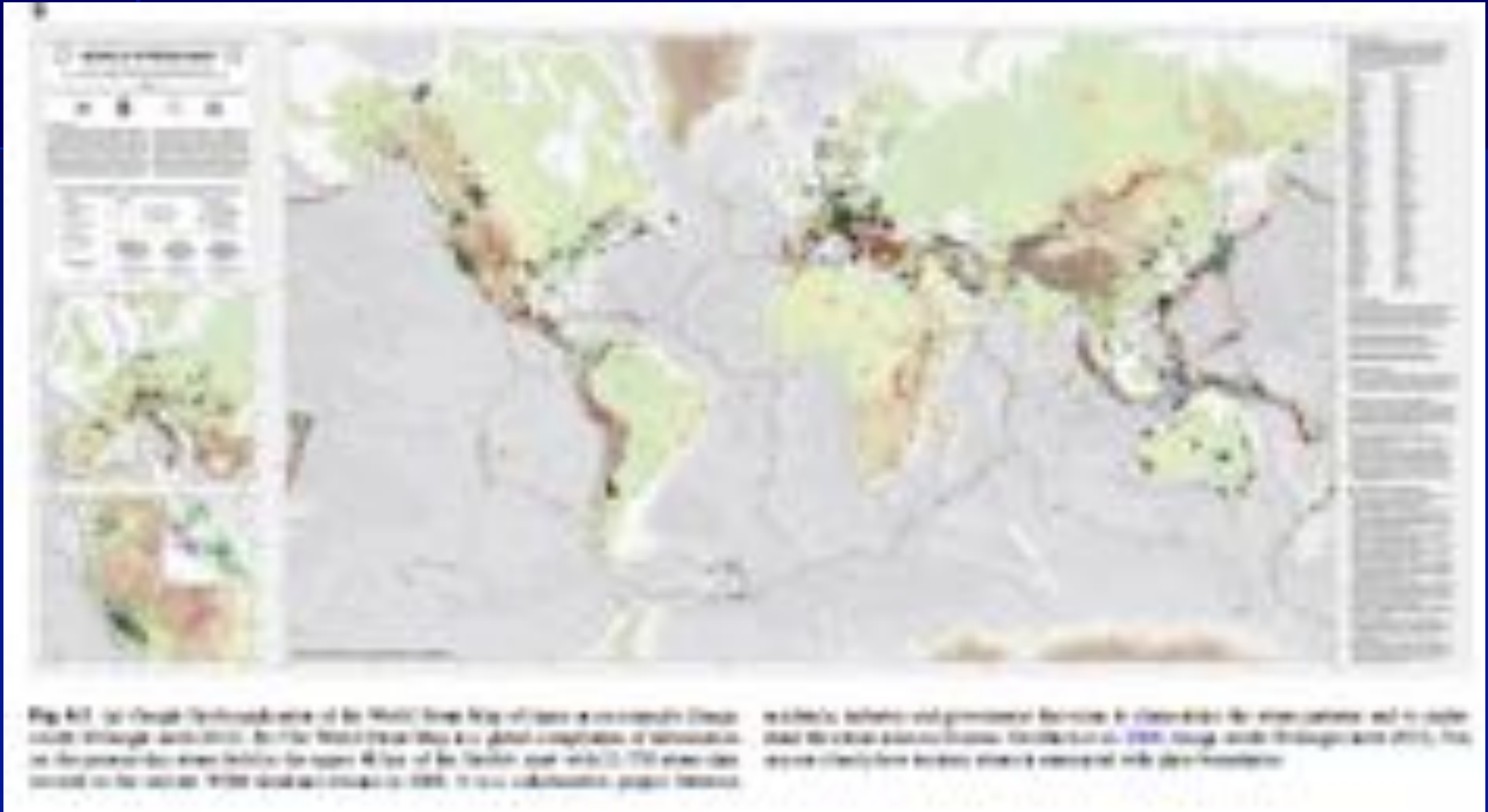


Google earth

构造地貌是由地壳运动直接形成的或受地质构造控制而形成的地貌类型。

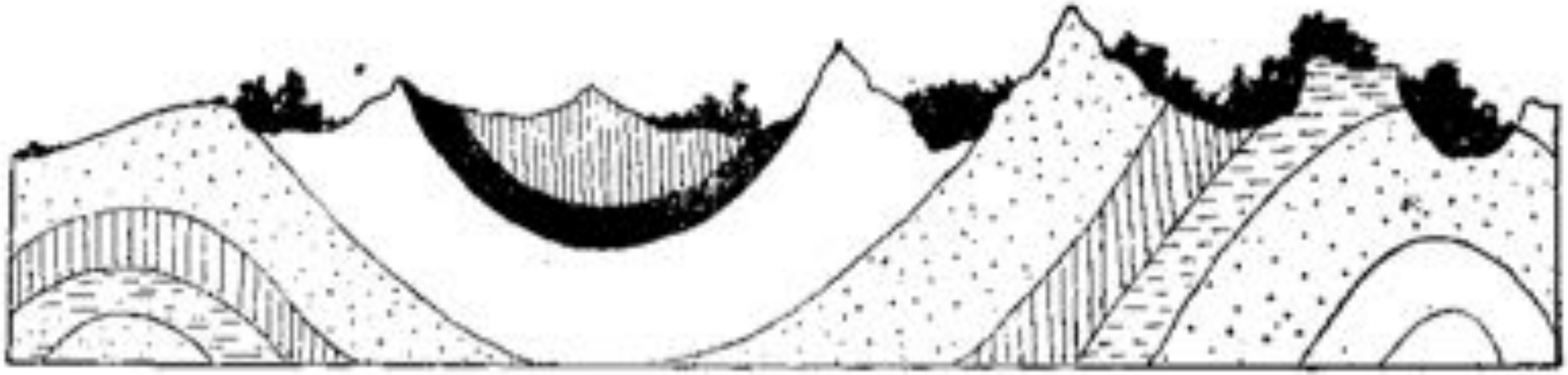

图 6　褶皱山剖面

【逆地形：加拿大落基山脉班夫公园的沛托湖】

- **地形倒置—背斜成谷、向斜成山。**
- **沛托湖**是加拿大艾伯塔省落基山脉班夫**国家公园**的一个冰川湖，可以通过冰原公路直接抵达。沛托湖海拔高度为1880米，湖泊面积为5.3平方公里。
- 名称源于班夫地区早期的一个向导和管理员埃比尼泽·威廉·沛托。**每年夏季，大量冰川岩粉流入湖水中，这些岩石的微粒使湖水呈现出明亮的的翠蓝色。**沛托湖的水来源于沛托溪，出口是米斯塔亚河。


布托湖
Image © 2015 DigitalGlobe
Image Parks Canada

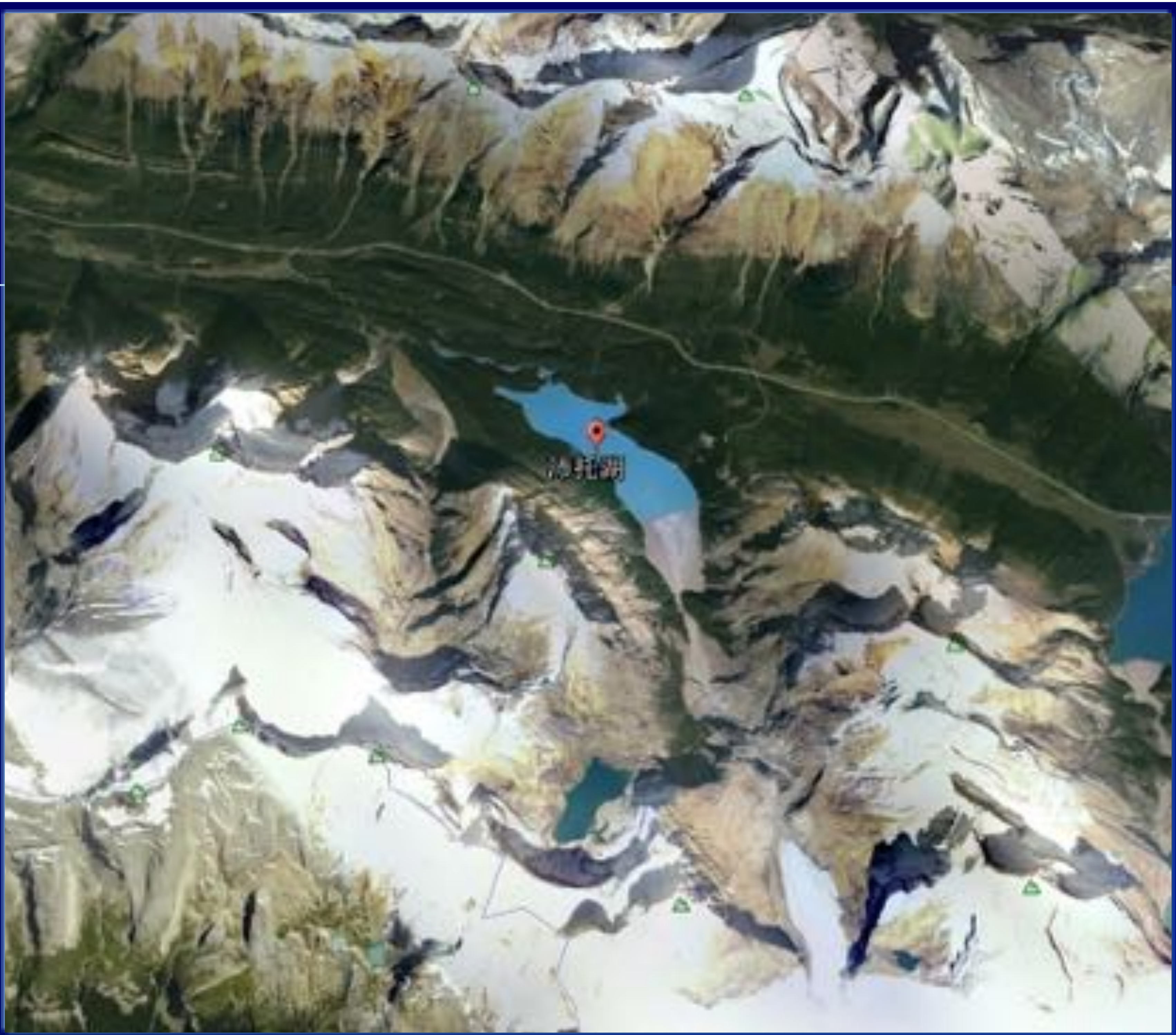


a
Google

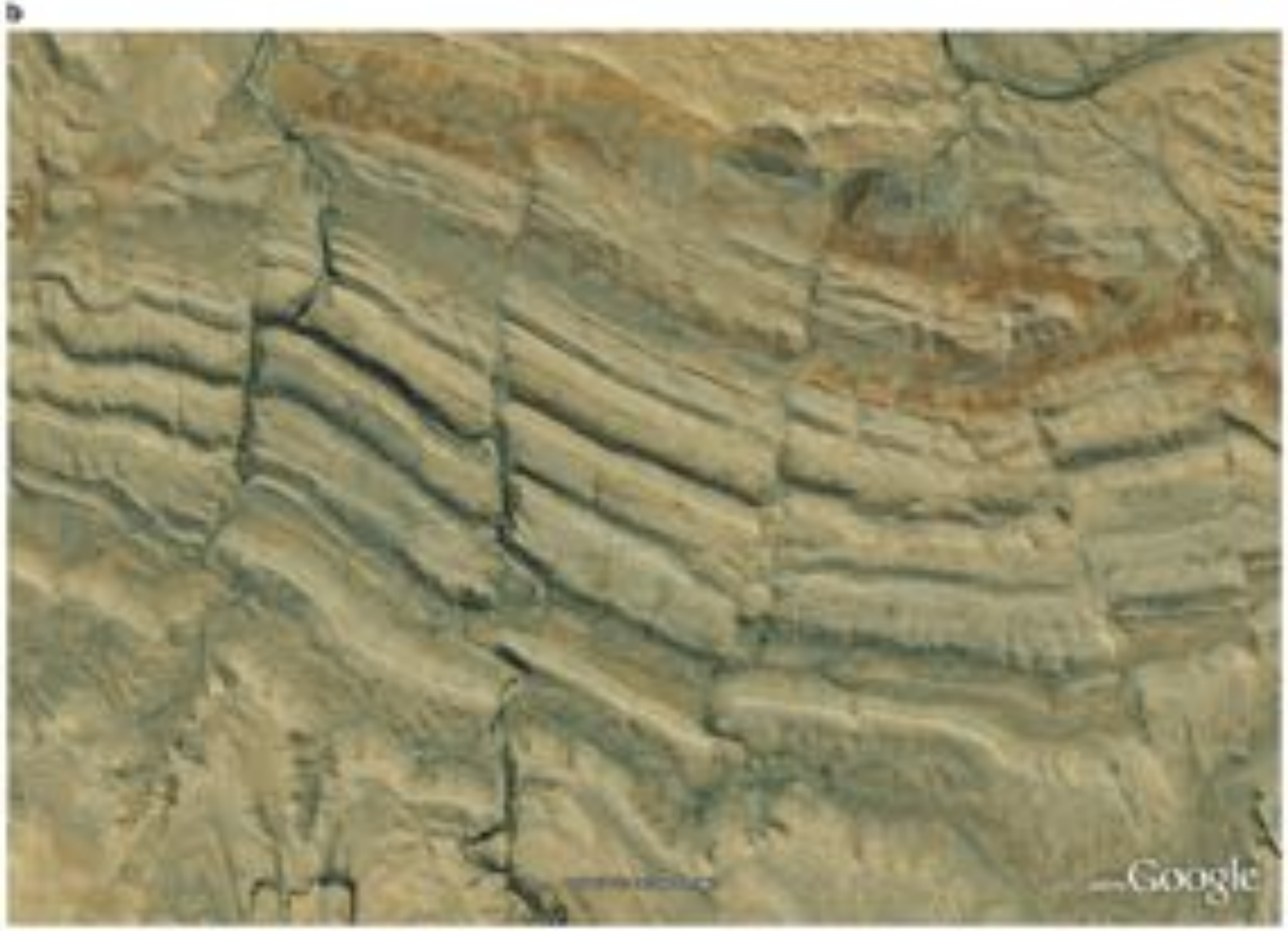
b
Google

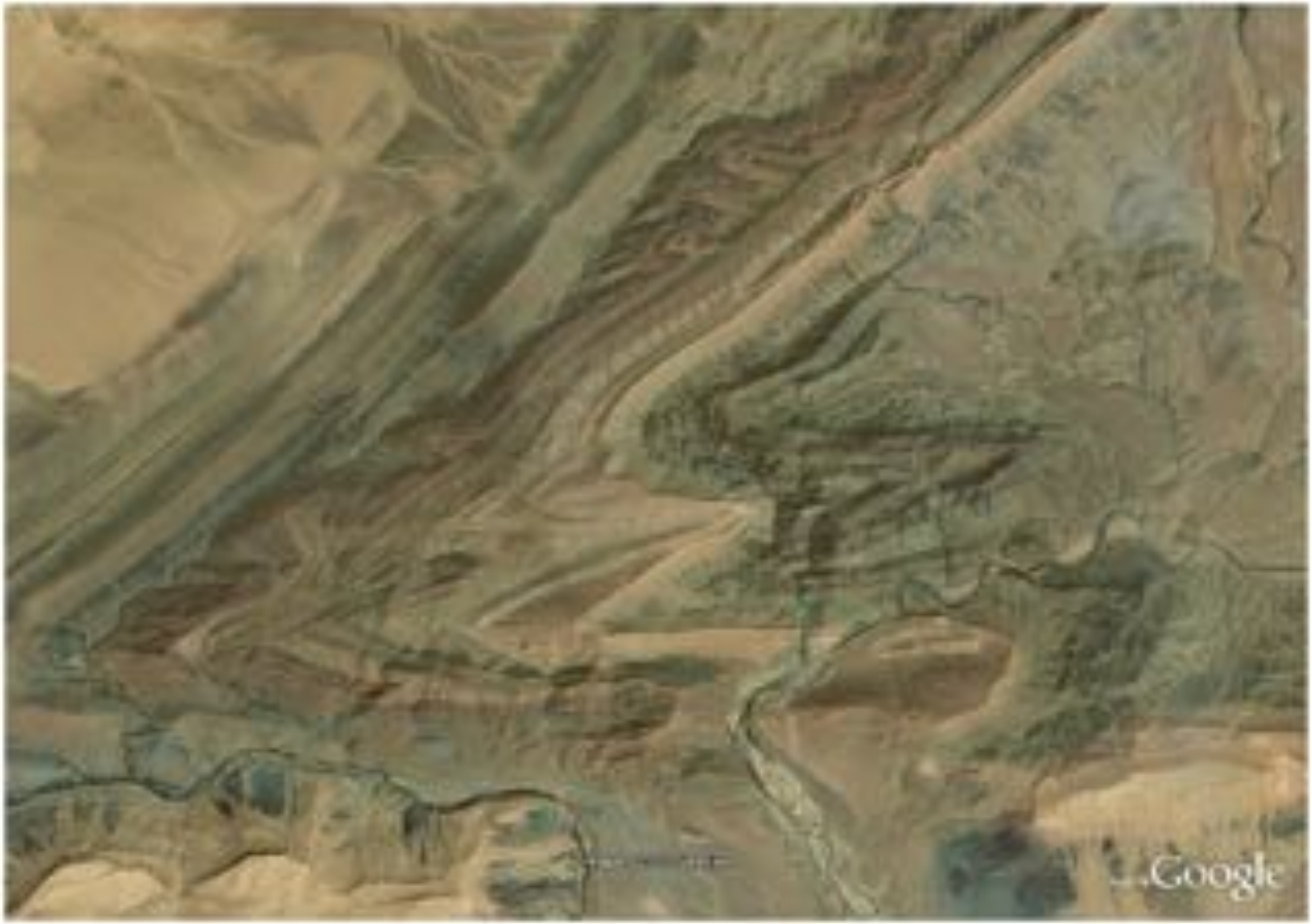
Google

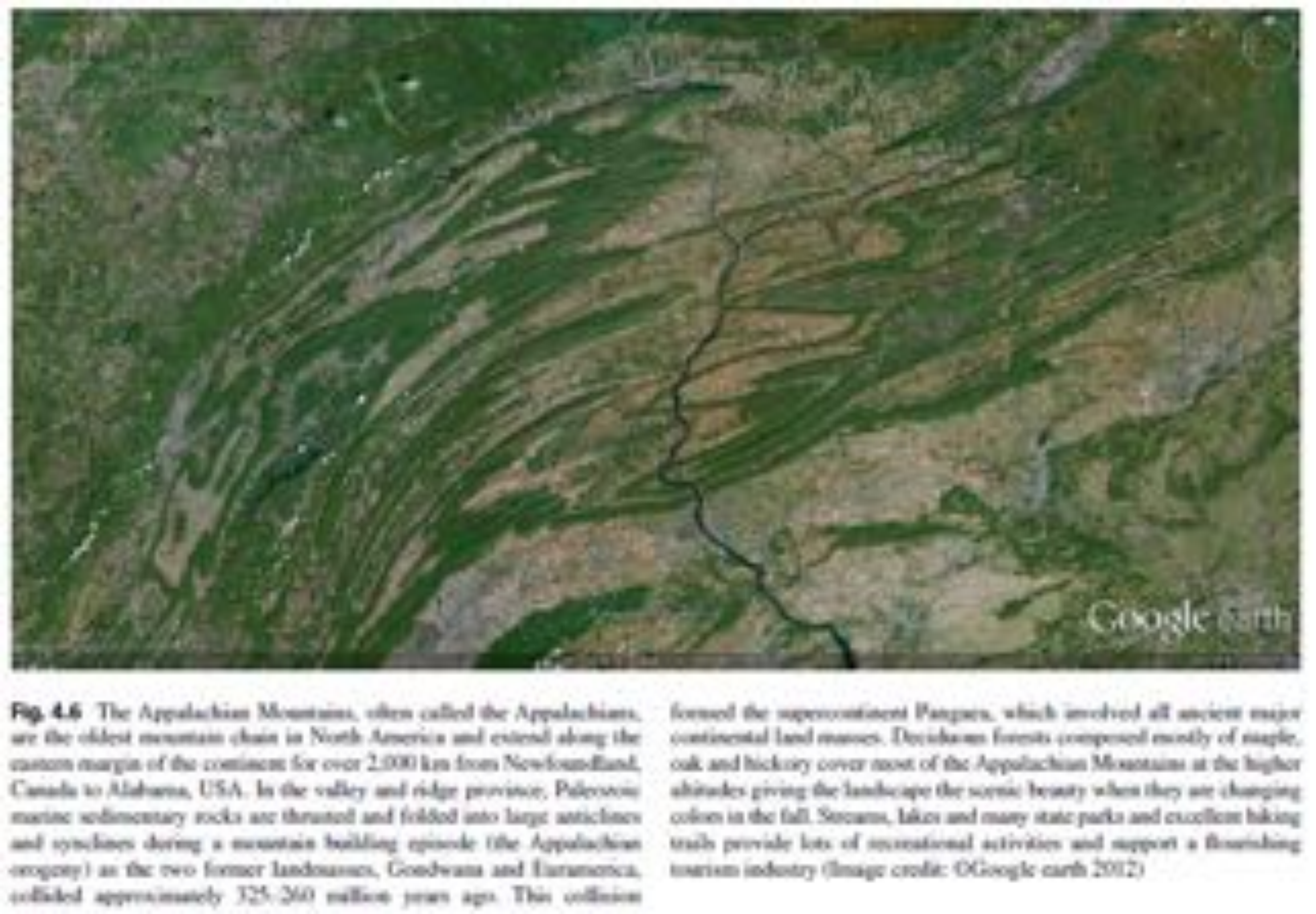

Fig. 4.6 The Appalachian Mountains, often called the Appalachians, are the oldest mountain chain in North America and extend along the eastern margin of the continent for over 2,000 km from Newfoundland, Canada to Alabama, USA. In the valley and ridge province, Paleozoic marine sedimentary rocks are thrusted and folded into large anticlines and synclines during a mountain building episode (the Appalachian orogeny) as the two former landmasses, Gondwana and Euramerica, collided approximately 325–260 million years ago. This collision formed the supercontinent Pangaea, which involved all ancient major continental land masses. Deciduous forests composed mostly of maple, oak and hickory cover most of the Appalachian Mountains at the higher altitudes giving the landscape the scenic beauty when they are changing colors in the fall. Streams, lakes and many state parks and excellent hiking trails provide lots of recreational activities and support a flourishing tourism industry (Image credit: ©Google earth 2012)

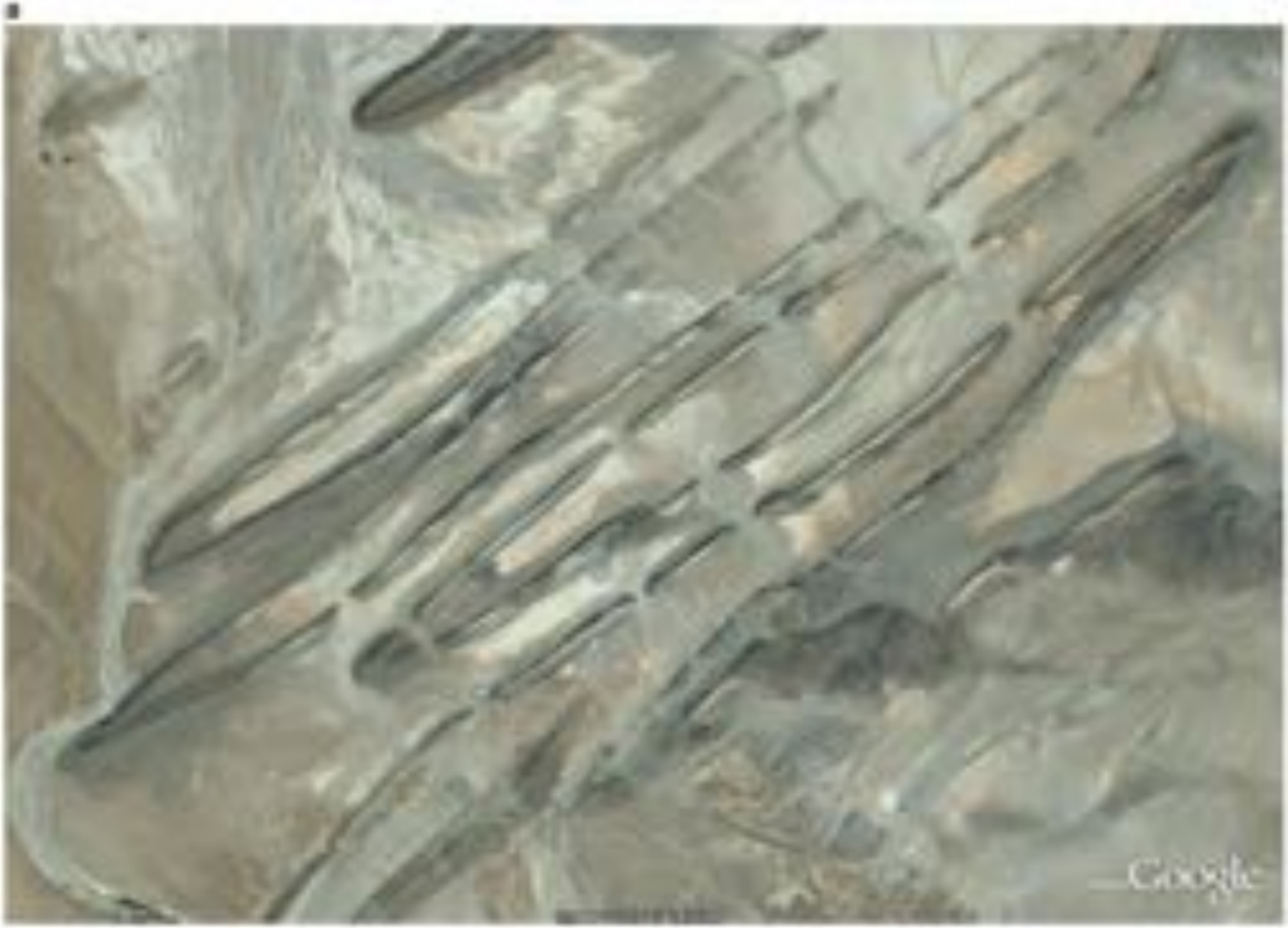

Fig. 4.8 (a, b) Sweeping folding structures north of Morocco's Anti-Atlas. The Anti-Atlas range formed in the Palaeozoic era during the same orogeny as the Appalachians. (a) An enlarged section of (b) (Image credit: ©Google earth 2012)


Google


c
Google

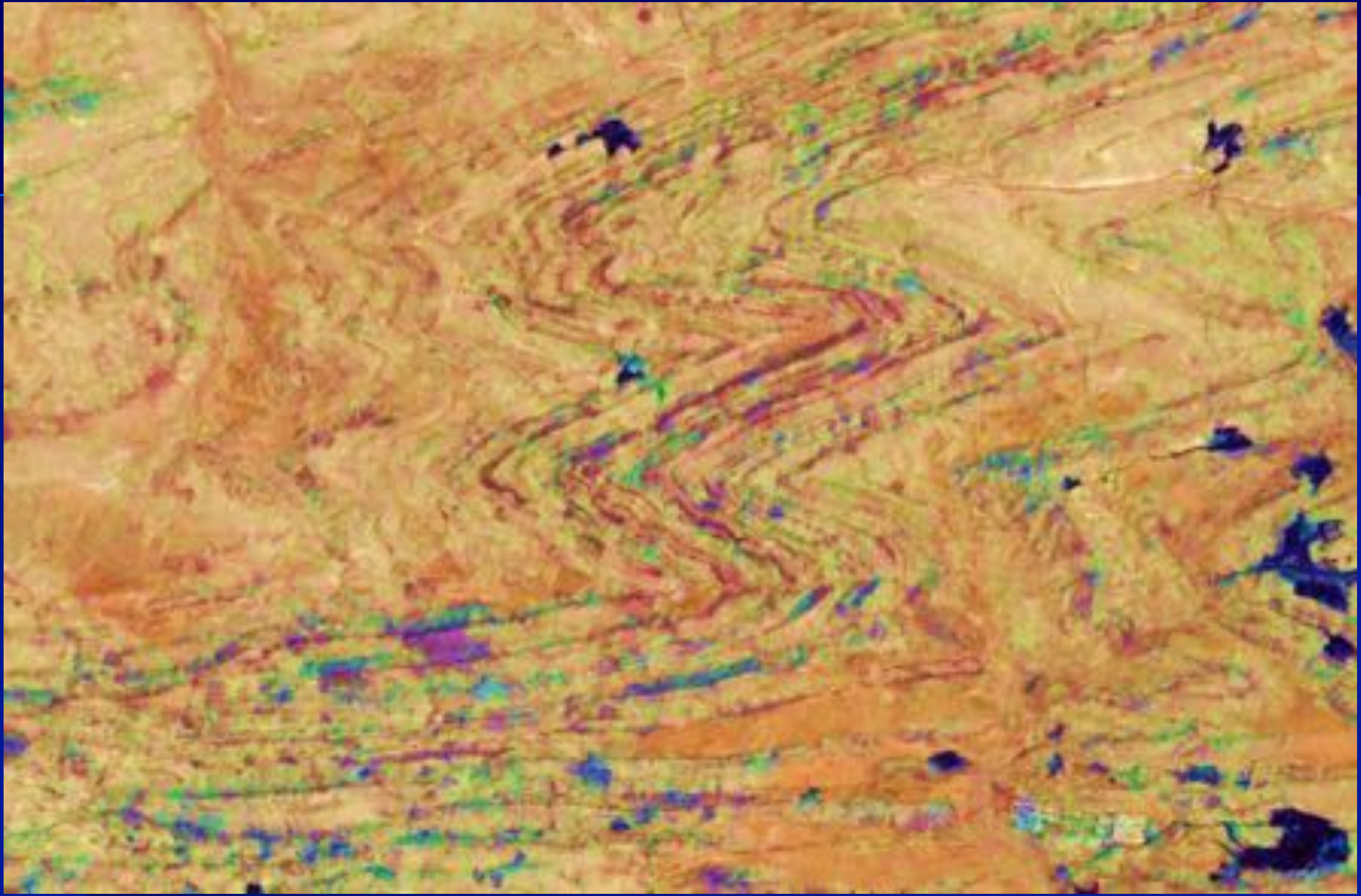

Fig. 4.9 The Finke River in central Australia crosses an anticline structure of 45 km width at *24°09'S* and *132°52'E*. Rock strata abruptly dip towards the north and south, and the anticline hinge plunges towards the west in its western part: the character of an anticline with the oldest strata in the center is evident. The valley of the Finke River is an incredibly old river system that follows exactly the same course for the past 15–20 million years and generally flowed along the same path for 100 million years. It has existed before the anticline structure was exhumed by uplifting and denudation, but the river kept its course and incised this valley in pace with the uplift. This keeping pace is called "antecedence" because the river is older than the structure it is cutting. Aboriginal mythology believes that the Finke River was formed when the Rainbow Serpent thrust north from Lake Eyre (Image credit: ©Google earth 2012)


b

Fig. 4.13 The famous synclinal structure of Wilpena Pound, Flinders Ranges (South Australia) forms an almost closed basin. Mountain ranges surrounding the remnant valley have been eroded away during the last several million years. The higher walls of Wilpena Pound are composed of quartzite, a metamorphic rock converted from sandstone by elevated temperature and pressure, which is very resistant to weathering (Image credit: ©Google earth 2012)

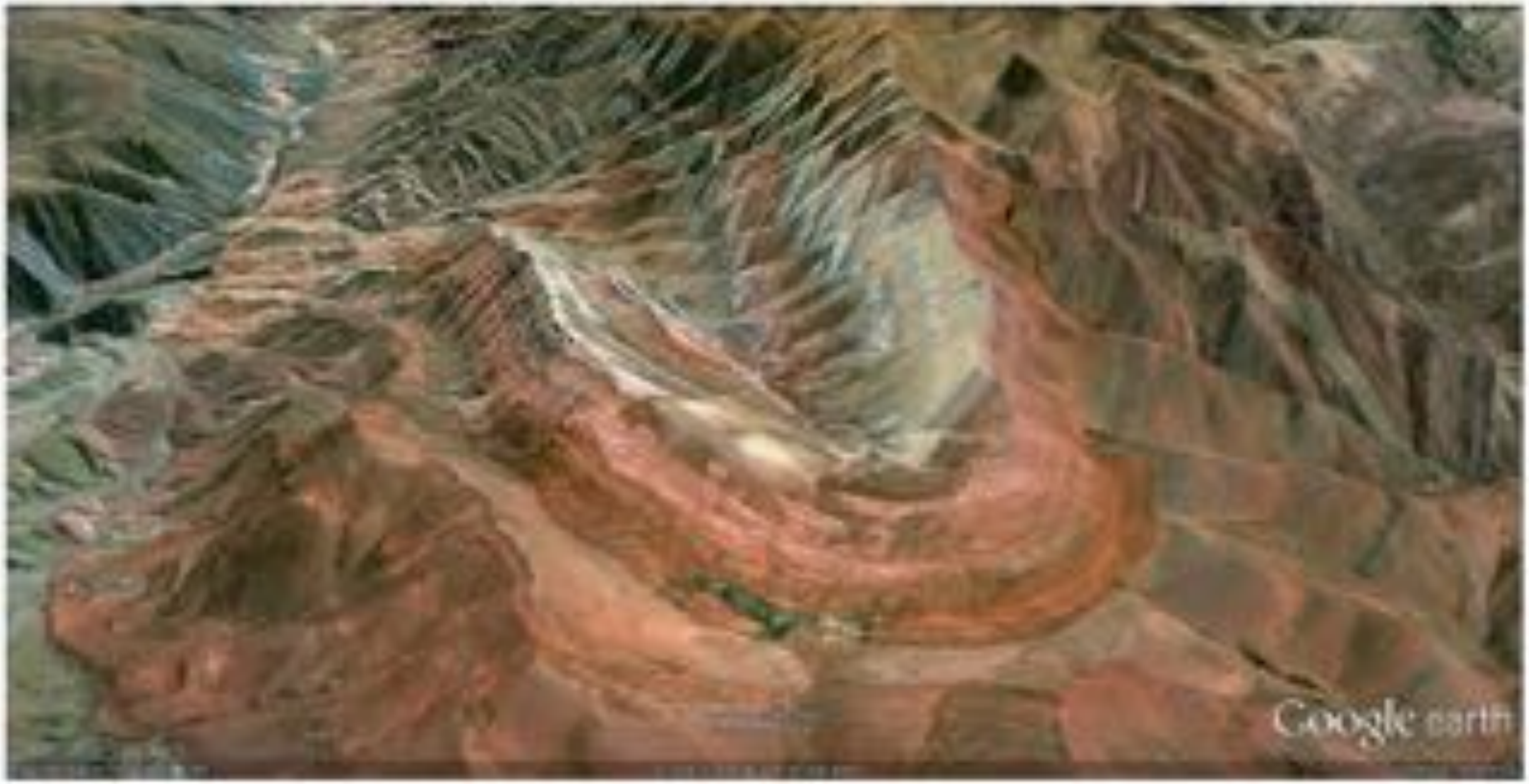

Fig. 4.14 A beautiful syncline in the Andes Mountains of northwest Argentina, exposing Jurassic rock formations. Large-scale erosion accompanying the uplift during the Andean orogeny has removed the adjacent (anticline) parts of these rock formations, but the trough-like syncline persisted. Picture-perfect cuestas have developed towards the center of the structure, where inclined layers of sedimentary rocks of different colors are incised by draining channels (Image credit: ©Google earth 2012)

Fig. 4.10 Complex deformation patterns in the vast and spectacular sedimentary rocks of the MacDonnell Ranges near Alice Springs in central Australia. Folds are disturbed by faulting, as a result of crustal compression. Viewed from above, they speak eloquently of the caterpillar dreaming that is at the heart of local Aboriginal mythology of the Arrernte people, the traditional custodians of this area of Australia. For them, this is where ancestral creation beings – including caterpillars and wild dogs – travelled the land, naming and shaping prominent elements in the vast landscape. The scene is about 50 km wide centred at about 24°22'S and 132°07'E (Image credit: ©Google earth 2012)

Fig. 4.11 Overview of the detailed pictures shown in Figs. 4.9 and 4.10. The compressional folding structures are easy to follow in this image, 112 km wide and centered near 24°12'S and 132°43'E. The Gosse's Bluff impact crater (see Chap. 5) is visible in the northern par of the image (Image credit: ©Google earth 2012)

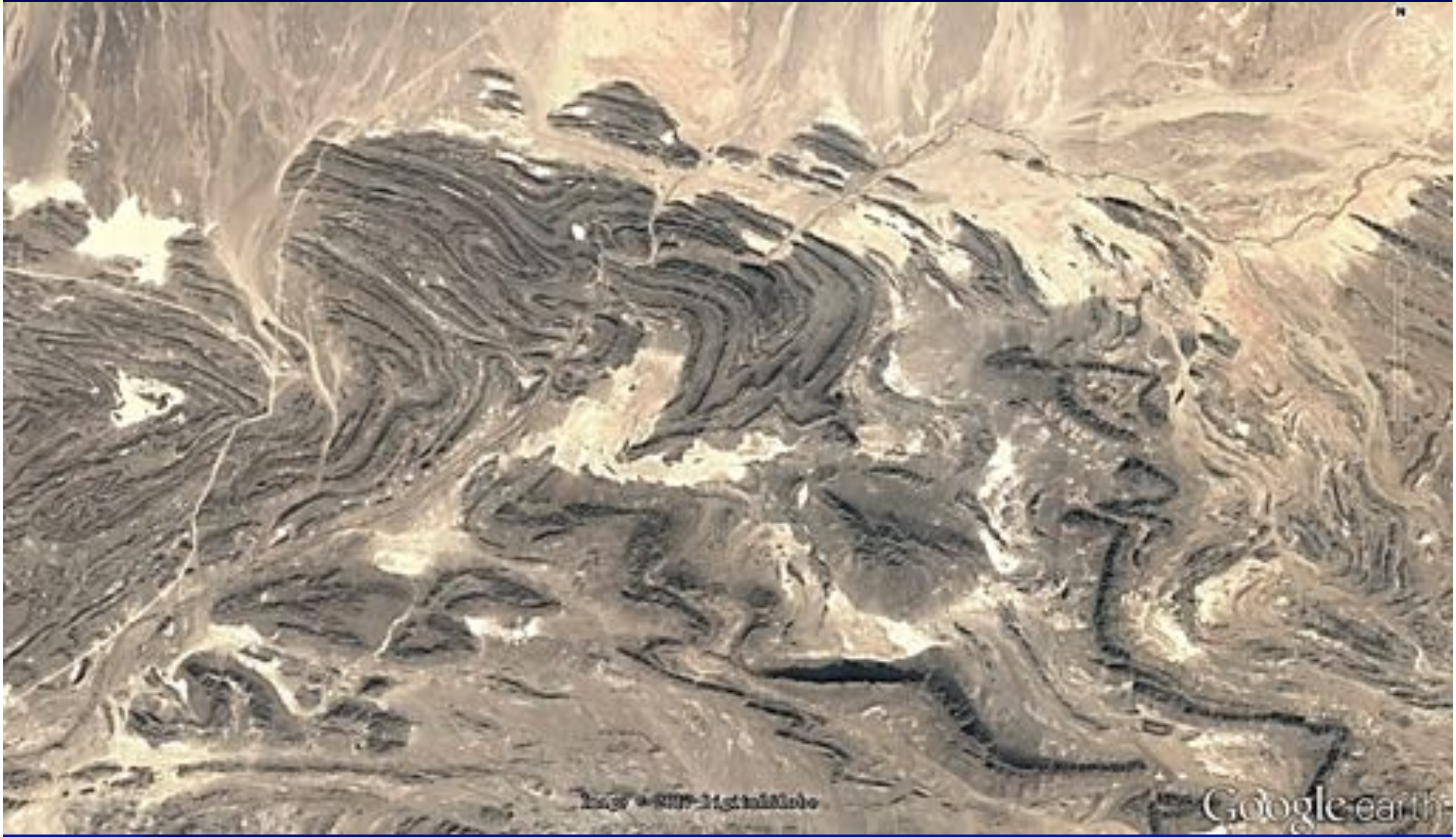
Image © [illegible] DigitalGlobe
Google earth

Fig. 4.15 If the inclination of rock layers is significant (here with about 8° to the south in southern Morocco), the cuestas show a differentiated dissection by infrequent, but severe rainfalls (28°39'N, 9°44'W, 38 km wide) (Image credit: ©Google earth 2012)


Google


a
b


Image Landsat / Copernicus
Google earth

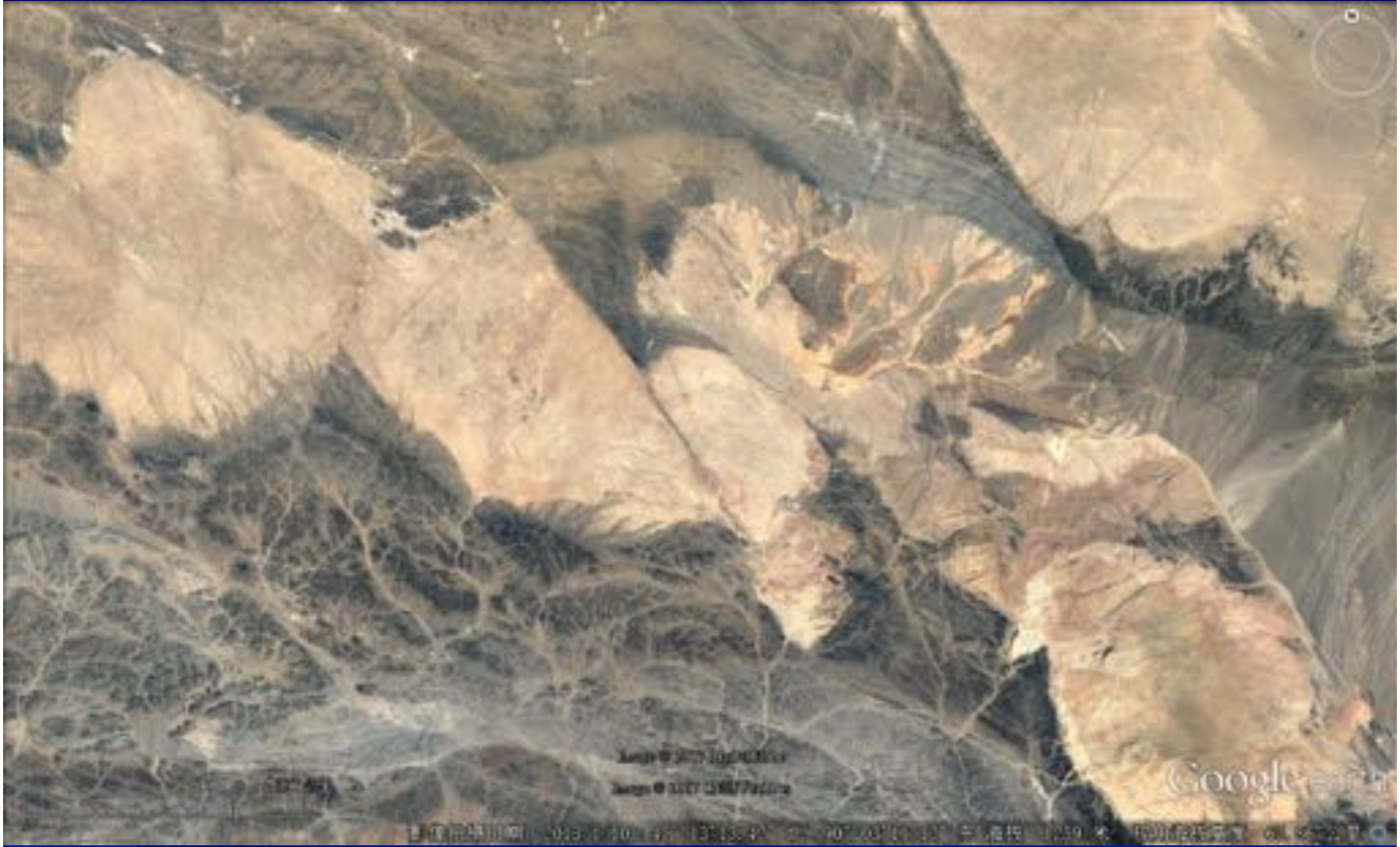
Google earth

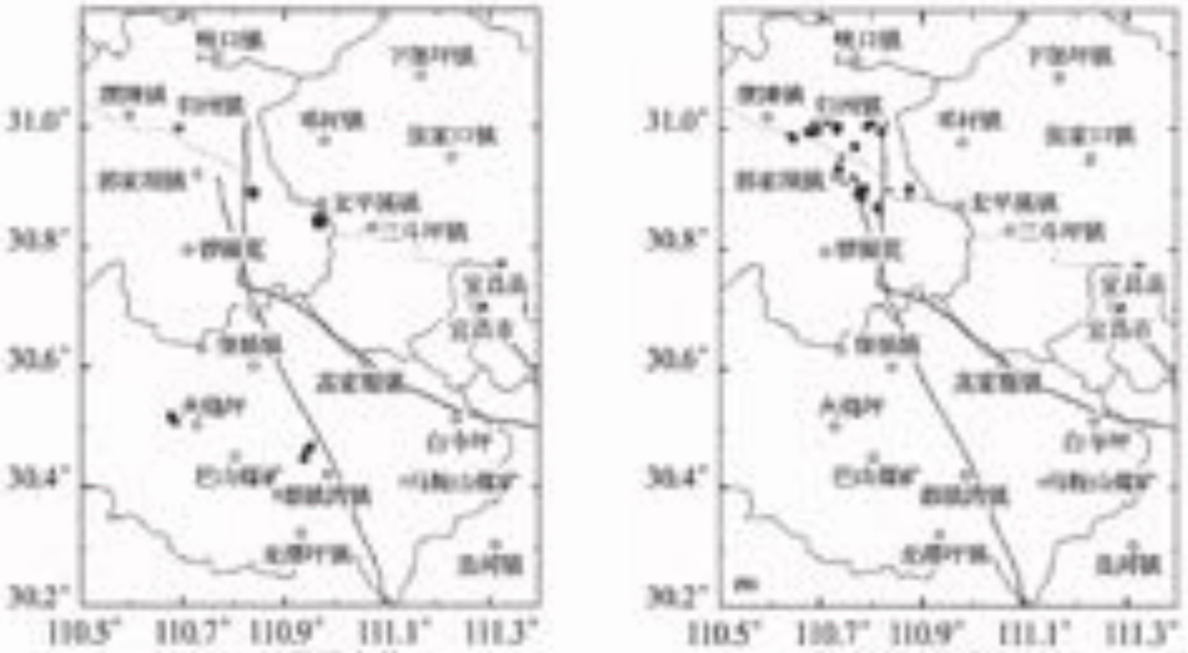

(a) 2003-06月蓄水前

(b) 2003-06~2006-09

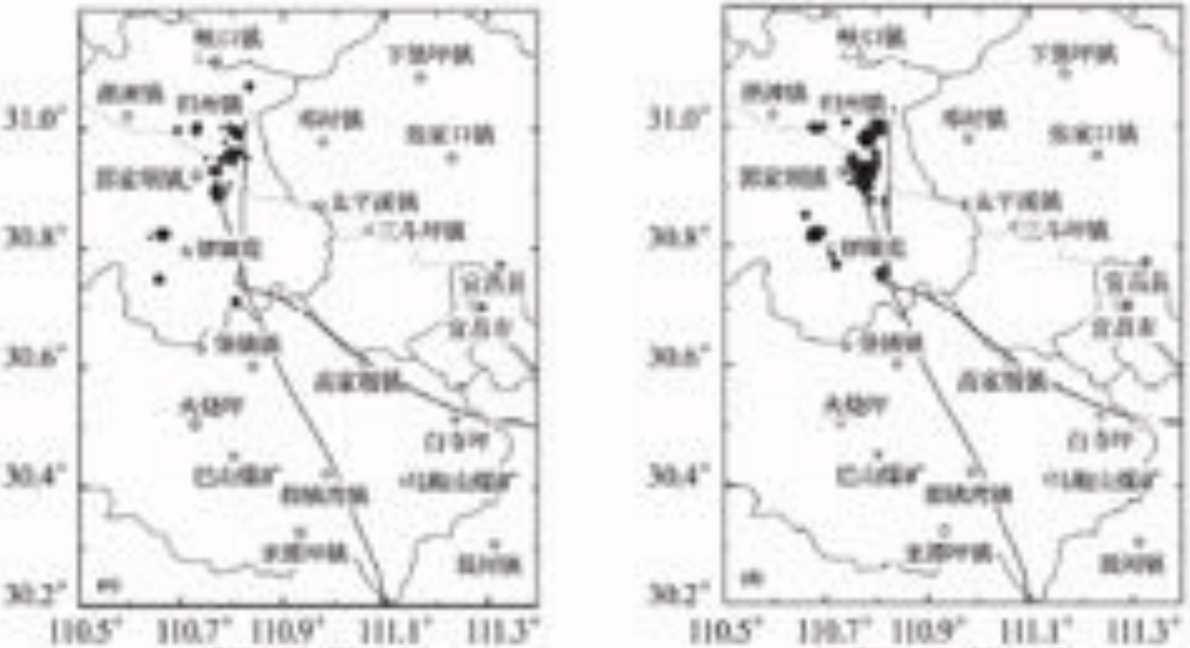

(c) 2006-09~2008-09

(d) 2008-09~2011-12


Google earth

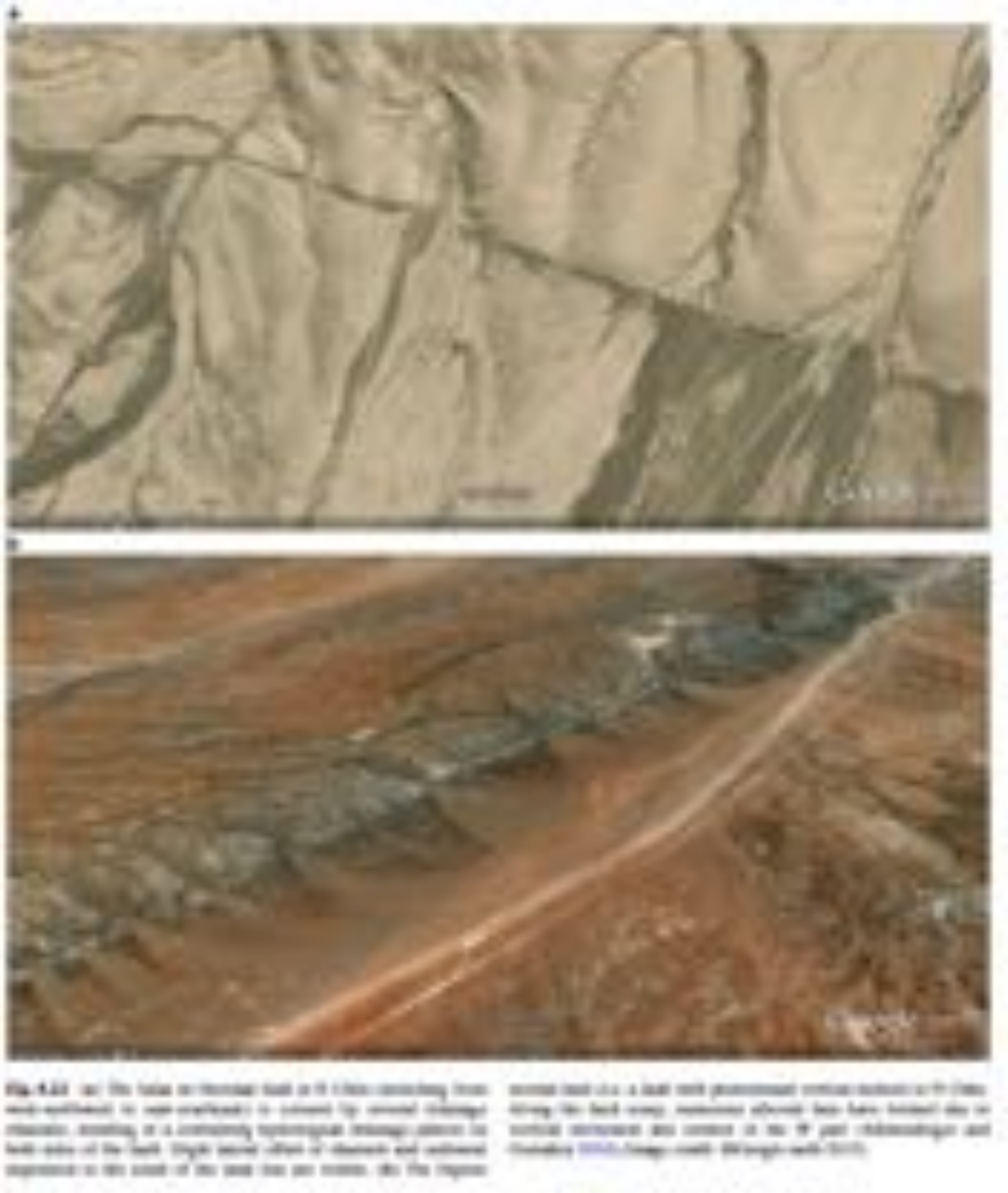

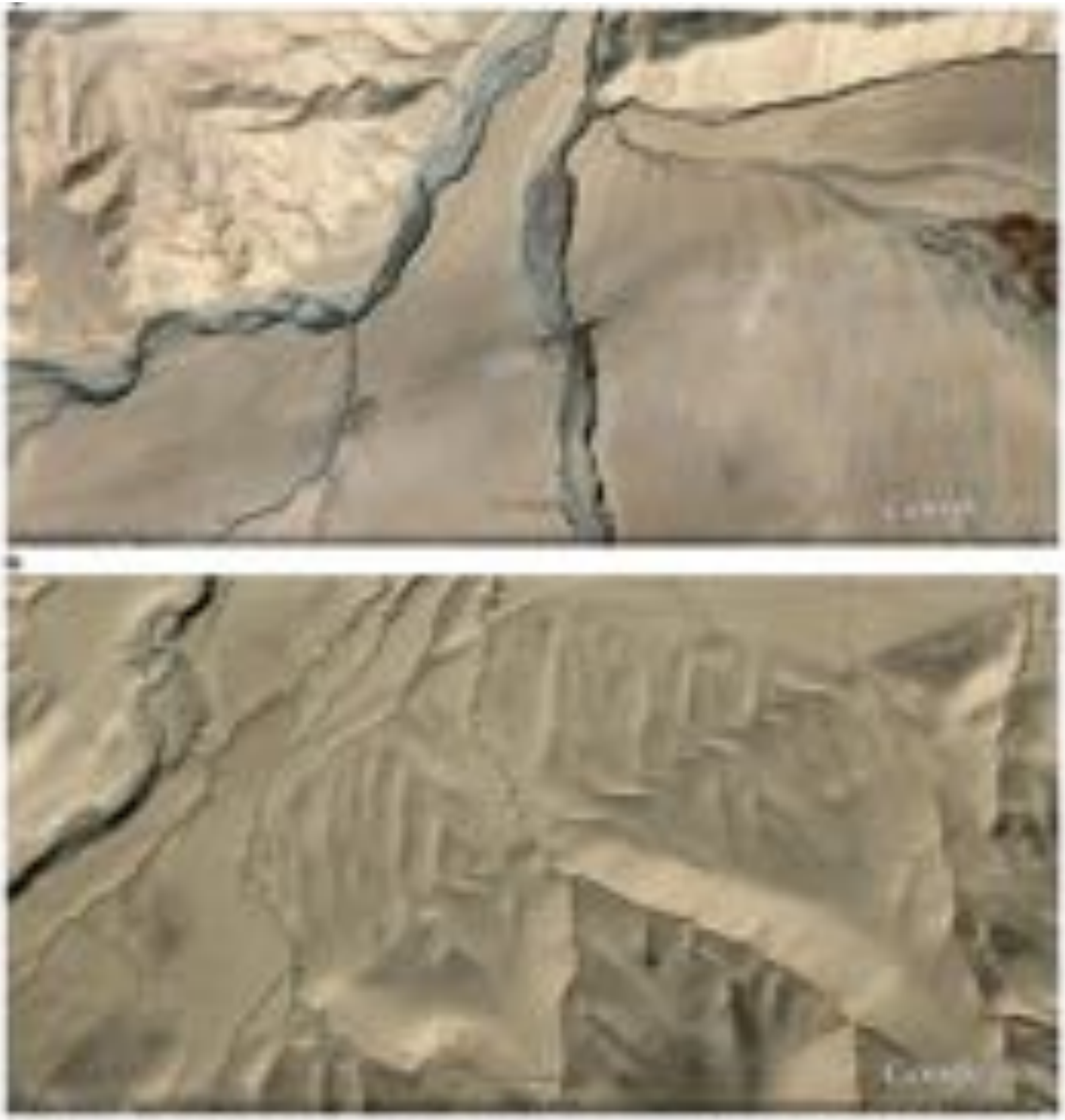
Google
Google


Google earth

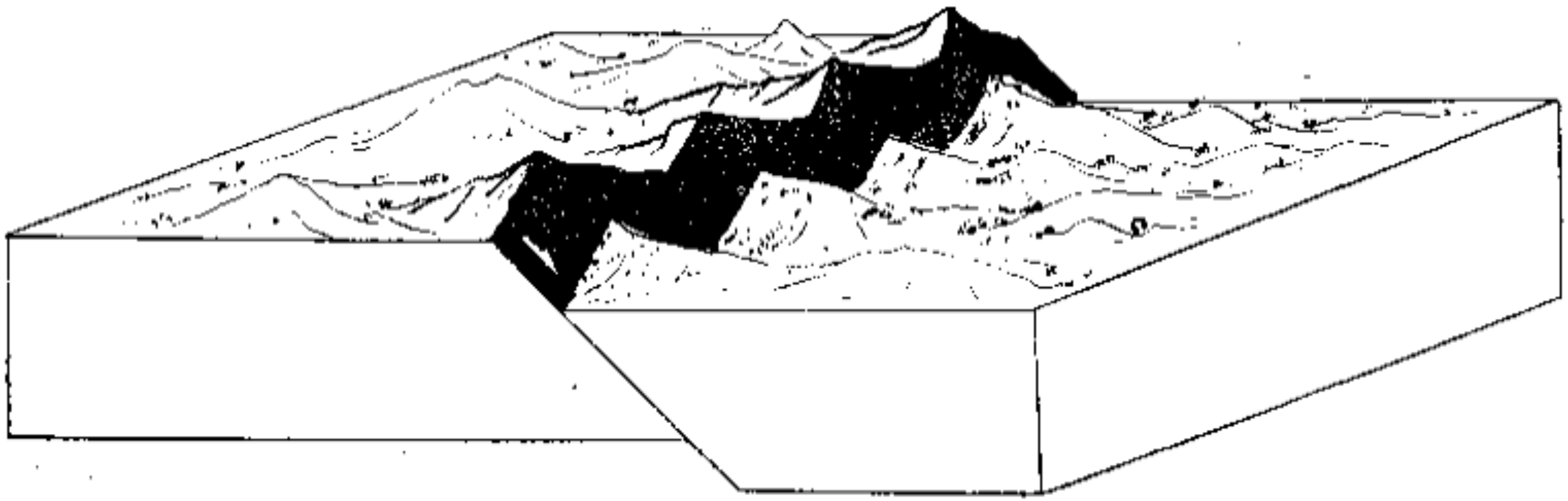

图 9　正断层形成的地貌示意图


Google earth

Fig. 4.24 A joint pattern in a limestone landscape in southern Andalusia, Spain, at *36°57′N, 4°33′W*. Scene is 3.7 km wide (Image credit: ©Google earth 2012)

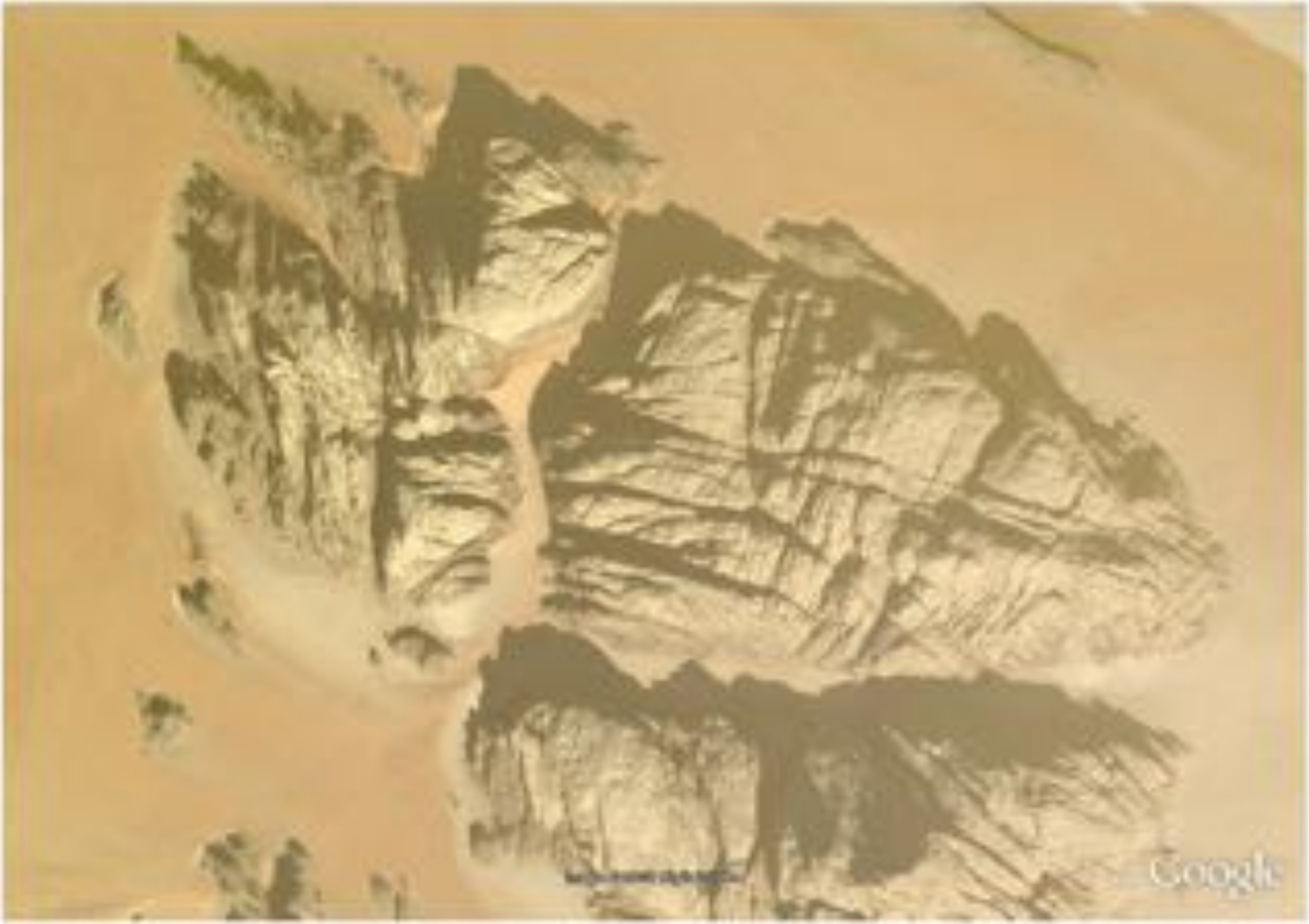

Fig. 4.26 The rock formation in southern Jordan *(29°37′1.29″N, 35°29′34.34″E)* has been deeply incised by erosion along the main joints – more and more small jointing patterns are exposed by ongoing weathering and subsequent erosion during infrequent but heavy rains (6 km wide scene) (Image credit: ©Google earth 2012)

a

Fig. 4.28 (a) Intensely weathered joints in very old rocks (about 2 billion years) in northwest Australia at *12°50'S, 133°21'E* (10 km wide section). There is a "hierarchy" of dominant primary and secondary joint patterns, which likely is either the result of different tectonic stress or just an expression of time of exposure to weathering processes to explore even the tiniest weak fractures in the rock. (b) Detail of the landscape in Fig. 4.8a, 5 km wide (Image credit: ©Google earth 2012)

Fig. 4.31 (a, b) The Arches National Park in Utah, USA, exhibits fine examples of jointing caused by an anticline uplift of a salt dome which has stretched and pulled apart the overlying rock strata (38°47'N, 109°35'W; about 4.5 km wide scene). (c) Detailed image showing secondary joints cross-cutting the dominant joints. Width of this image is just 2 km (Image credit: ©Google earth 2012)

Fig. 4.34 Upheaval Dome is a salt intrusion with a cap of gypsum pushing up the top sandstone layers in Canyonlands National Park, Utah, USA, at *38°26′N* and *109°55′W*. The round structure has a diameter of about 3.2 km. In earlier days, the feature was interpreted to be of volcanic origin or as an impact crater (Image credit: ©Google earth 2012)

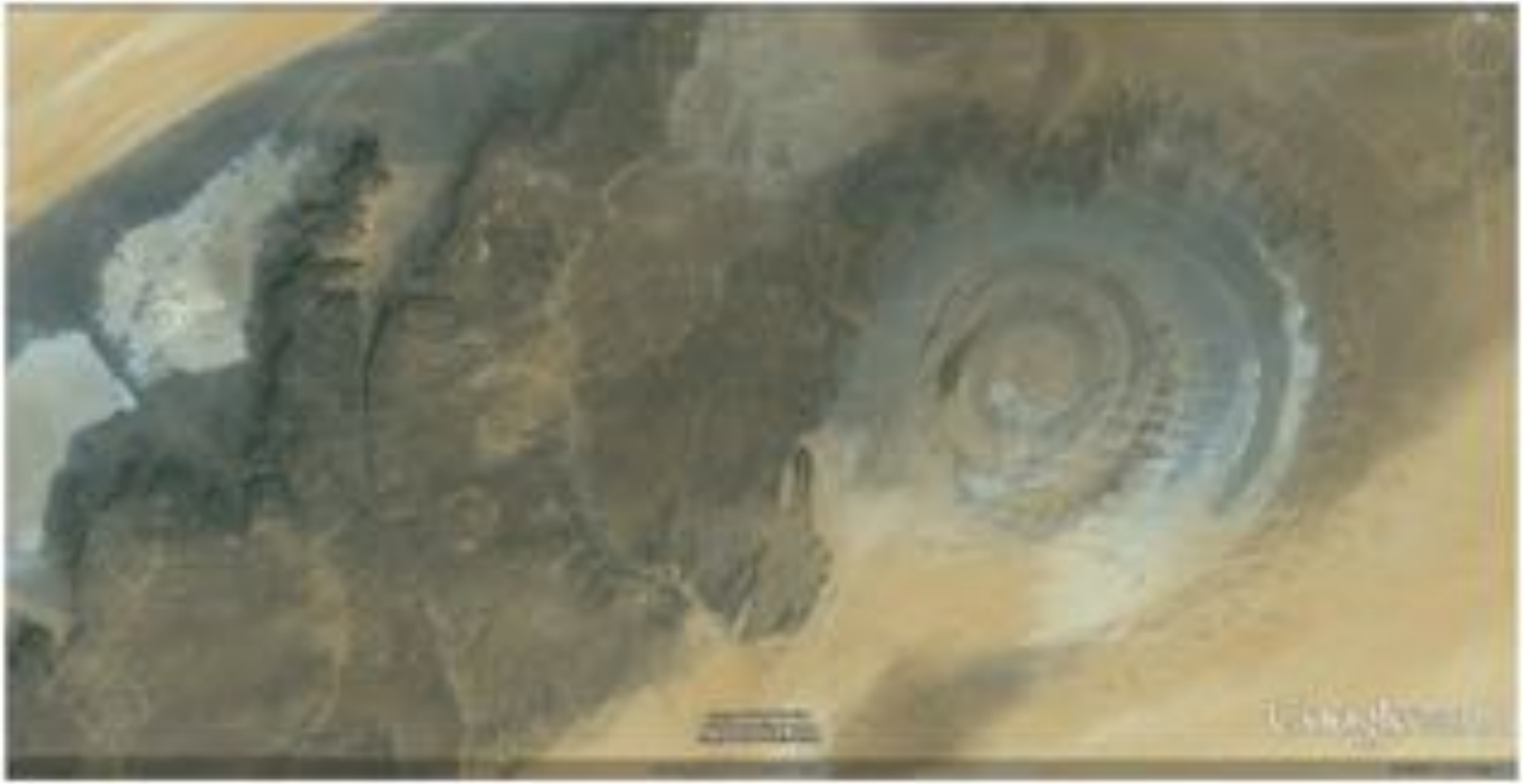

Fig. 4.35 The famous Richat Structure. This prominent circular feature in the Sahara Desert of Mauritania (northwest Africa) has attracted much attention since the earliest space missions because it forms a conspicuous bull's-eye that has become a landmark for shuttle crews in the otherwise rather featureless expanse of the desert. Initially interpreted as a meteorite impact structure because of its high degree of circularity, it is now thought to be merely a symmetrical uplift that has been sculptured bare by erosion. Palaeozoic quartzites form the resistant beds outlining the structure (Image credit: ©Google earth 2012)

Fig. 4.38 (a, b) In central Patagonia (Argentina) at *37°51'S* and *69°44'W*, layers of rock strata in a mudstone/siltstone sequence can be distinguished by their changing colors (Image credit: ©Google earth 2012)

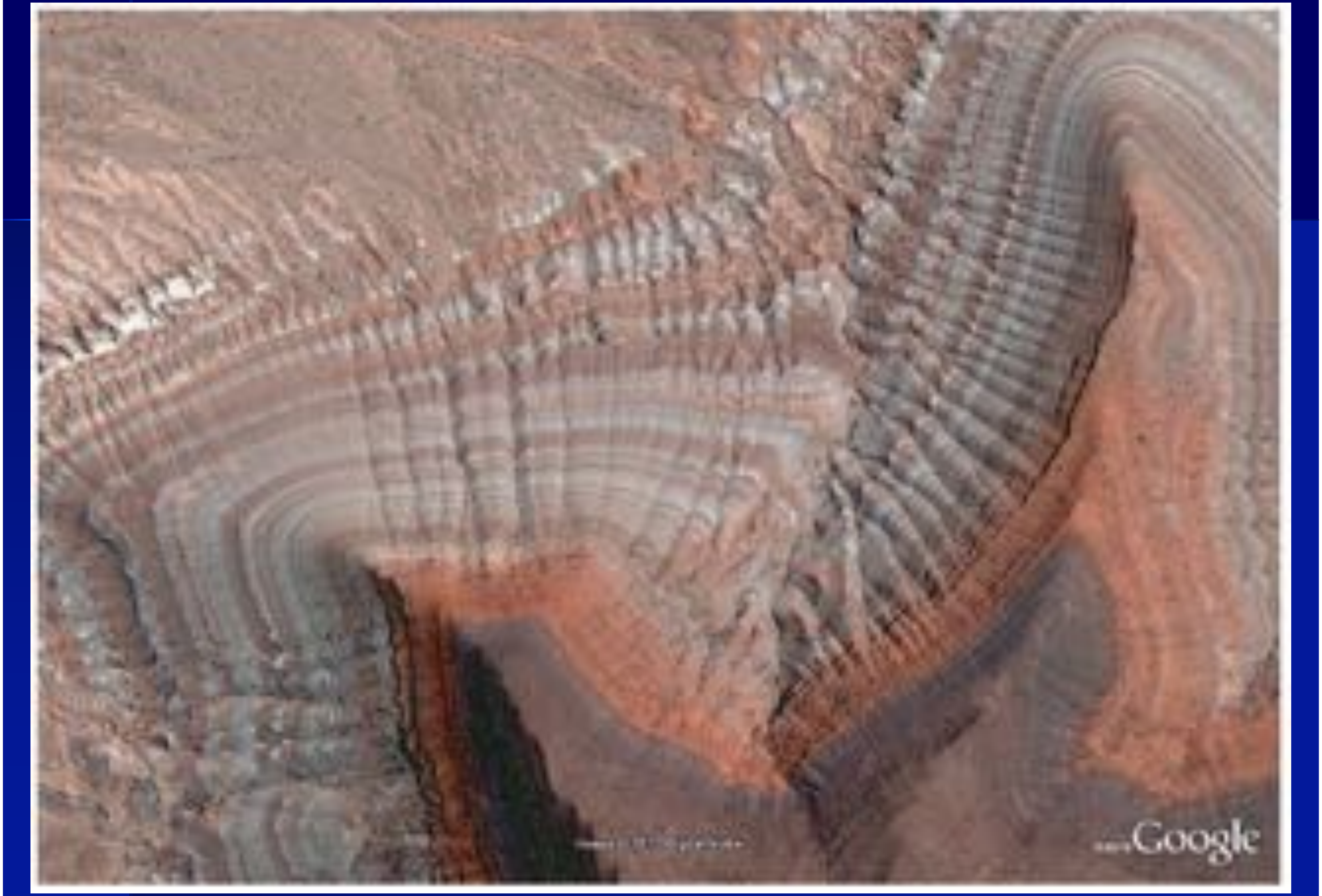
Google

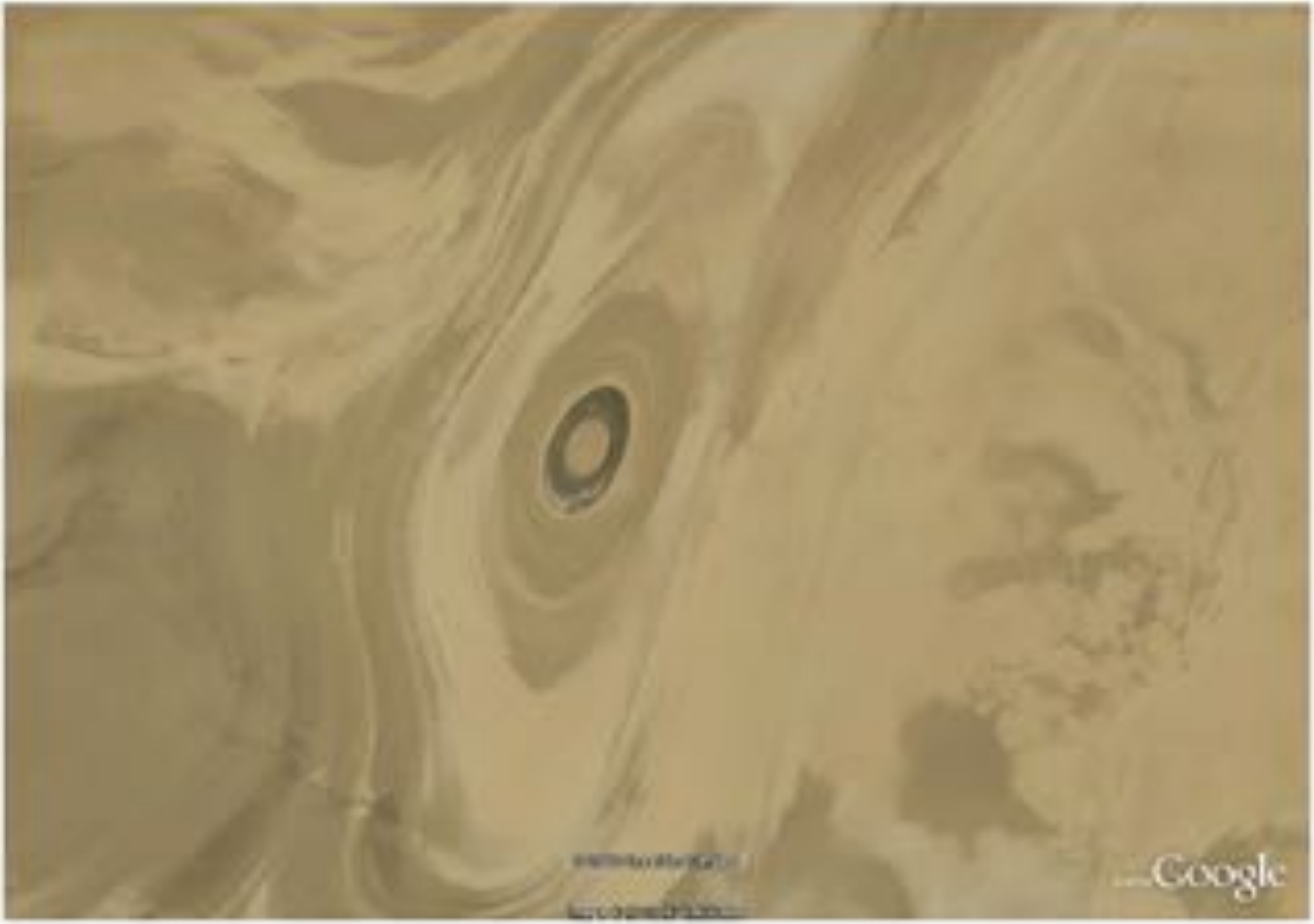

Fig. 4.39 In northern Iran, wind erosion expose different mudstone and sandstone sequences in ancient basins (related to salt tectonics) at about *34°42′N* and *53°11′E*. Width of scene is 12 km (Image credit: ©Google earth 2012)

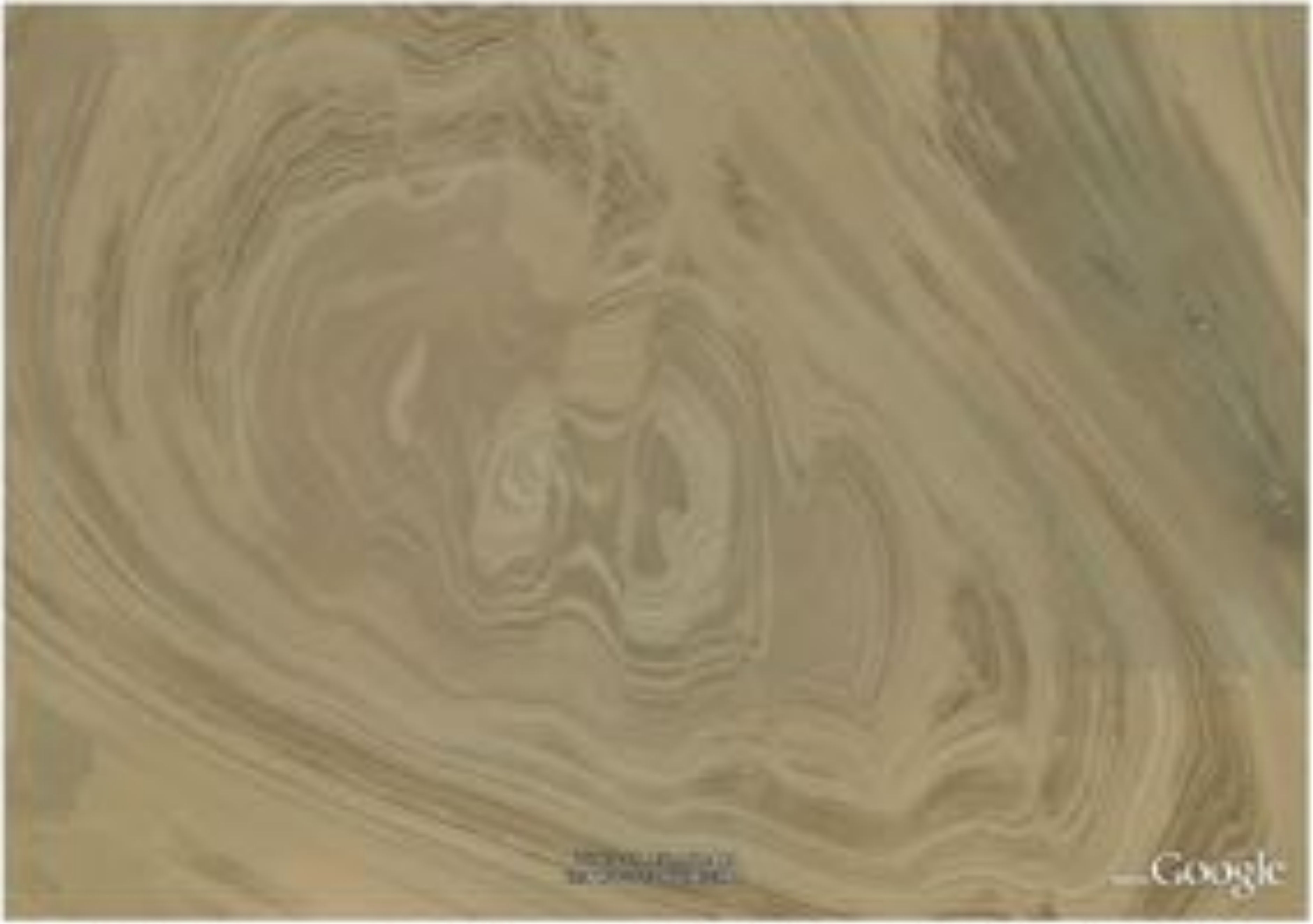

Fig. 4.40 (a, b) Deformation of exposed silt and clay layers in northern Iran at 34°38'N and 54°02'E and 34°51'N and 53°47'E. Width of scene is approximately 6 km (Image credit: ©Google earth 2012)


Google

外力作用

撞击坑

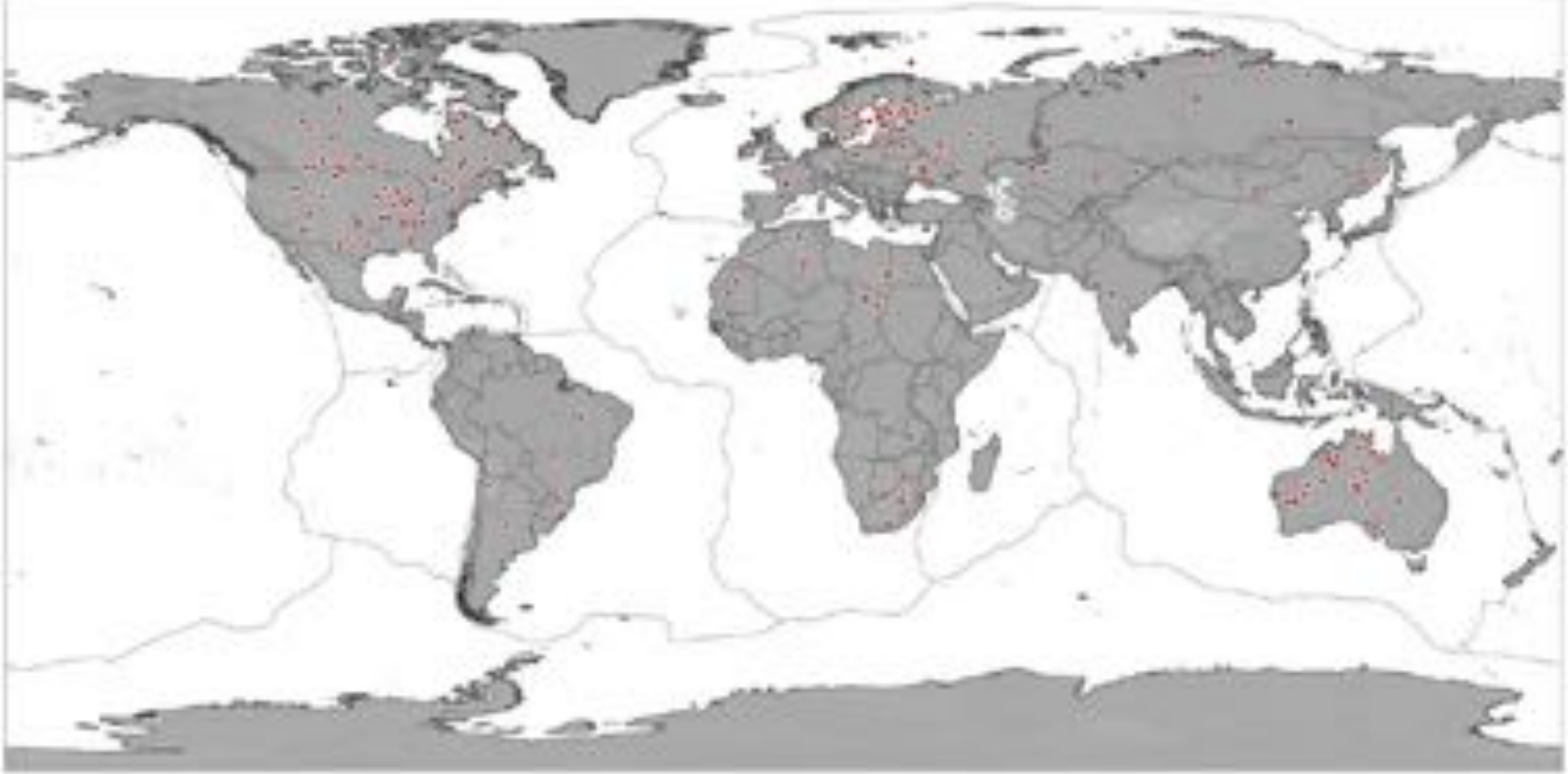

Fig. 5.1 Confirmed impact craters on the continental landmasses of the Earth based on the Earth Impact Database (URL: http://www.passc.net/EarthImpactDatabase/)

Fig. 5.2 The Meteor or Barringer Crater in northern Arizona (USA) is the best preserved crater on Earth with a diameter of 1.2 km and a depth of 170 m. It has been formed about 49,000 years ago when an iron-nickel meteorite with a diameter of approximately 50 m and a weight of 300,000 tons travelling at 11 km/s struck the ground. During the explosion (believed to be equal to about 10 megatons of TNT) the sandstone and limestone rock formations were bent upwards to form the outer ring. Impacts of this size statistically occur on Earth every 1,000 years (Image credit: ©Google earth 2012)

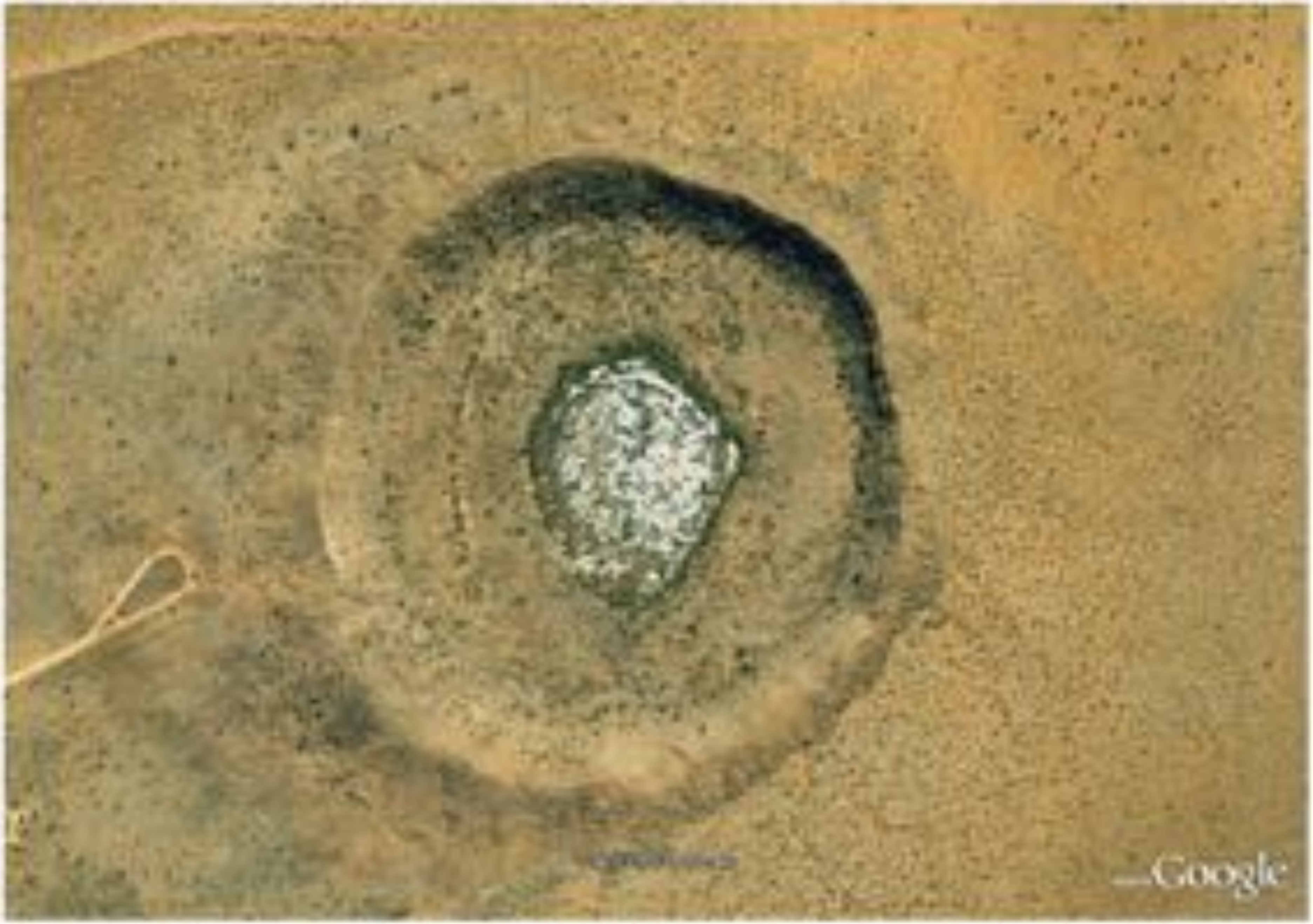

Fig. 5.3 Wolfe Creek Crater in Western Australia at about 19°10′S and 127°47′E. Diameter is 875 m with a depth of 60 m. The impactor is estimated to have had a weight of 50,000 tons of iron and nickel striking the ground at about 15 km/s. The age of the crater has been determined to be around 300,000 years (Image credit: ©Google earth 2012)

Fig. 5.4 Roter Kamm crater in Namibia at 27°45′S and 16°17′E with a diameter of 2.5 km, depth of 130 m and an age of 3.7 million years. It exhibits a perfect round form in very old gneiss but has been filled by shifting sand in the desert environment and will possibly be covered in the near future. Melt breccias found in the rim are strong evidence for an extraterrestrial impact (Image credit: ©Google earth 2012)

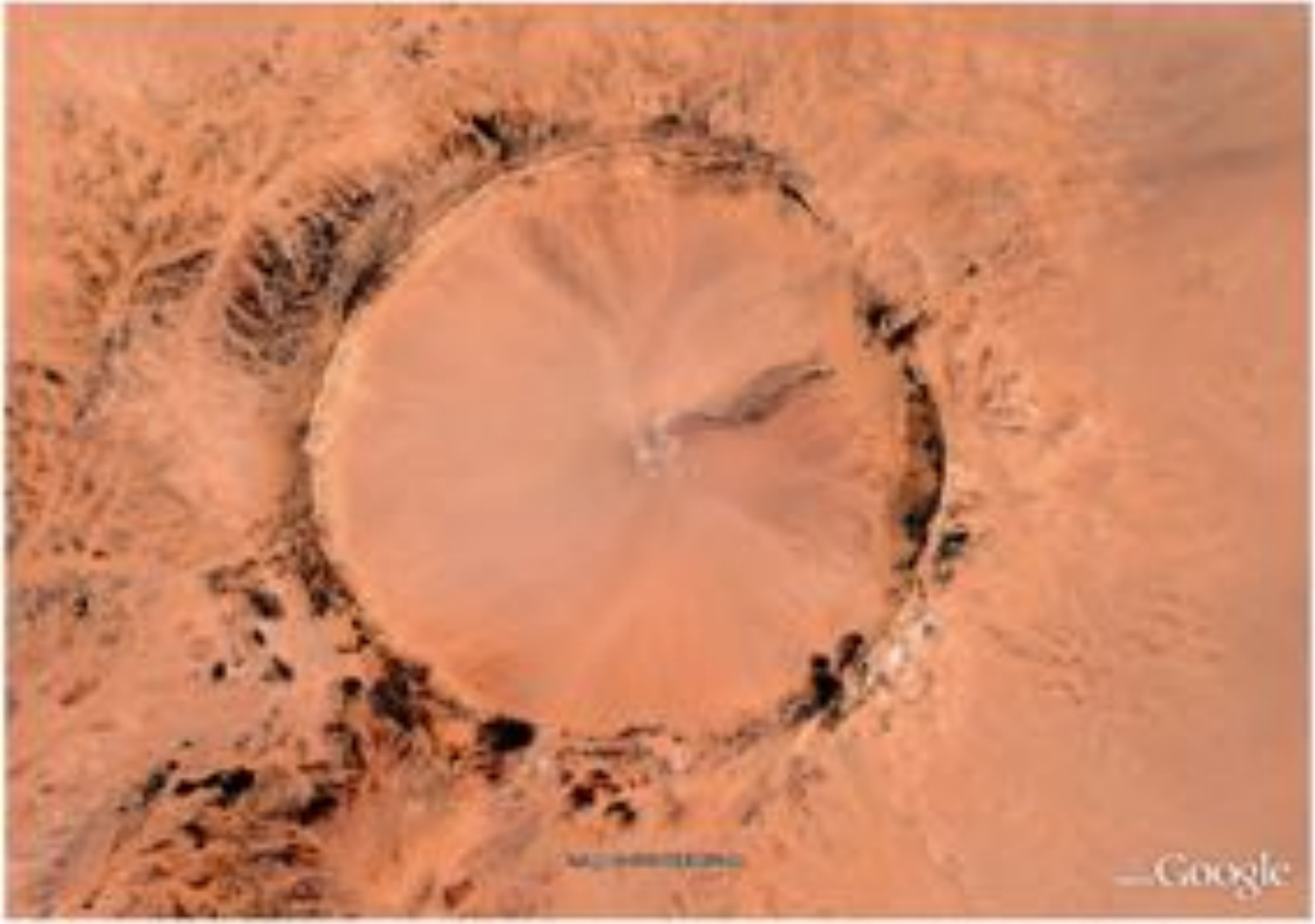

Fig. 5.5 The superbly preserved Tenoumer crater in Mauritania, north-west Africa, at about *22°55′N* and *10°24′W* has an age of only 22,000 years. The site is composed of very old Precambrian rocks. The diameter is around 1.9 km and its depth near 110 m, making the likely size of the impactor 200-m across or more (*Image credit*: ©Google earth 2012)

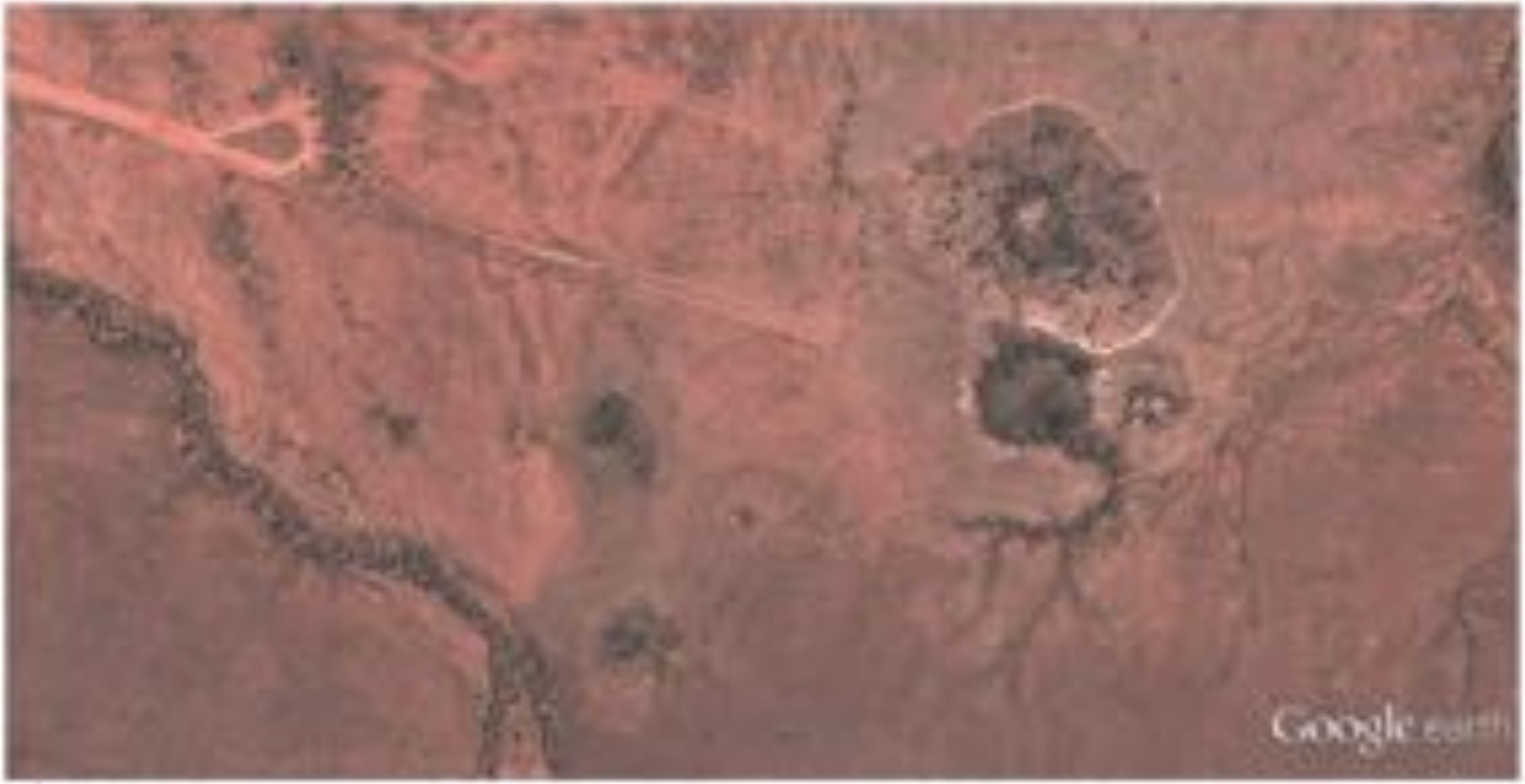

Fig. 5.6 The Henbury crater field in central Australia (Northern Territory). Aboriginal oral traditions about the crater field are sacred and secret to outsiders as well as other cultural knowledge about the physical world. The interested reader may refer to the excellent blog of Dr. Duane Hamacher (URL: http://aboriginalastronomy.blogspot.com.au/). Hamacher (2012) highlights an aboriginal oral story from the central desert regarding its cosmic origins closely parallels the scientific explanation: "*During the Dreaming, a group of sky-women were dancing as stars in the Milky Way. One of the women grew tired and placed her baby in a wooden basket, called a turna. As the women continued dancing, the turna fell and plunged into the earth. The baby fell and was covered by the turna, which forced the rocks upward, forming the circular mountain range. The baby's mother, the Evening Star, and father, the Morning Star, continue to search for their baby to this day*" (Image credit: ©Google earth 2012)

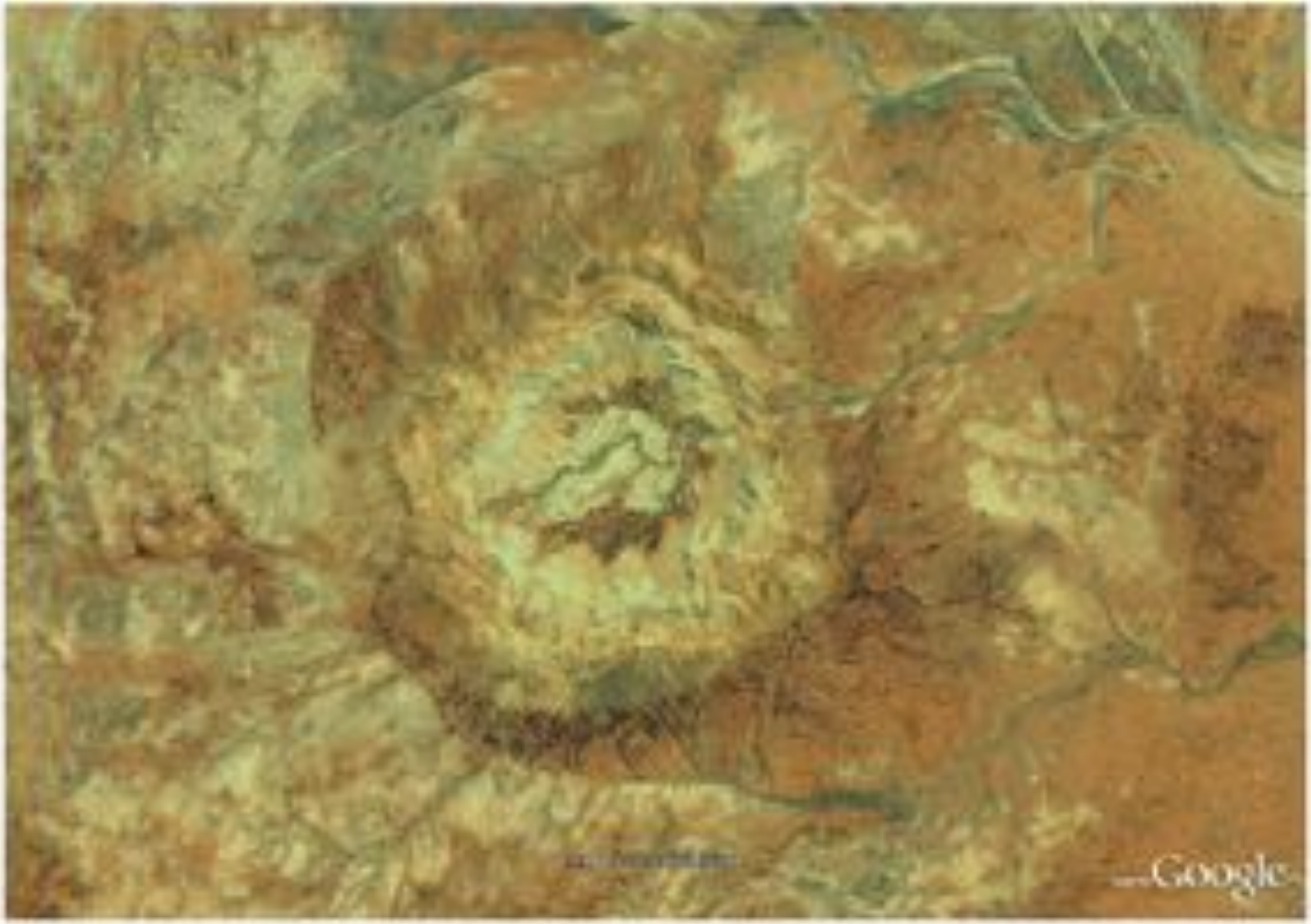

Fig. 5.7 Gosses Bluff impact crater in central Australia (Northern Territory) at 23°49'S and 132°18'E with a diameter of 22 km and a depth of 180 m was formed in less resistant rock which sustained rather strong weathering, relative to its young age in the geologic time scale (143 million years old). The meteorite may have had a diameter of about 1 km and originally caused a crater depth of 1.5 km. Shatter cones are conical fractures present at this site with typical markings produced by shock waves. The energy of the impact has been calculated to equal about 1 million Hiroshima bombs (Image credit: ©Google earth 2012)

Fig. 5.8 In the arid landscape of Australia, several old impact craters have been detected such as the complex Acraman crater in South Australia with its salt lake at 32°02'S and 135°26'E. The crater has a diameter of originally up to 90 km, but today only a ring-like structure close to 35 km in diameter is visible. Its age has been determined to be about 590 million years, but strong erosion has changed all original morphology. Shatter cones in the rock and shocked quartz minerals document the strong impact that has been estimated to equal 5.2 million megatons of TNT (Image credit: ©Google earth 2012)

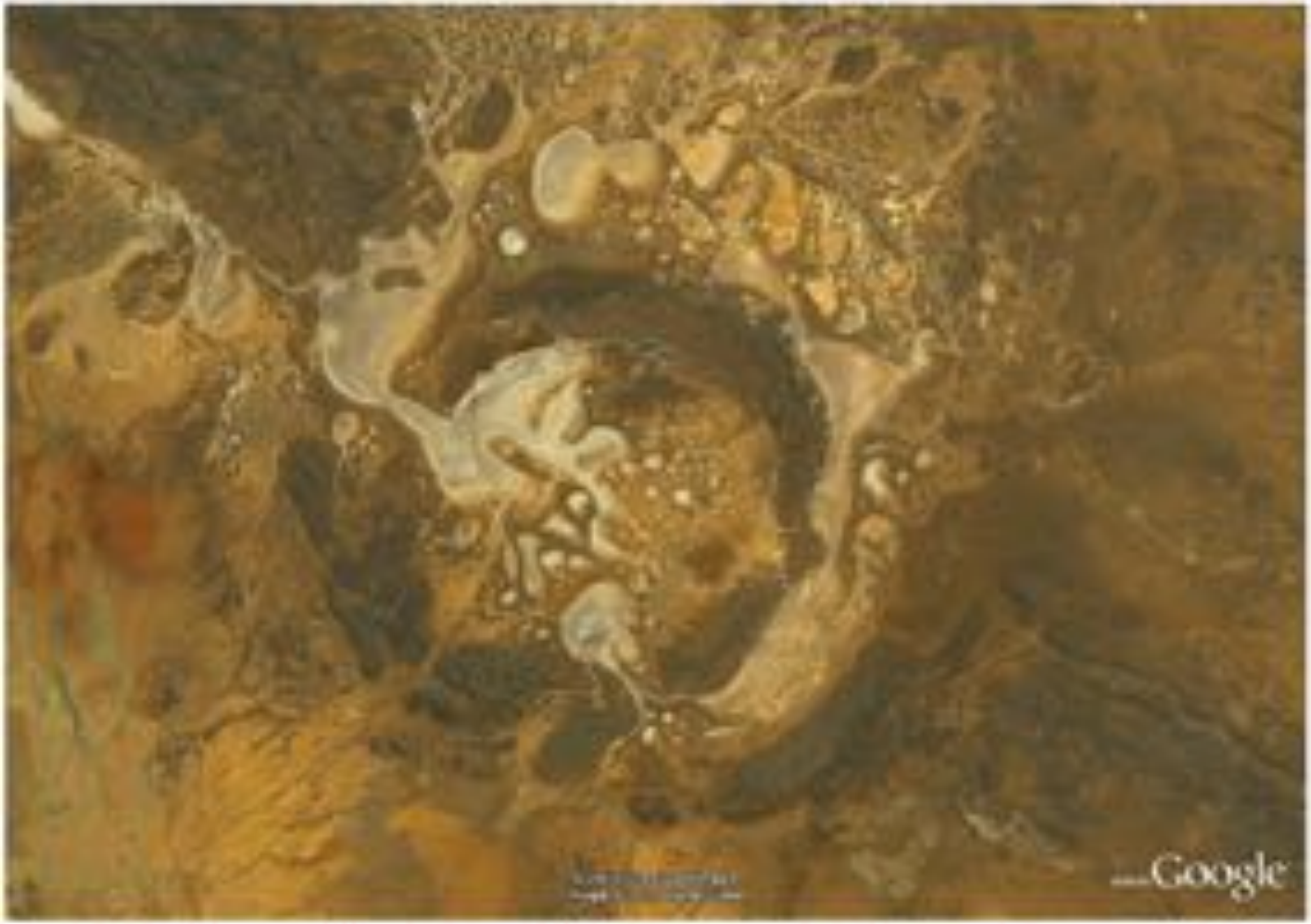

Fig. 5.9 The Shoemaker crater in Western Australia, at 25°53'S and 120°54'E with a diameter of about 30 km, belongs to the oldest impact structures on Earth with an estimated age of 1.63 billion years, although more recent measurements yielded a much younger age of only 568 ± 20 million years. Again shatter cones and the occurrence of shocked-quartz document the impact process in Archaean granitic rocks (Image credit ©Google earth 2012)

Fig. 5.10 The Clearwater impact craters (Quebec, Canada; Clearwater West with a diameter of 36 km, and Clearwater East with a diameter of 26 km) are both located around 56°08′N and 74°22′W. It is thought that a binary asteroid around 290 ± 20 million years ago hit the Earth. In the smaller crater (Clearwater east) the central bulge is hidden under water (Image credit: ©Google earth 2012)

b

喀斯特地貌

Fig. 7.1 (a) Typical karren features on a limestone rock in Greece. They are about 50 cm long and distinct in shape at the upper parts. Rainwater is acidic and erosive and it becomes increasingly more saturated with soluble carbonate and consequently less erosive as it flows downwards (Image credit: D. Kelletat). (b) Intersecting karren features tracing different joint patterns in limestone of the Aran Islands, Ireland (Image credit: A. Scheffers). (c) Karren landscape in the Judbarra/Gregory National Park (Northern Territory, Australia), developed in the carbonate and calcareous rocks of the Proterozoic Skull Creek Formation. A clear zonation of karren formation resulting from


b
c
Google


a
b


Google
b

[illegible]


a
b
Google earth


滴水岩
和尚洞
周家坡

块体运动


a
Google


b
c


a
Google Earth
b
Google Earth

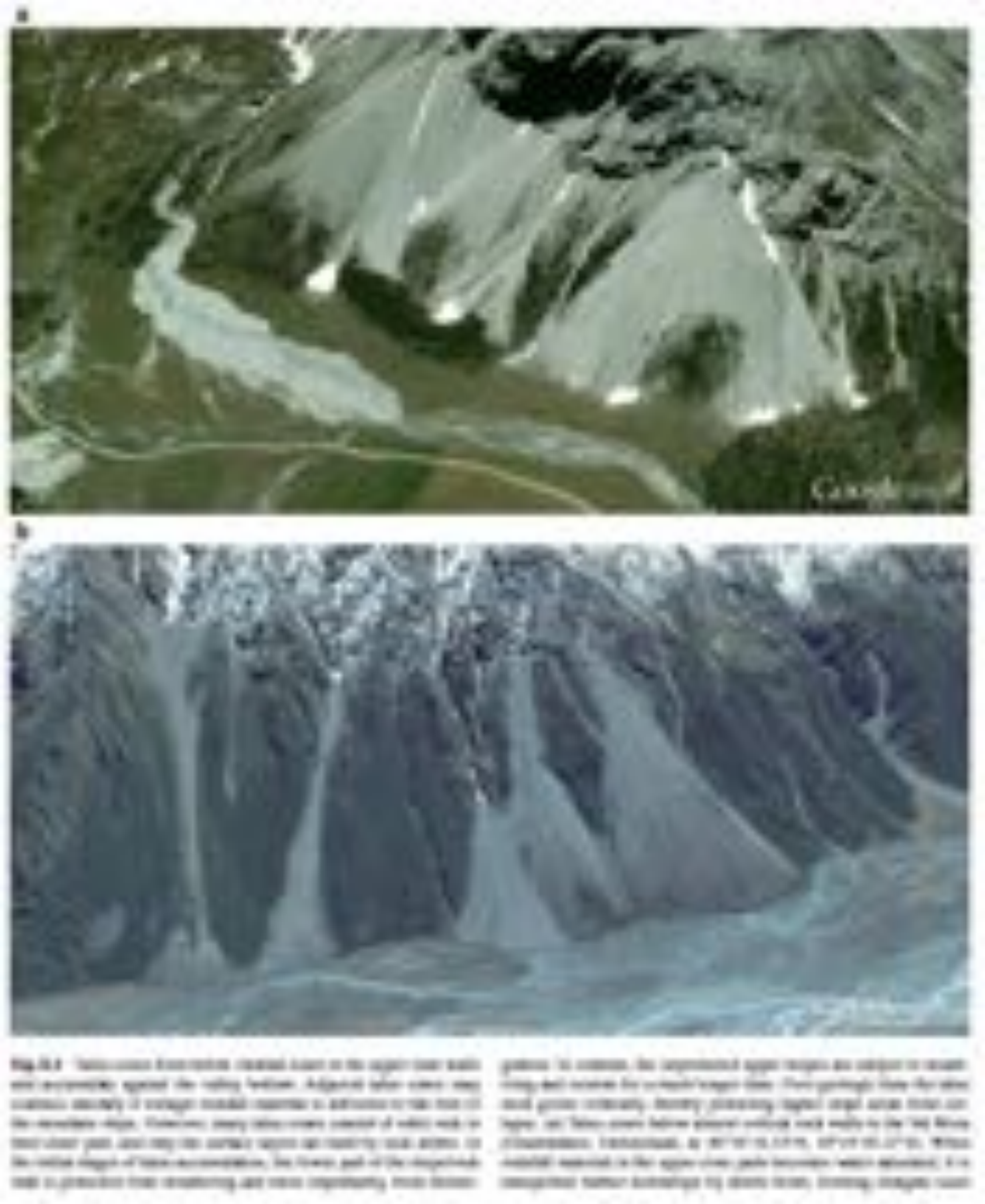
a
b

Fig. 8.3 (continued) and lobate deposits in the upper and lower parts of the cones, respectively. (**b**) Talus cones in the Southern Alps of New Zealand (upper Rakaia Valley, at *43°30′1.22″S, 170°58′43.61″E*). The typical sorting pattern with larger blocks in the lower, distal part of the talus cone is visible. (**c**) Talus cones (*right*) and lateral moraines (*left*) south of Bow Lake, Banff National Park, Canadian Rocky Mountains (*51°39′55.29″N, 116°27′29.96″W*). In addition to the rockfall material, debris flows may develop from the talus cones due to water saturation of rock debris sections (Image credit: ©Google earth 2012)

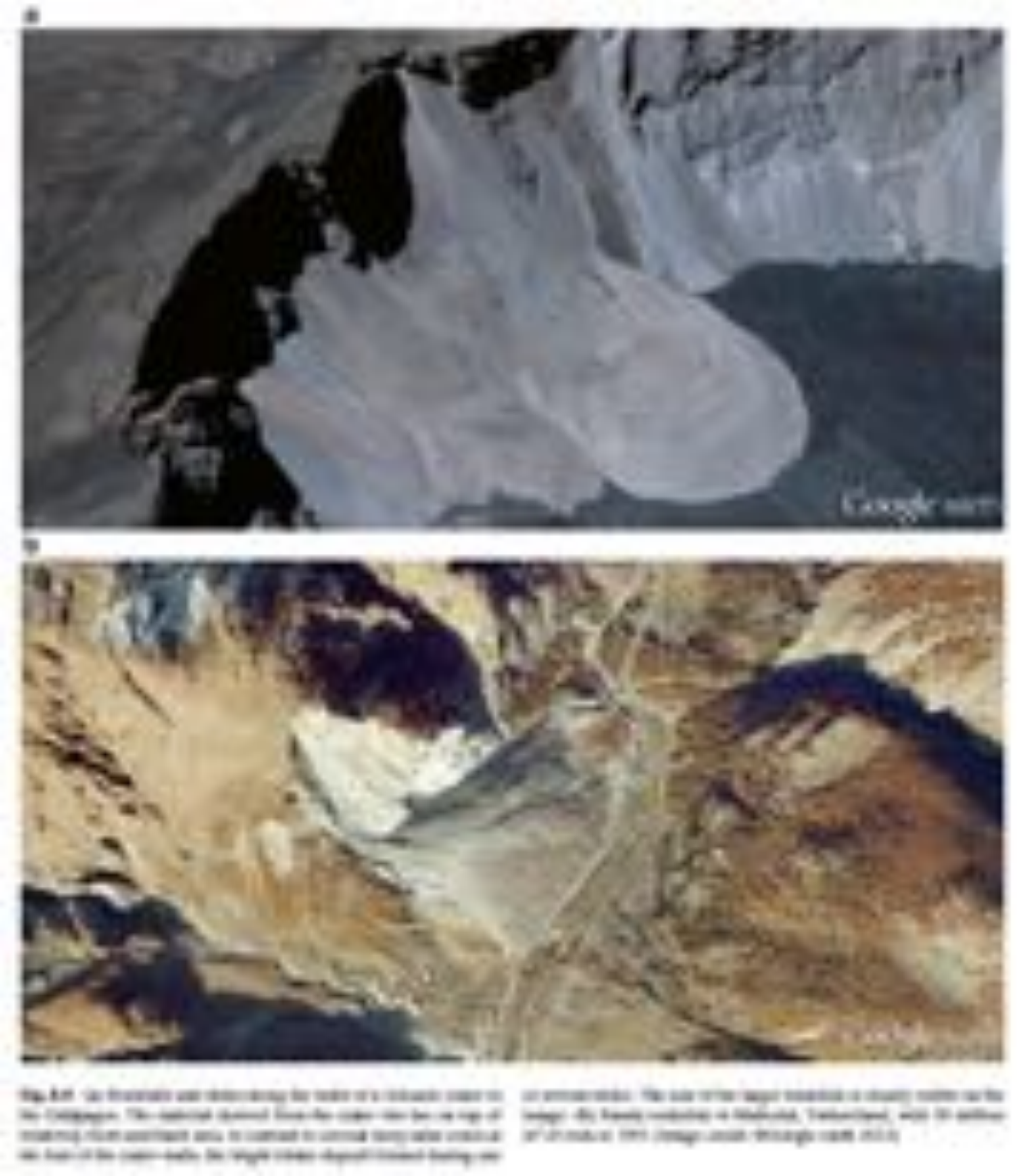
a
Google earth
b

Google earth


Google earth
影像拍摄日期: 2013
95°28'22.99" 东 海拔 2801 米 视角海拔高度 23.04 公里


Image © 2017 DigitalGlobe
4710 米
Google earth
影像拍摄日期: 2014/12/19 29° 56' 18.23" 北 95° 27' 48.29" 东 海拔 3991 米 视角海拔高度 18.36 公里

松散物质的运动


a
Google earth
b
Google earth


a
Google earth


Google earth

Google earth

河流地貌

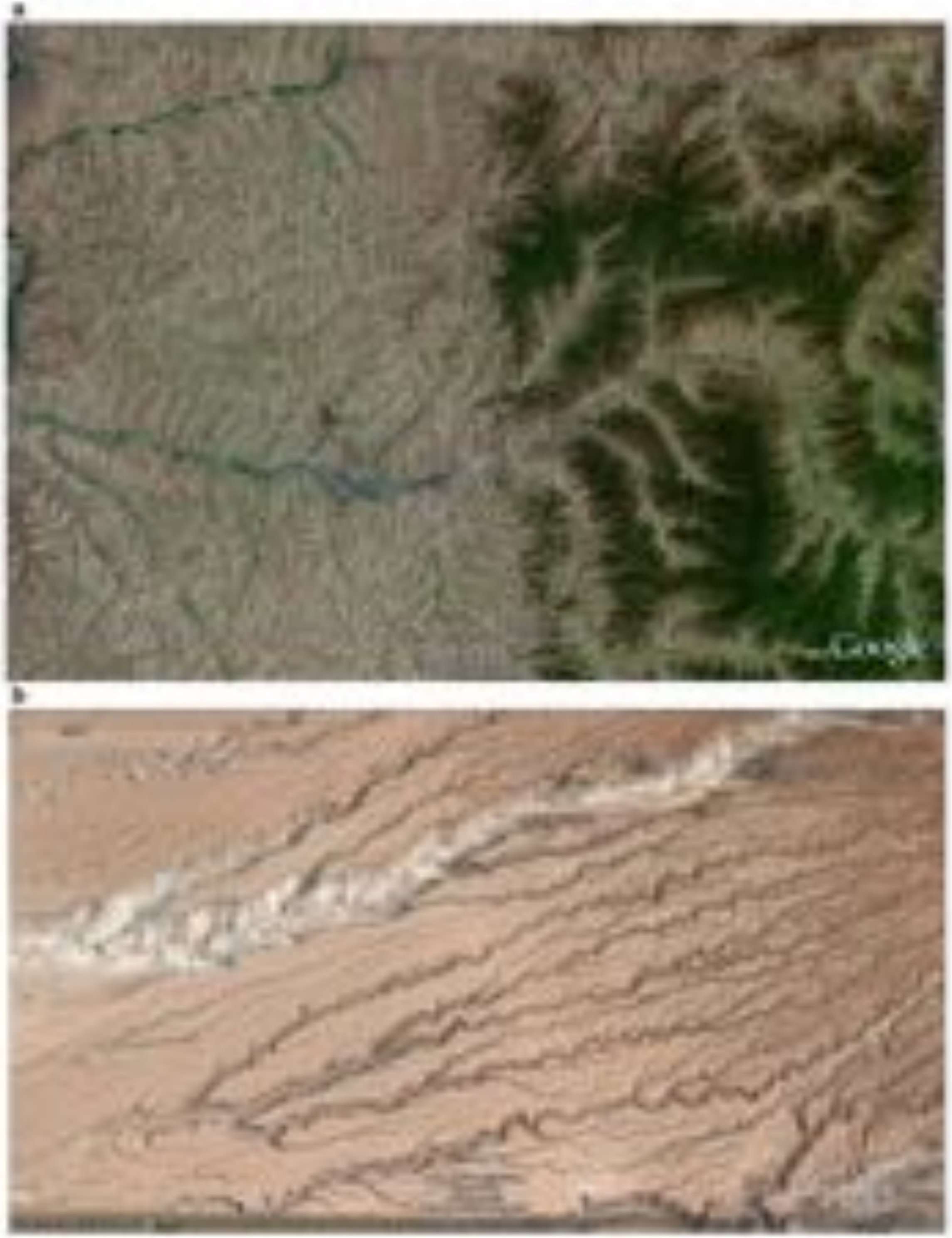
a
Google
b


a
b
Google earth
Google earth

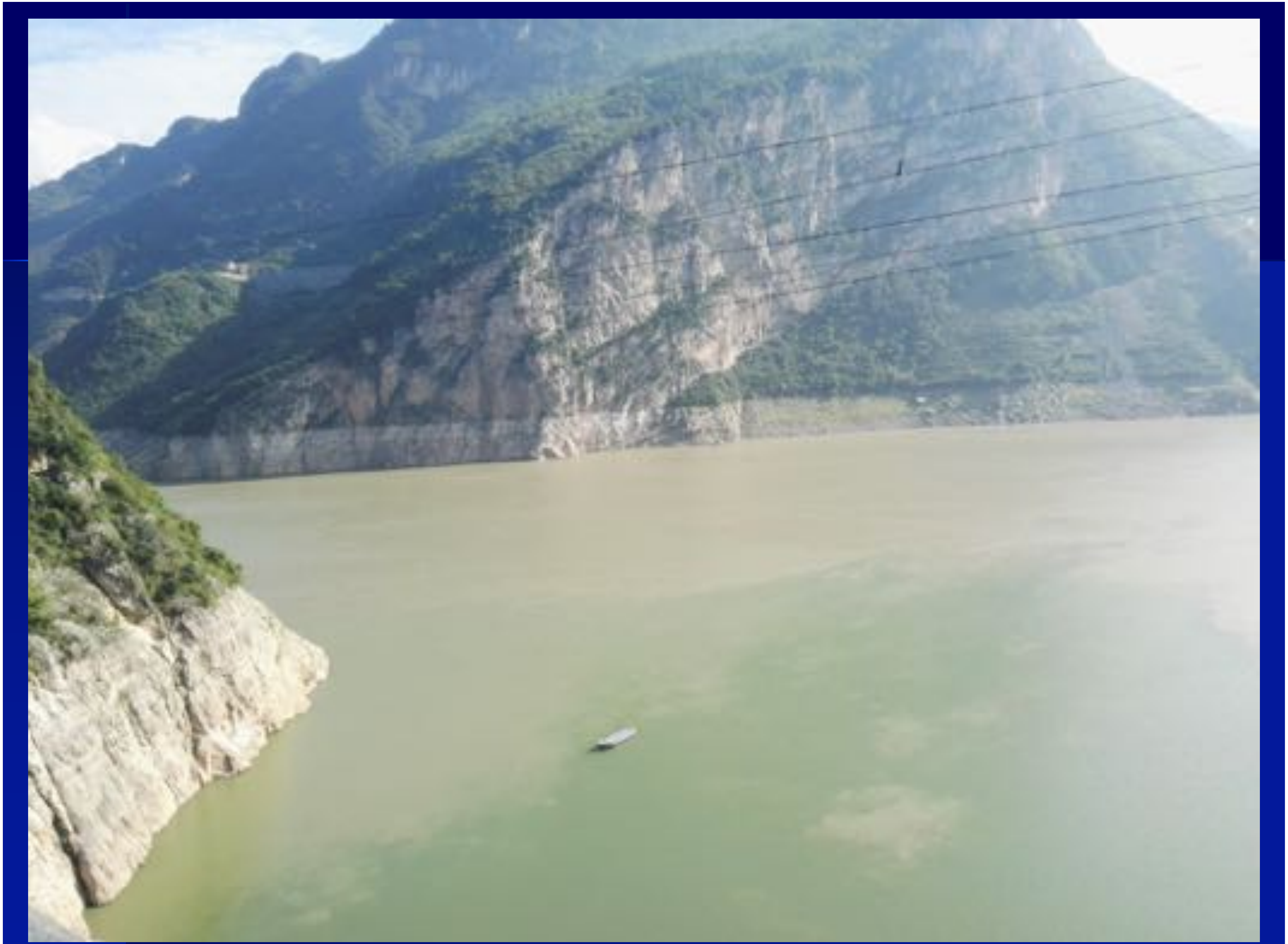

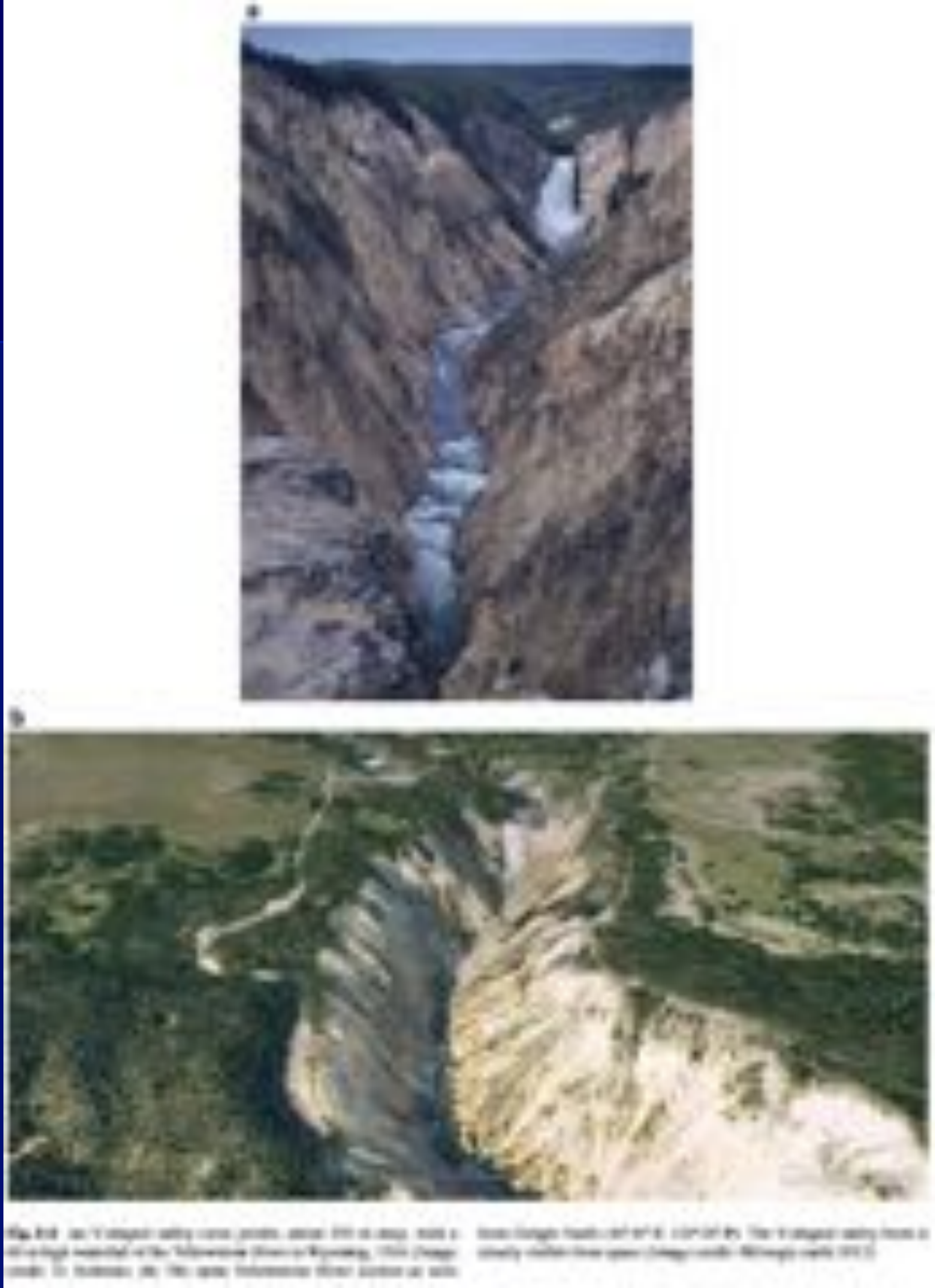
a
b


a
b

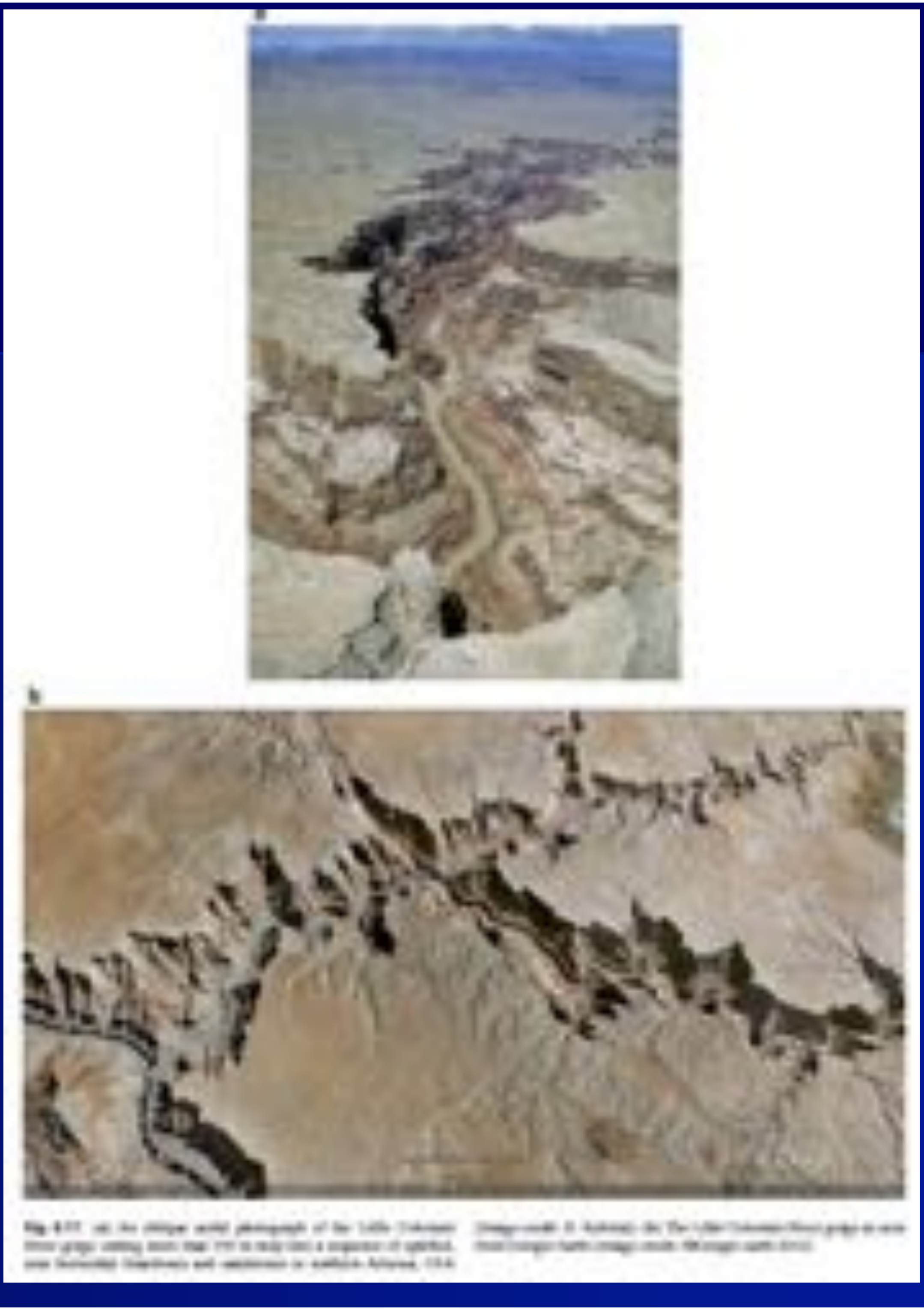
a
b


a
b


a
Google earth
b
Google earth

Fig. 8.15 Detail from the middle section of the Mississippi River at 33°22'N and 91°47'W. The meander shown (now an oxbow lake) is about 3 km wide (Image credit: ©Google earth 2012)


a
b


a
Google earth


b
c
Google earth
Google earth

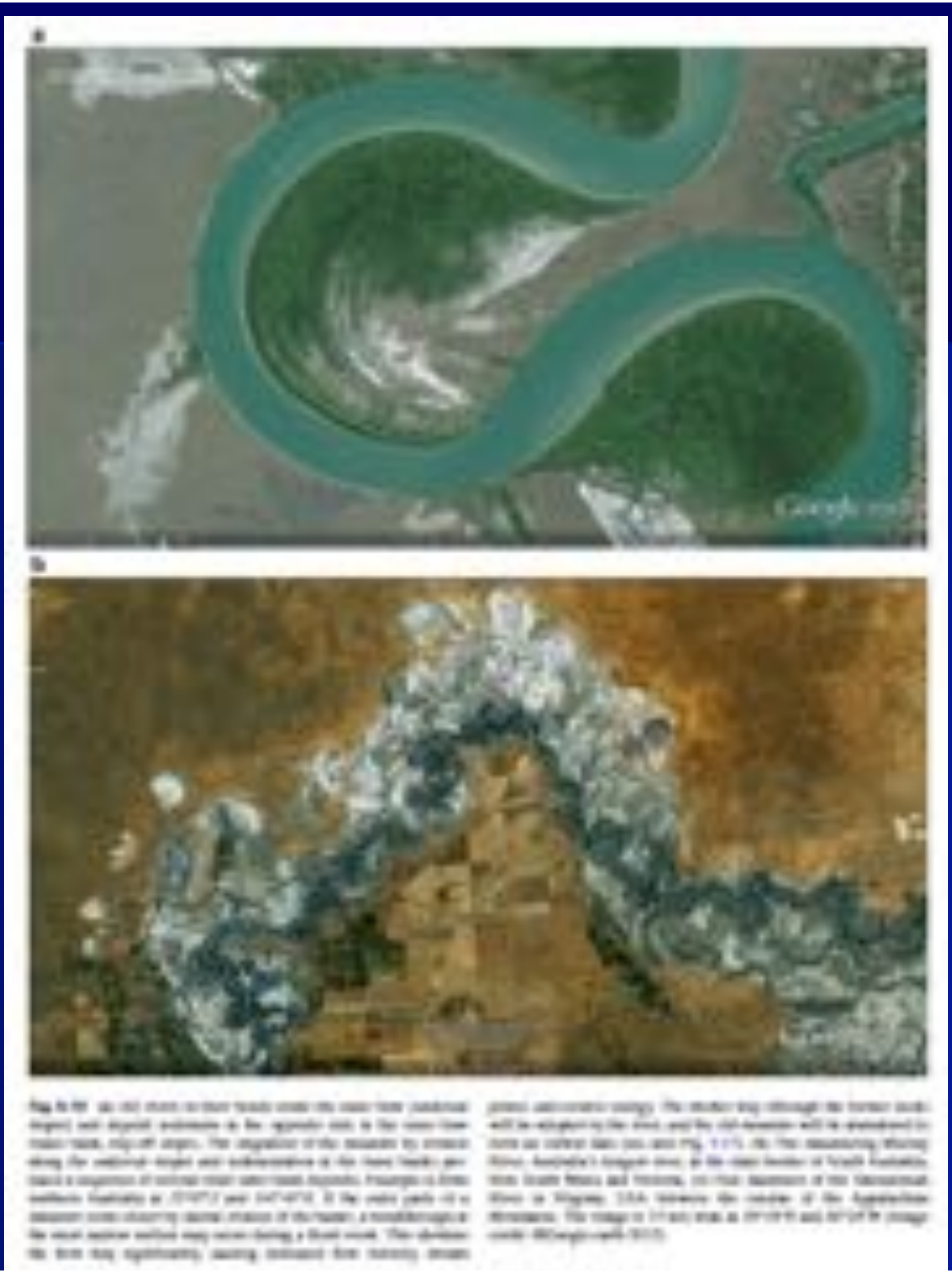
a
b


a
b

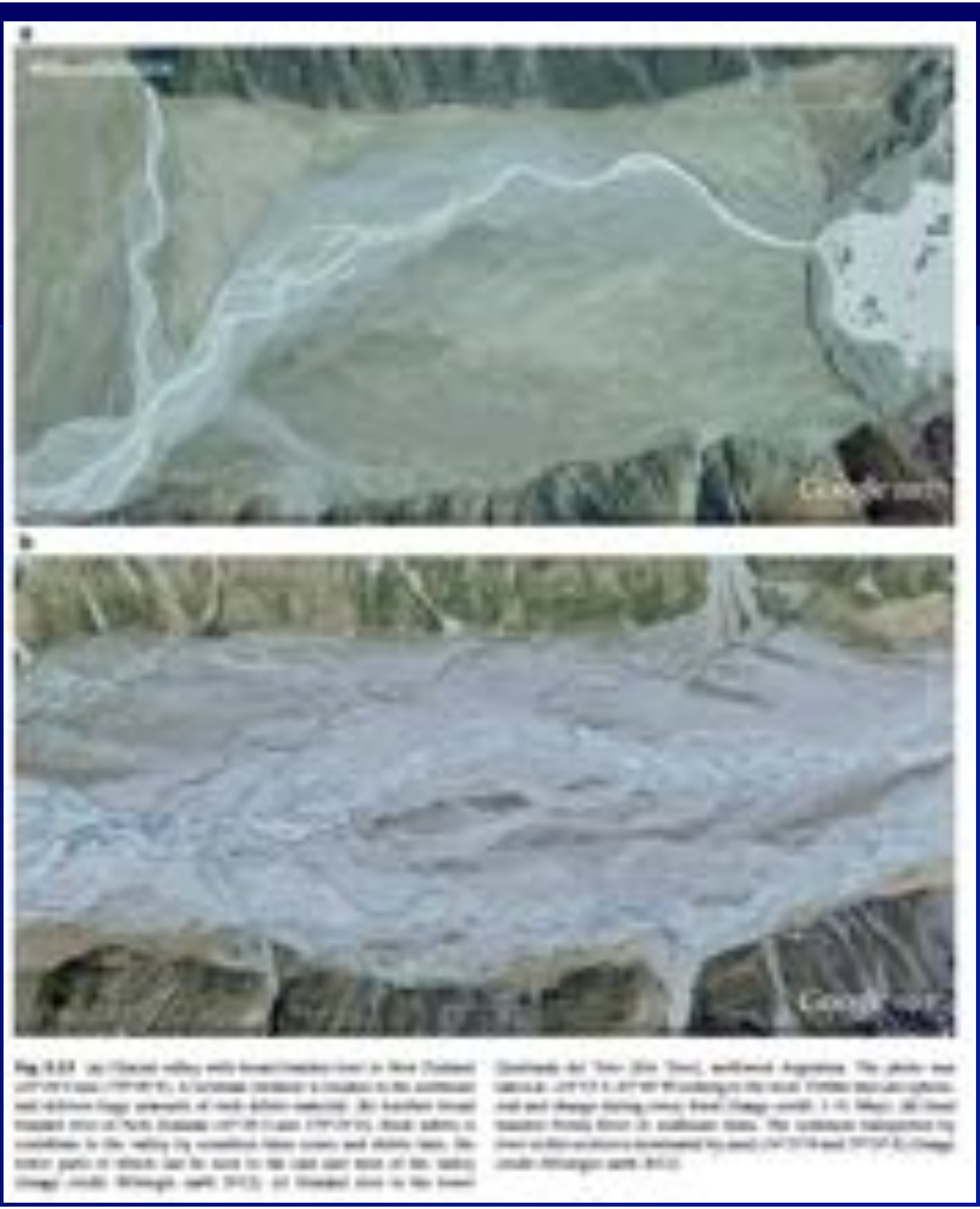
a
b
Google earth
Google earth


c
d

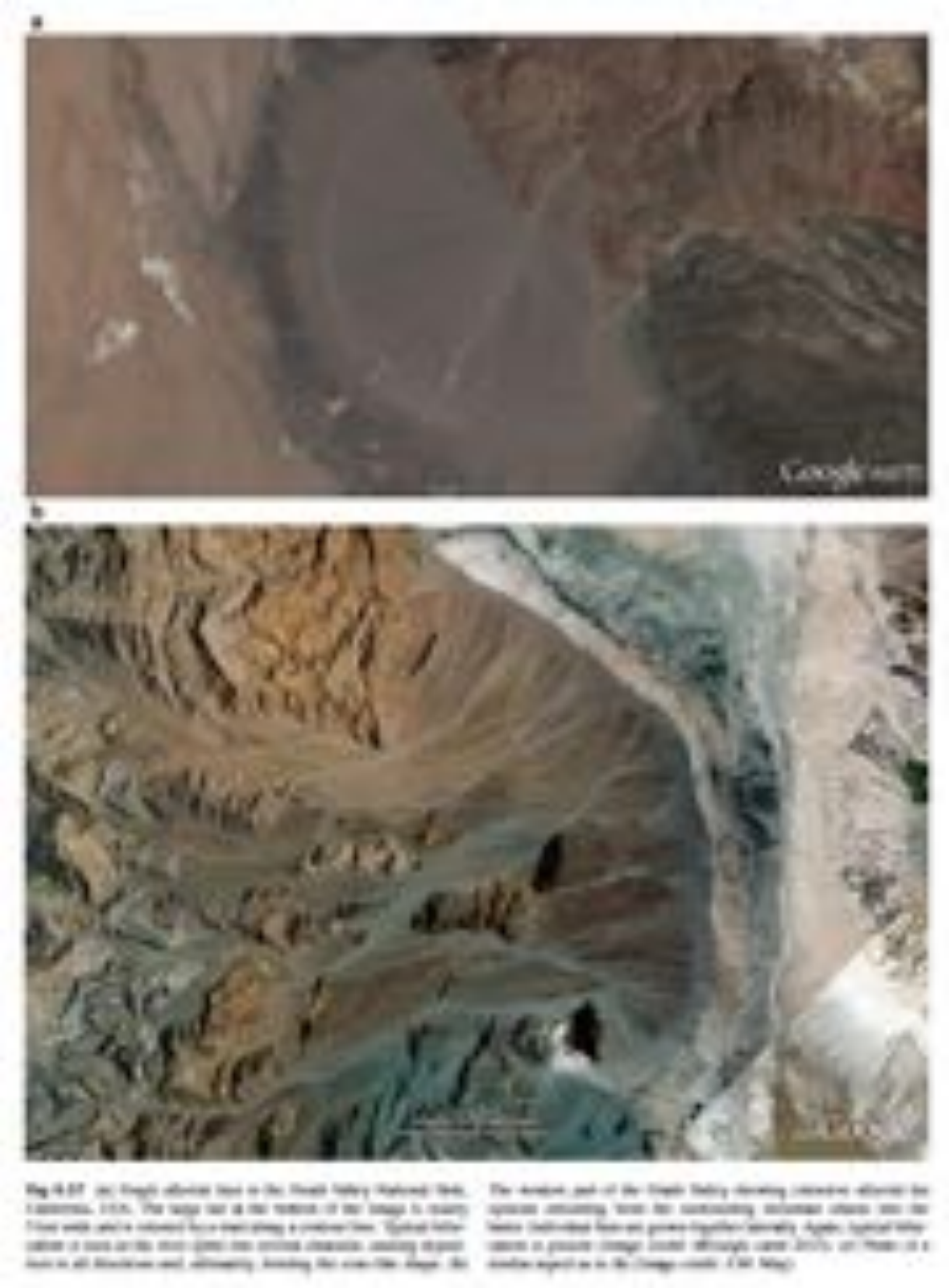
a
Google earth
b

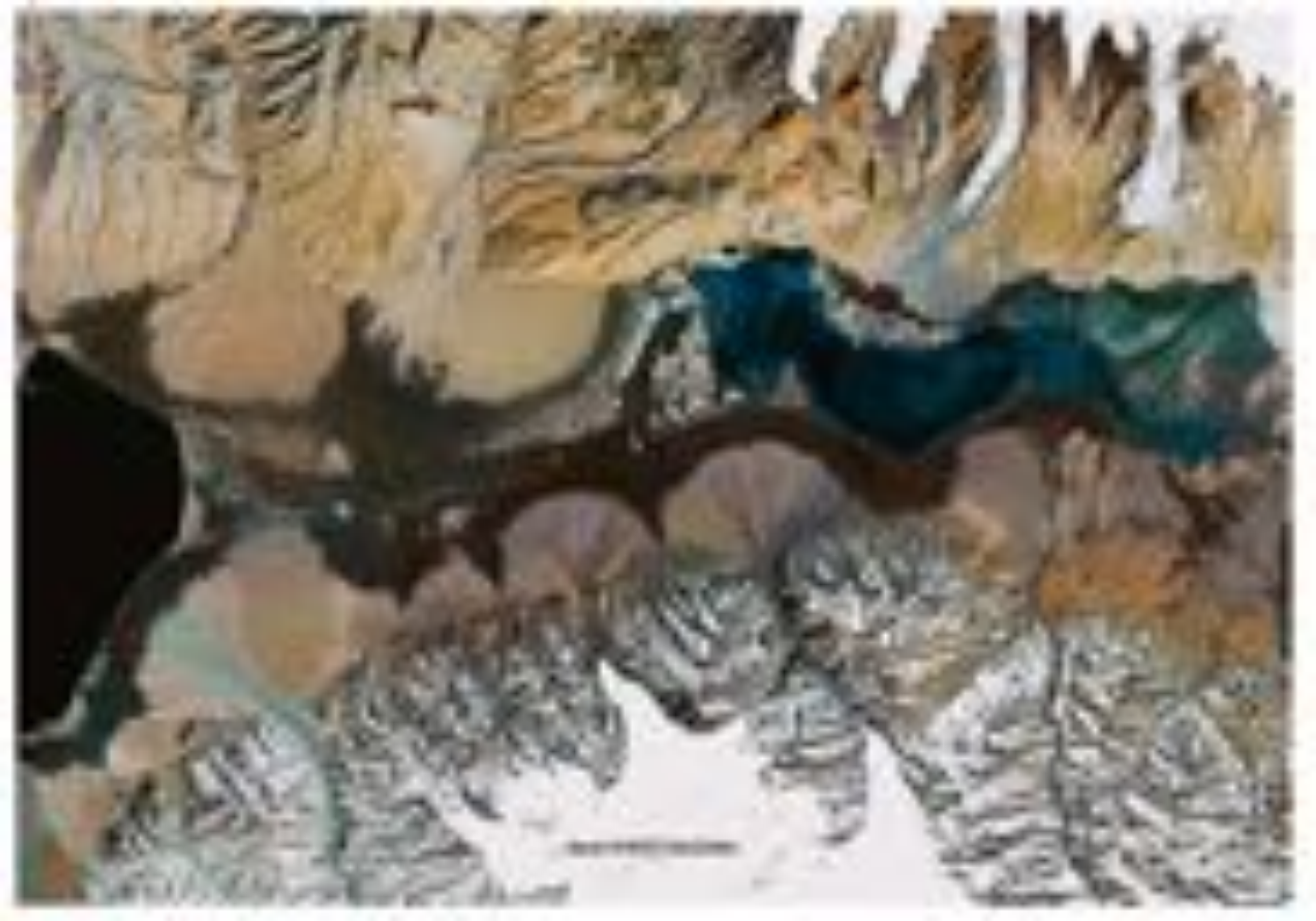

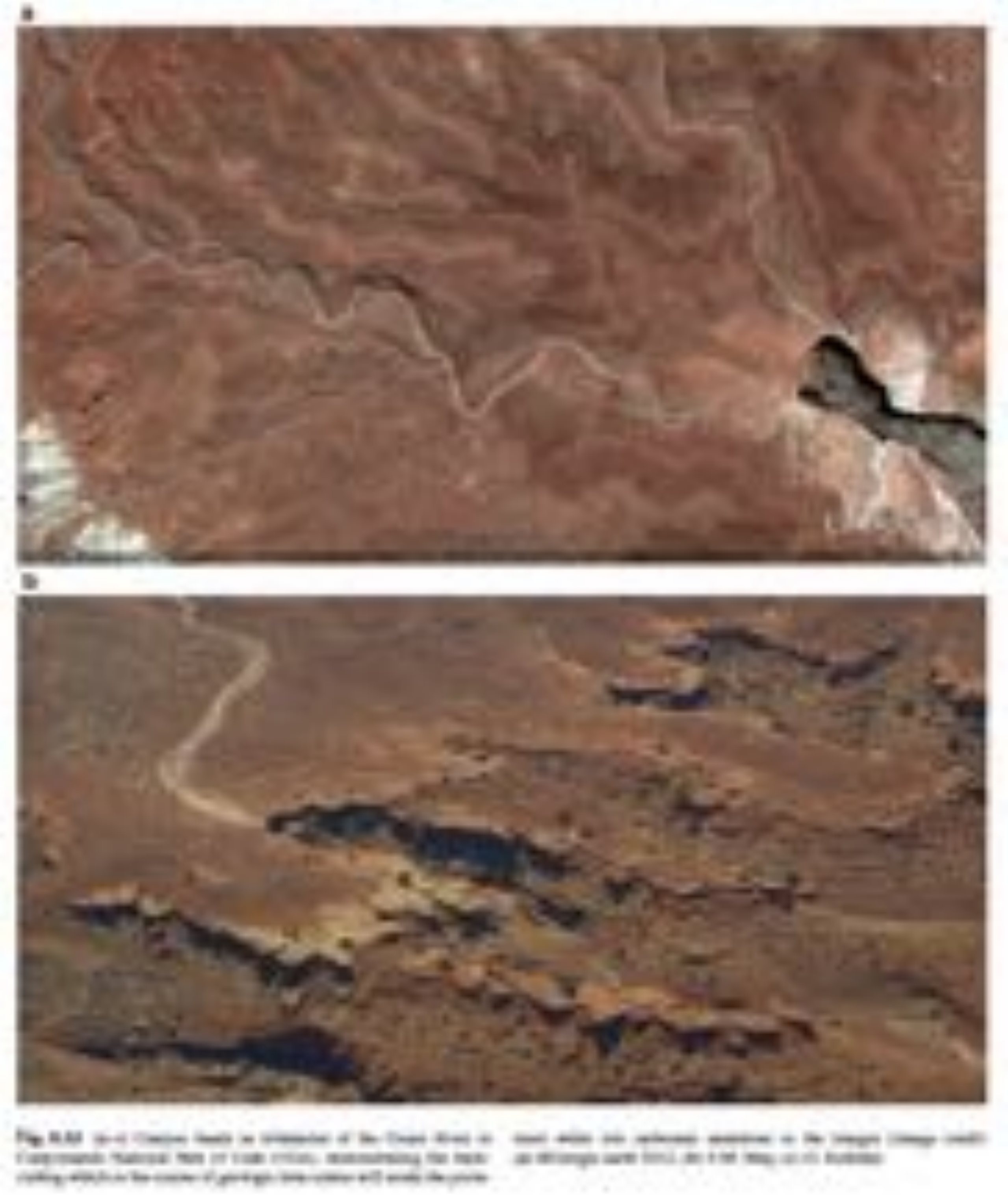
a
b


a
b


Goog
图像拍摄日期 2016/3/28 43° 00′18.70″ 北 81° 9′58.72″ 东 海拔 1406 米 视角海拔高度


Google earth
d
Google earth

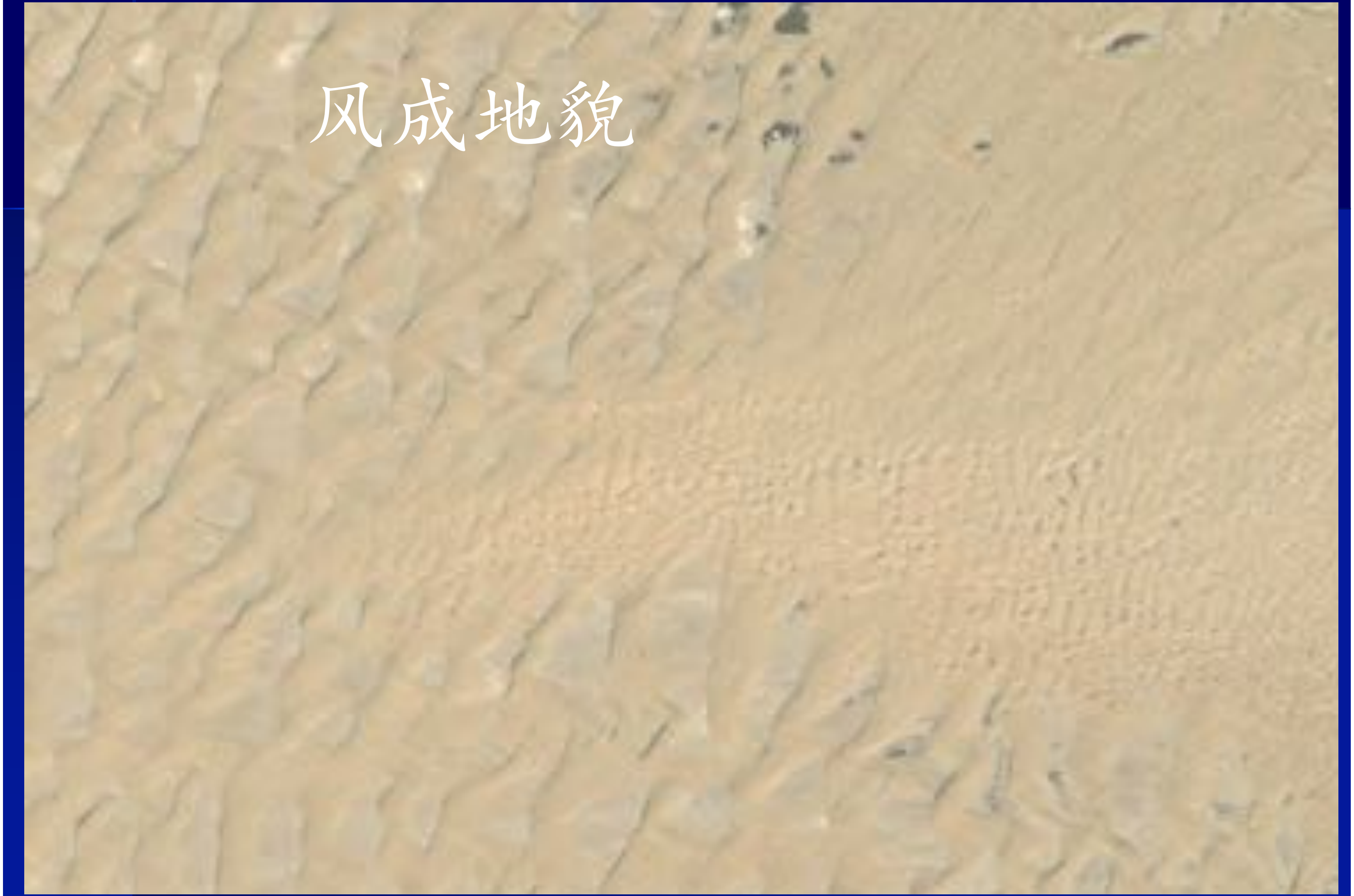

风成地貌


Google earth

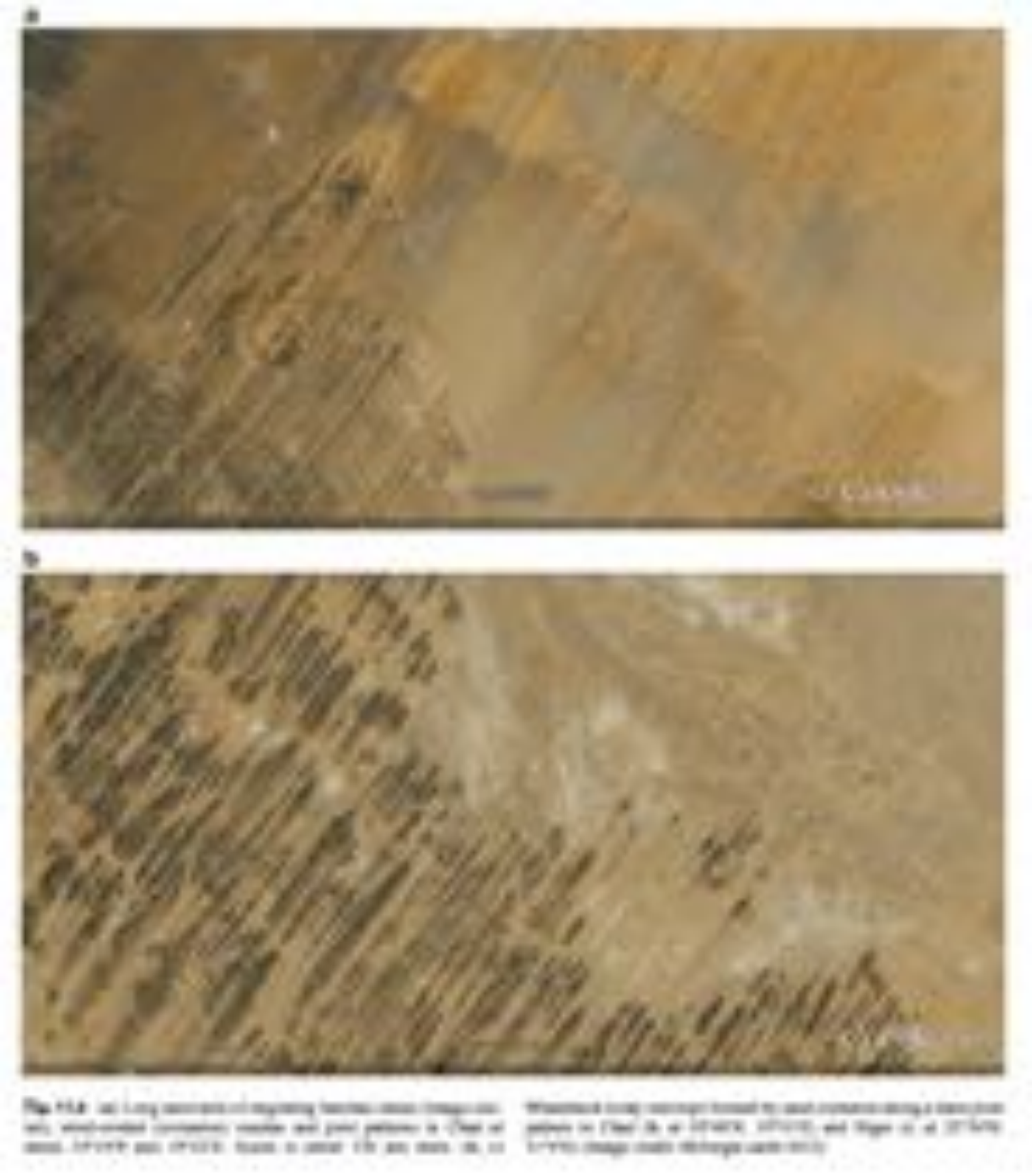
a
b

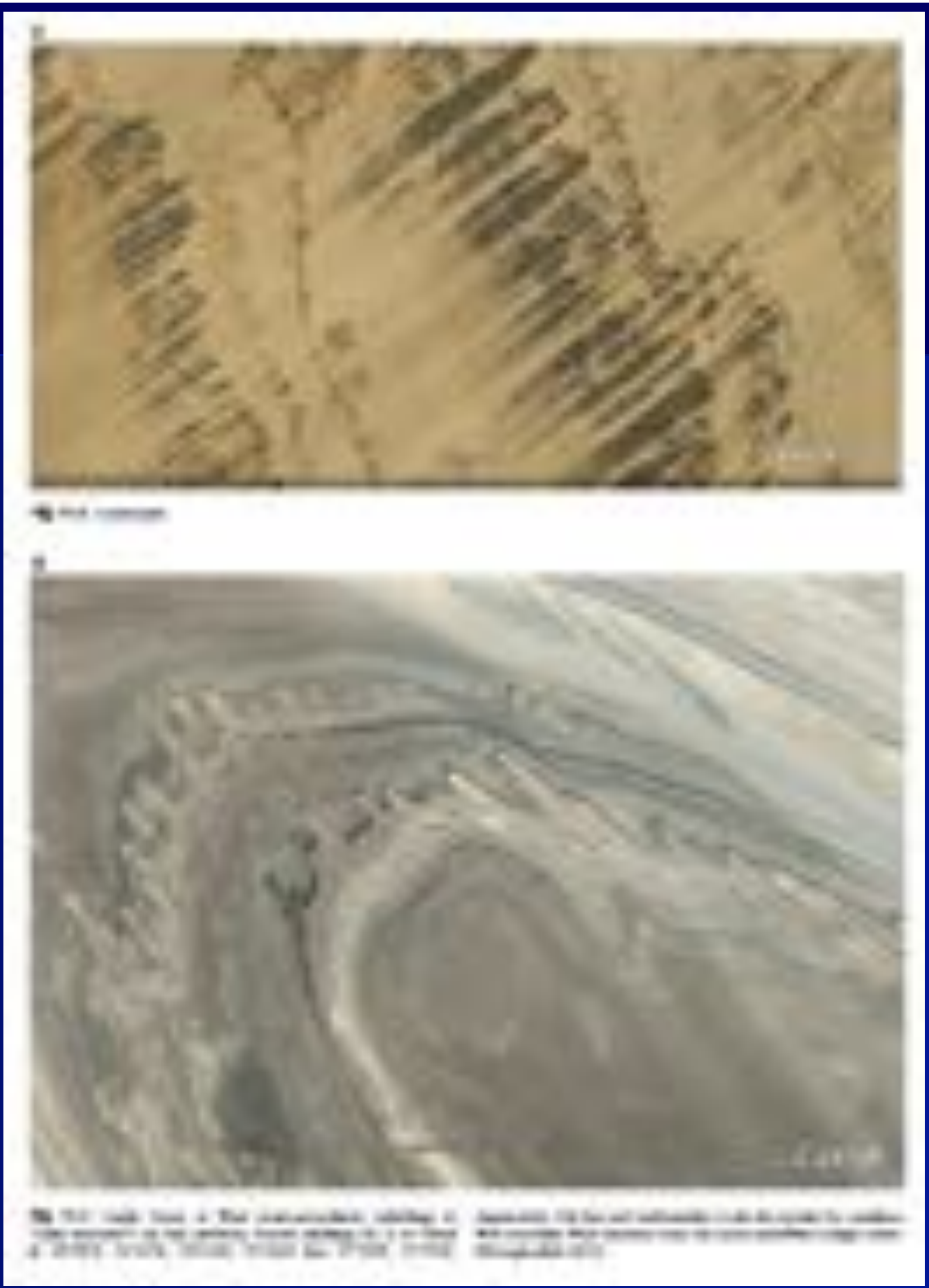

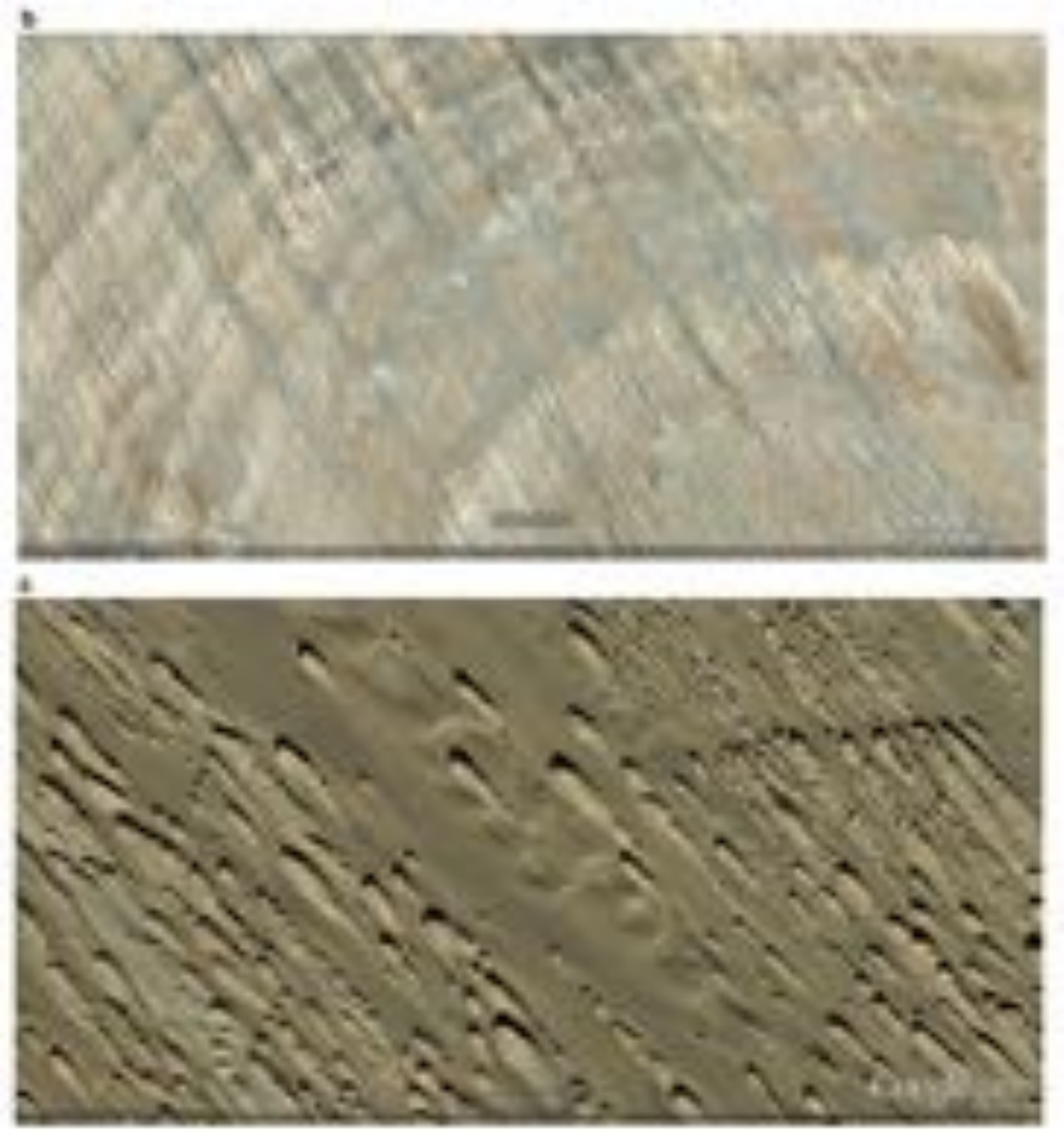
b

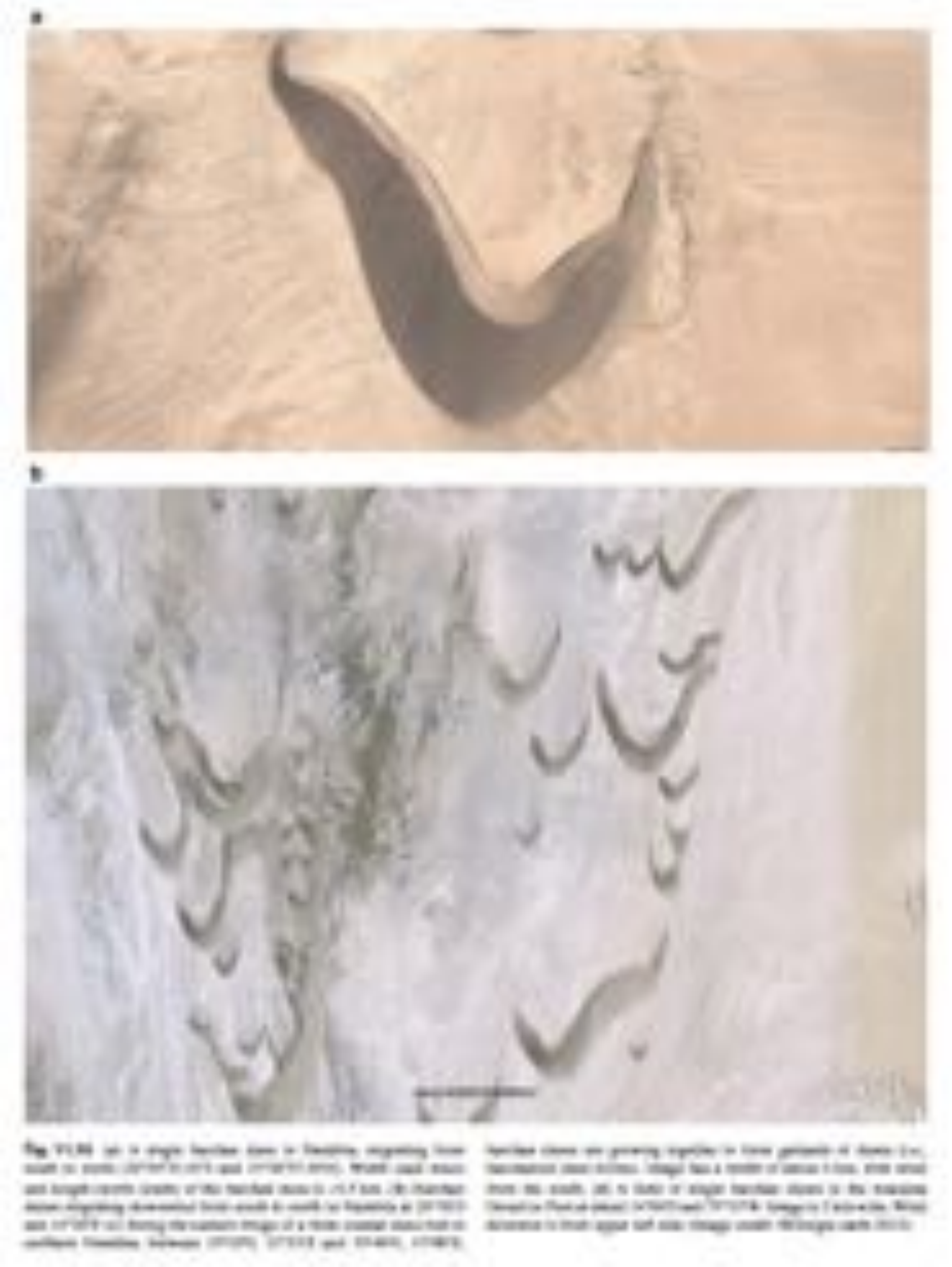
a
b

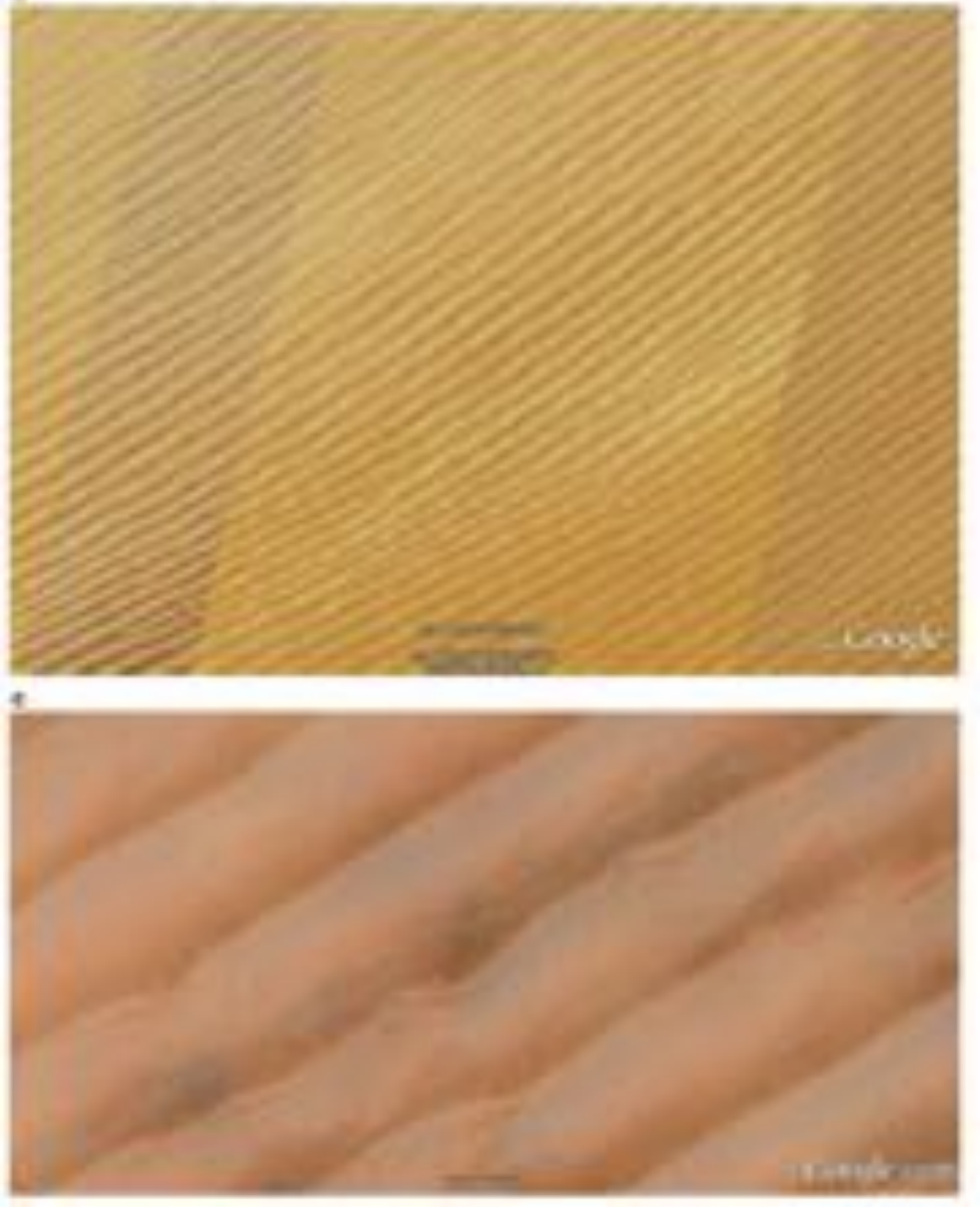
Google

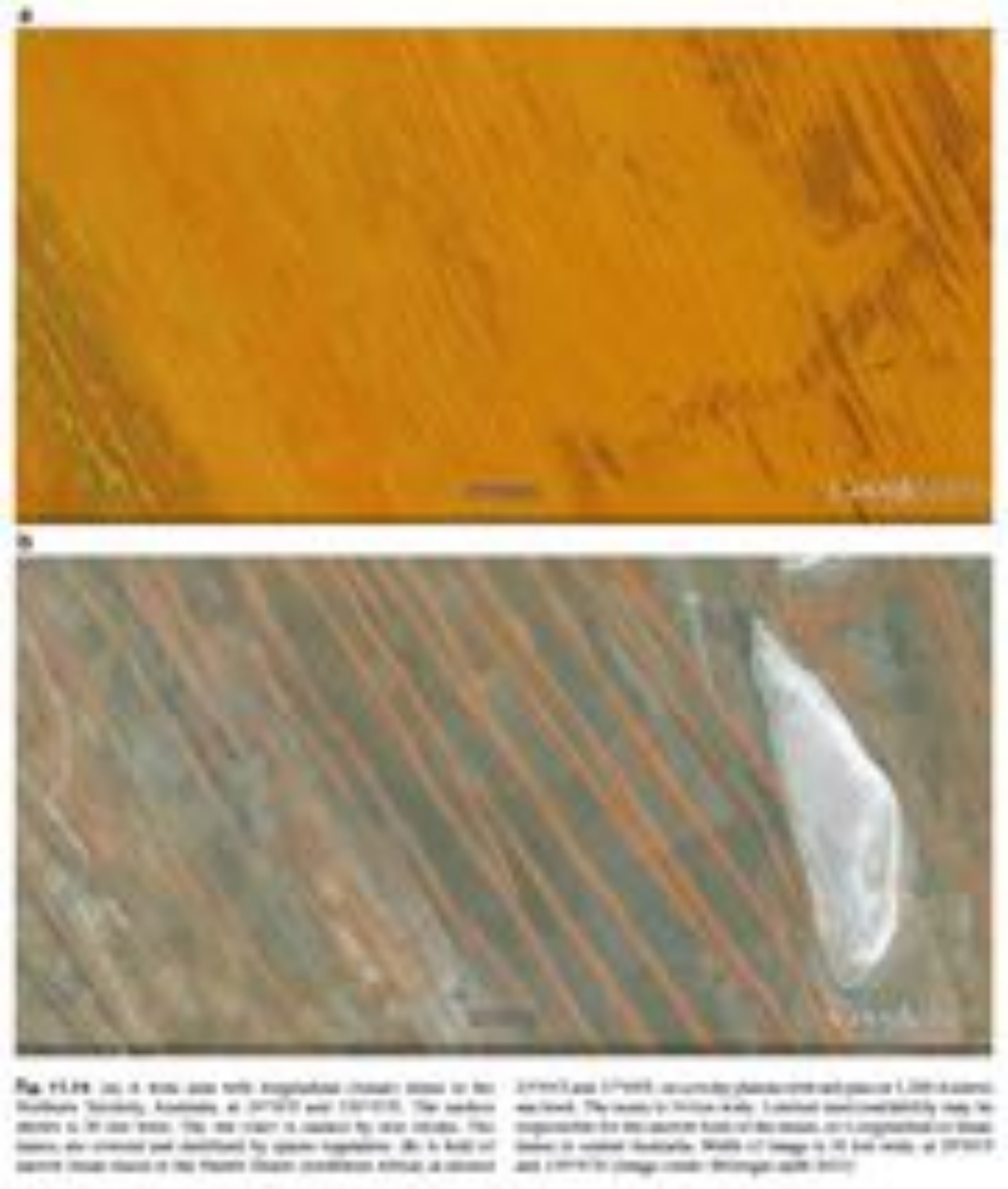
a
b

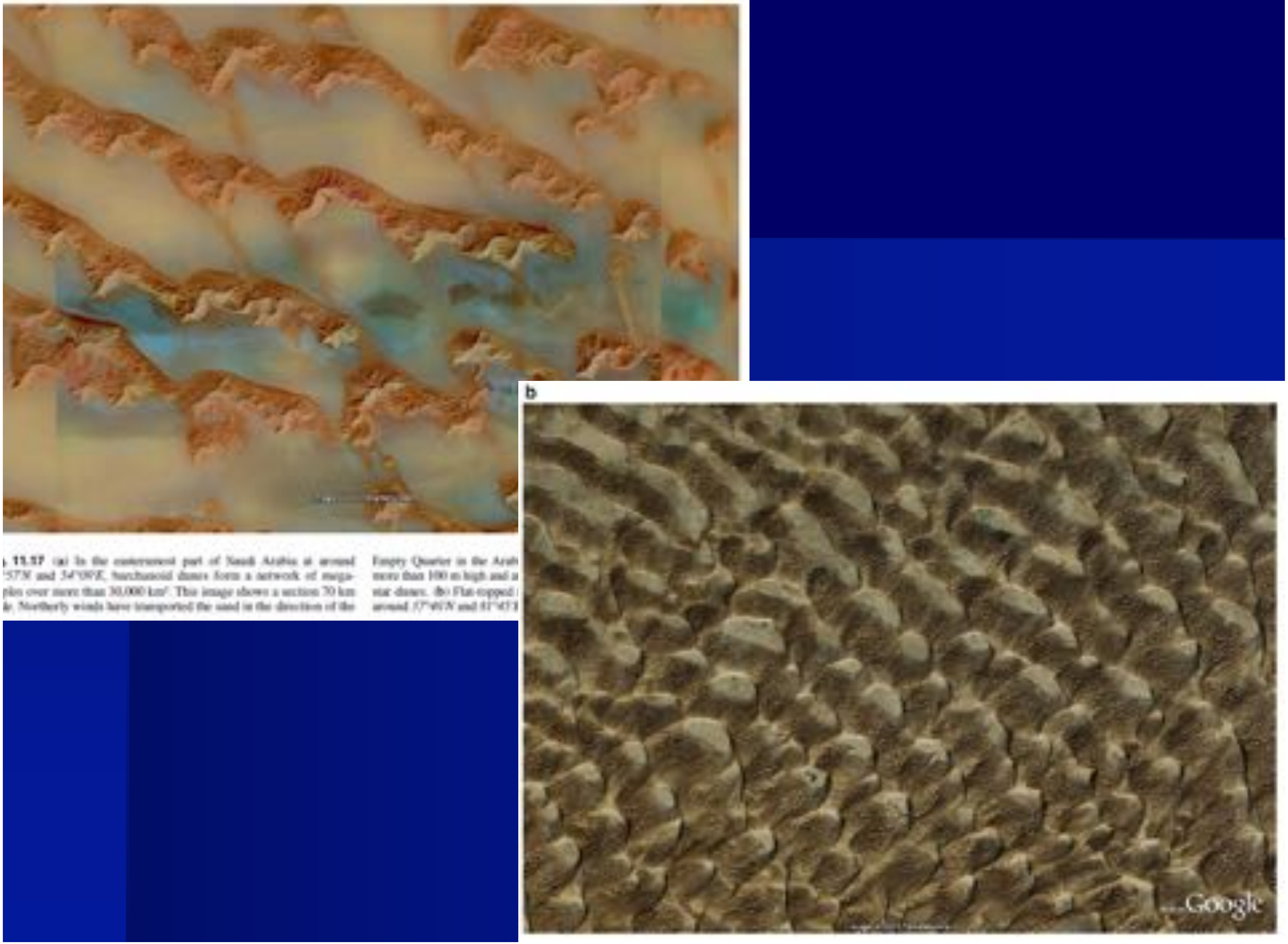

11.17 (a) In the easternmost part of Saudi Arabia at around
57′N and 54°09′E, barchanoid dunes form a network of mega-
ples over more than 30,000 km². This image shows a section 70 km
le. Northerly winds have transported the sand in the direction of the

Empty Quarter in the Arab
more than 100 m high and a
star dunes. (b) Flat-topped
around 37°40′N and 81°45′

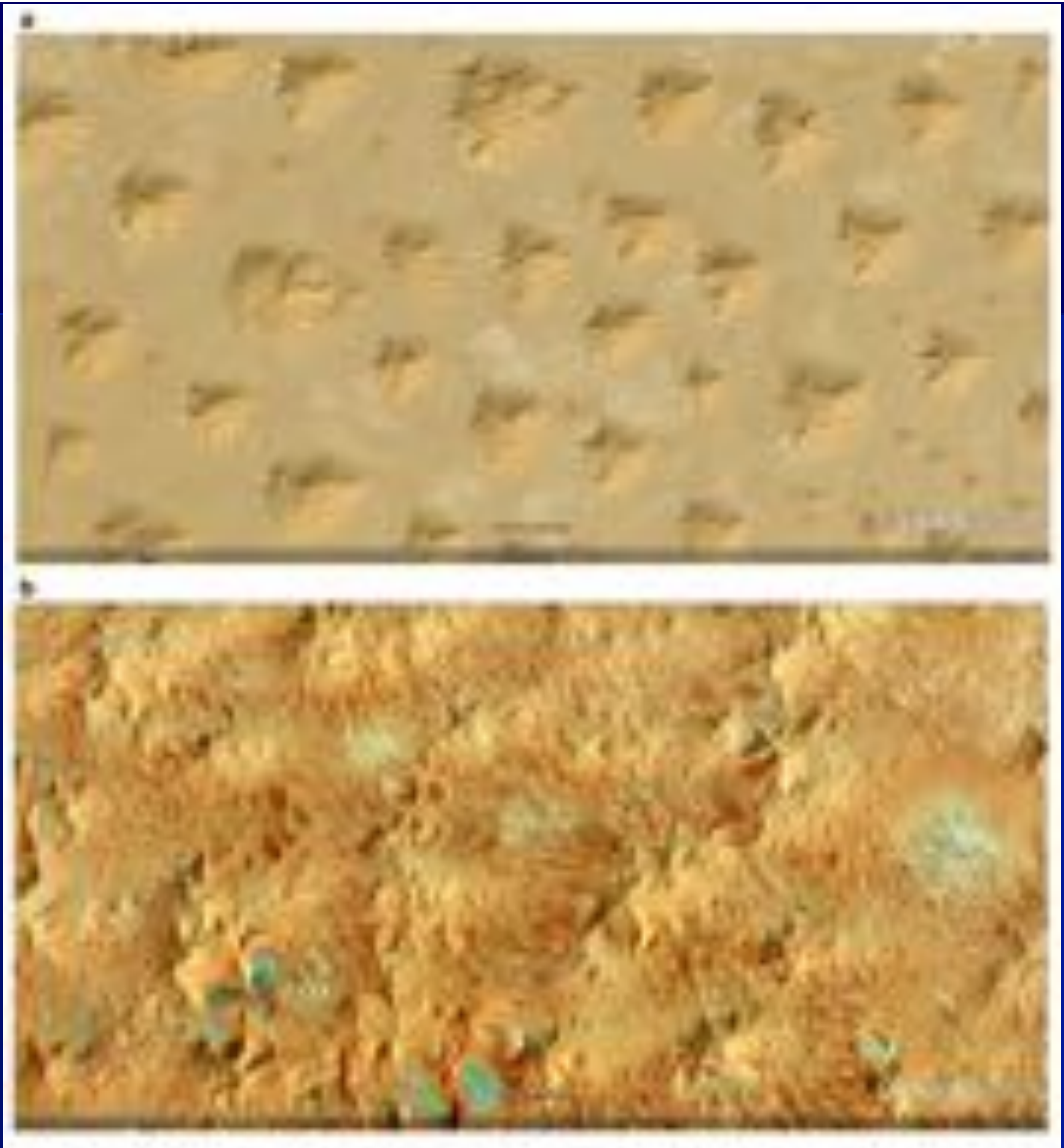
a
b

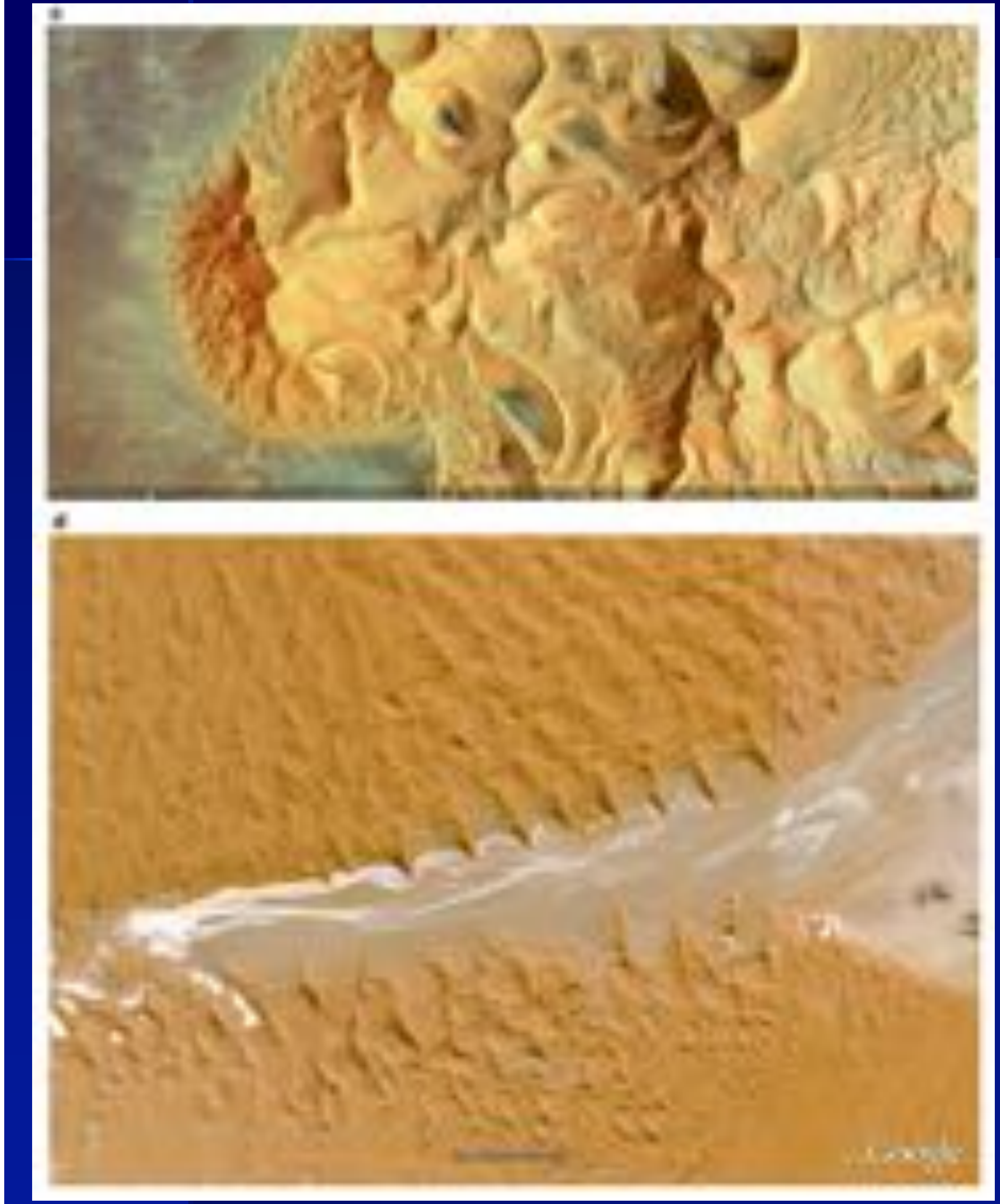
Google

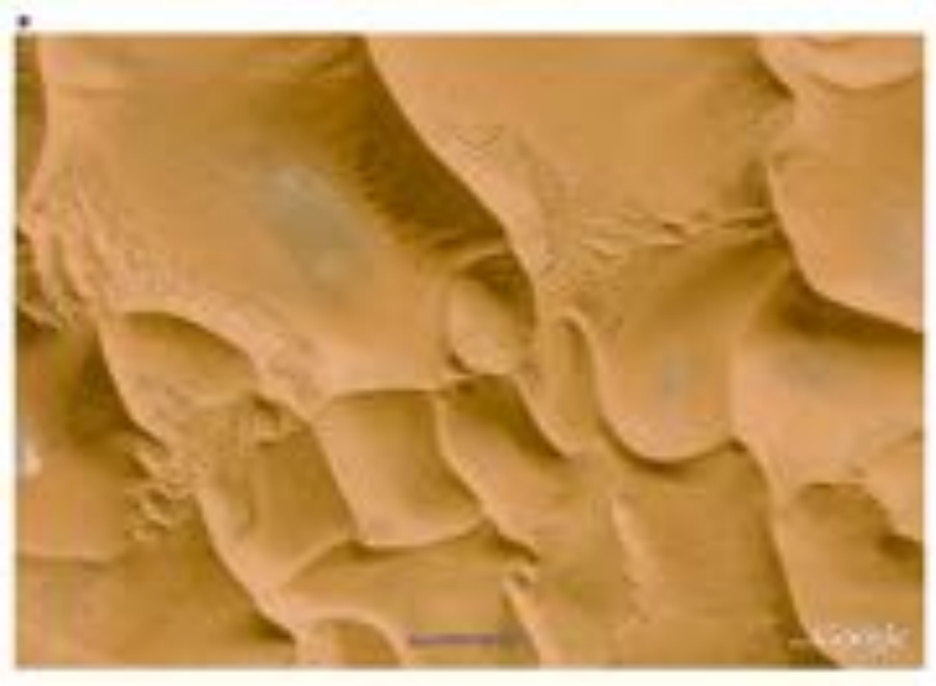
Google

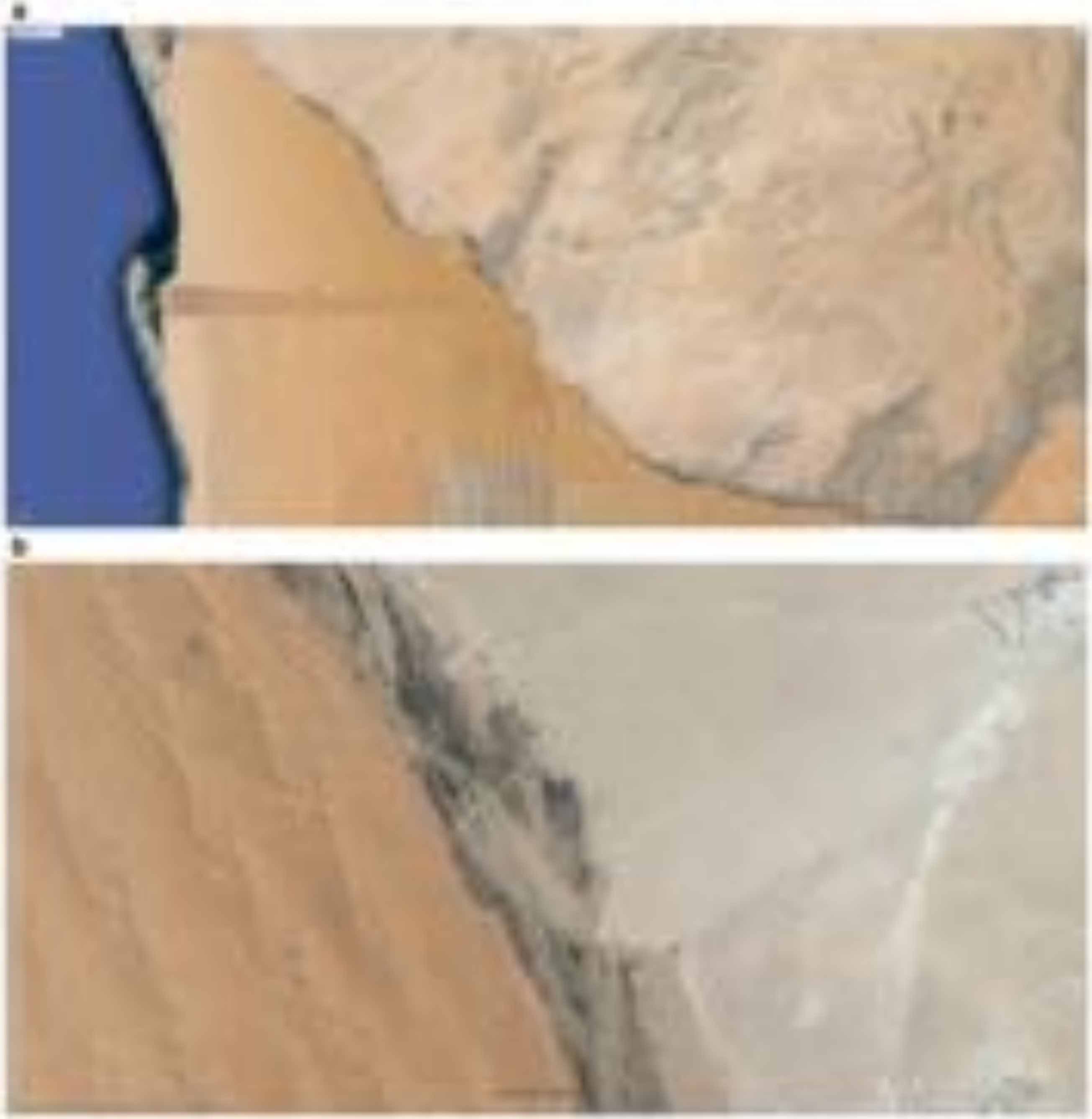
a
b

冰川地貌

g 12.1 (a) A series of different snowfalls from one winter is preserved on an alpine pass. Each darker stratum represents a phase of melting, where snow disappeared but other particles have been enriched from the remnants of the old snow. Similar records are developed in a same manner in glacial ice over much longer time periods (Image credit: D. Kellner). (b) This 450 Swiss Alps (46°30'05.40"N, 8°26' its body of ice, which represent dust and dirt within the snow an credit: ©Google earth 2012)

Fig. 12.2 Ice crystals from an alpine valley glacier, grown together with a diameter of up to more than 10 cm each. White tiny spots in the left upper part of the image are small bubbles of air in the ice (Image credit: D. Kelletat)

Fig. 12.3 (a) Dirt layers on this Chilean glacier are particles from volcanic eruptions, like tuff, ash and cinder. These may derive from a single eruption with different rhythms and therefore show material of different grain size. (b) In this Chilean glacier tongue the dirt layers

from volcanic eru
defined layers even
parts of the glacier
©Google earth 201

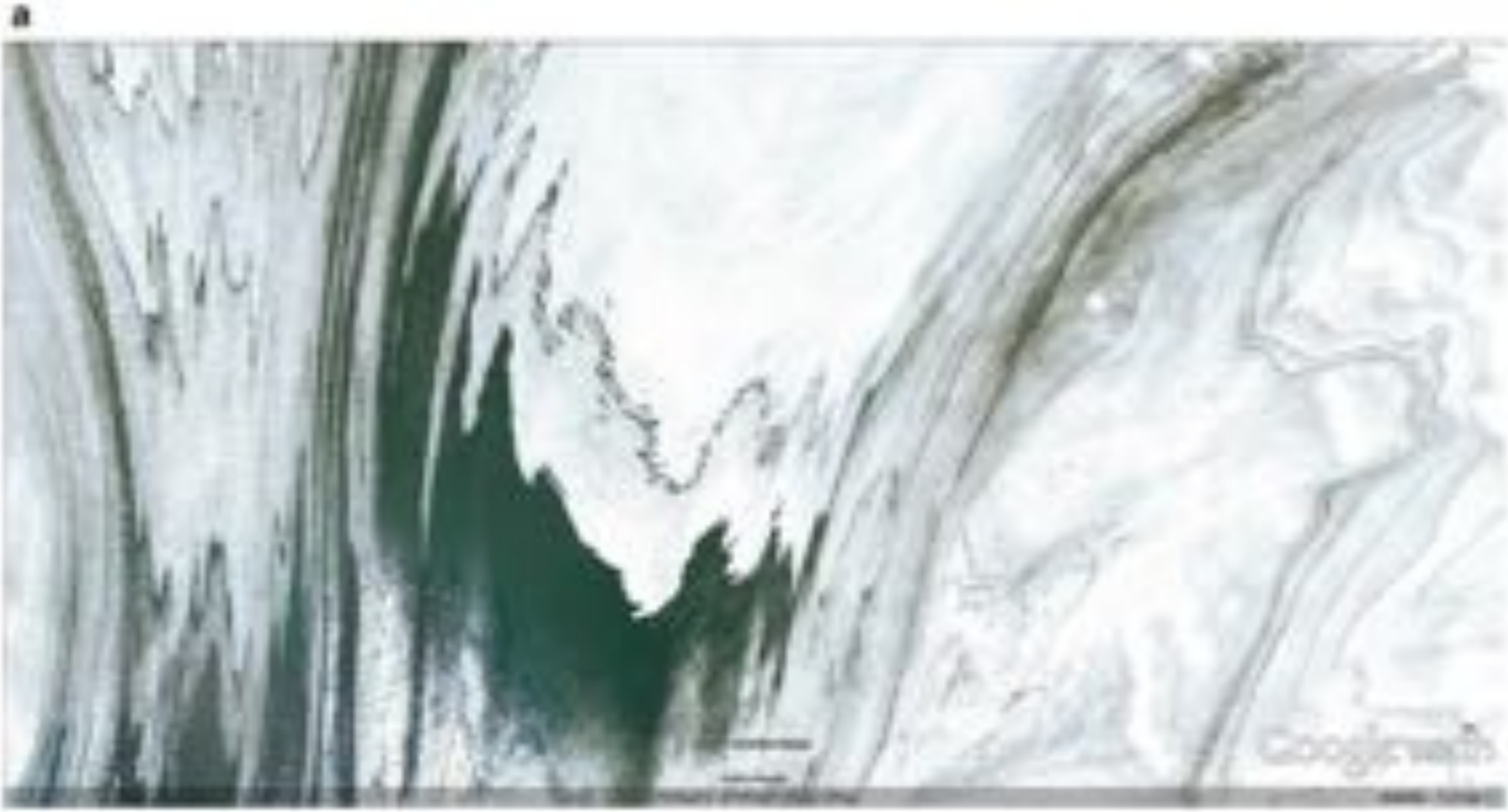
a
Google earth

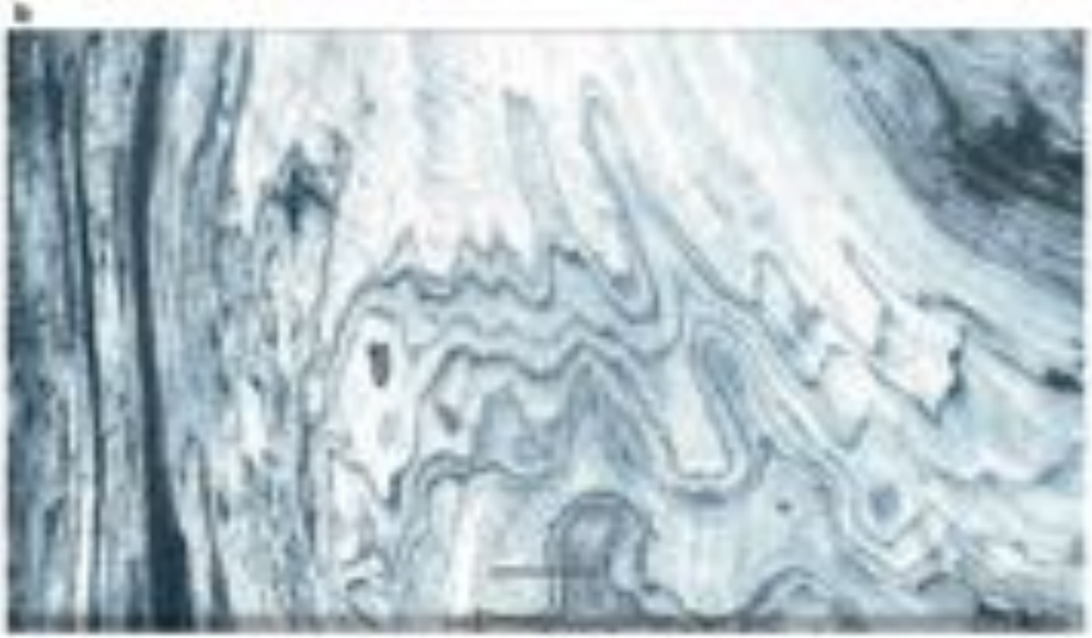

Fig. 13.4 (continued)

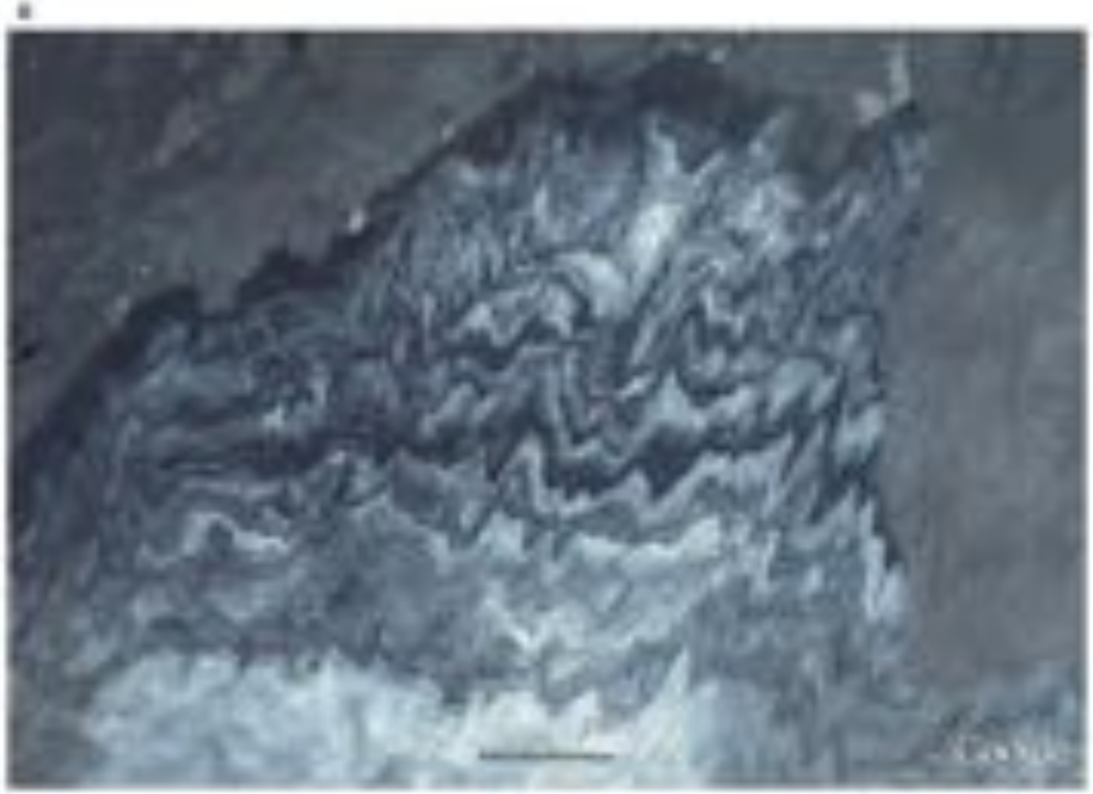

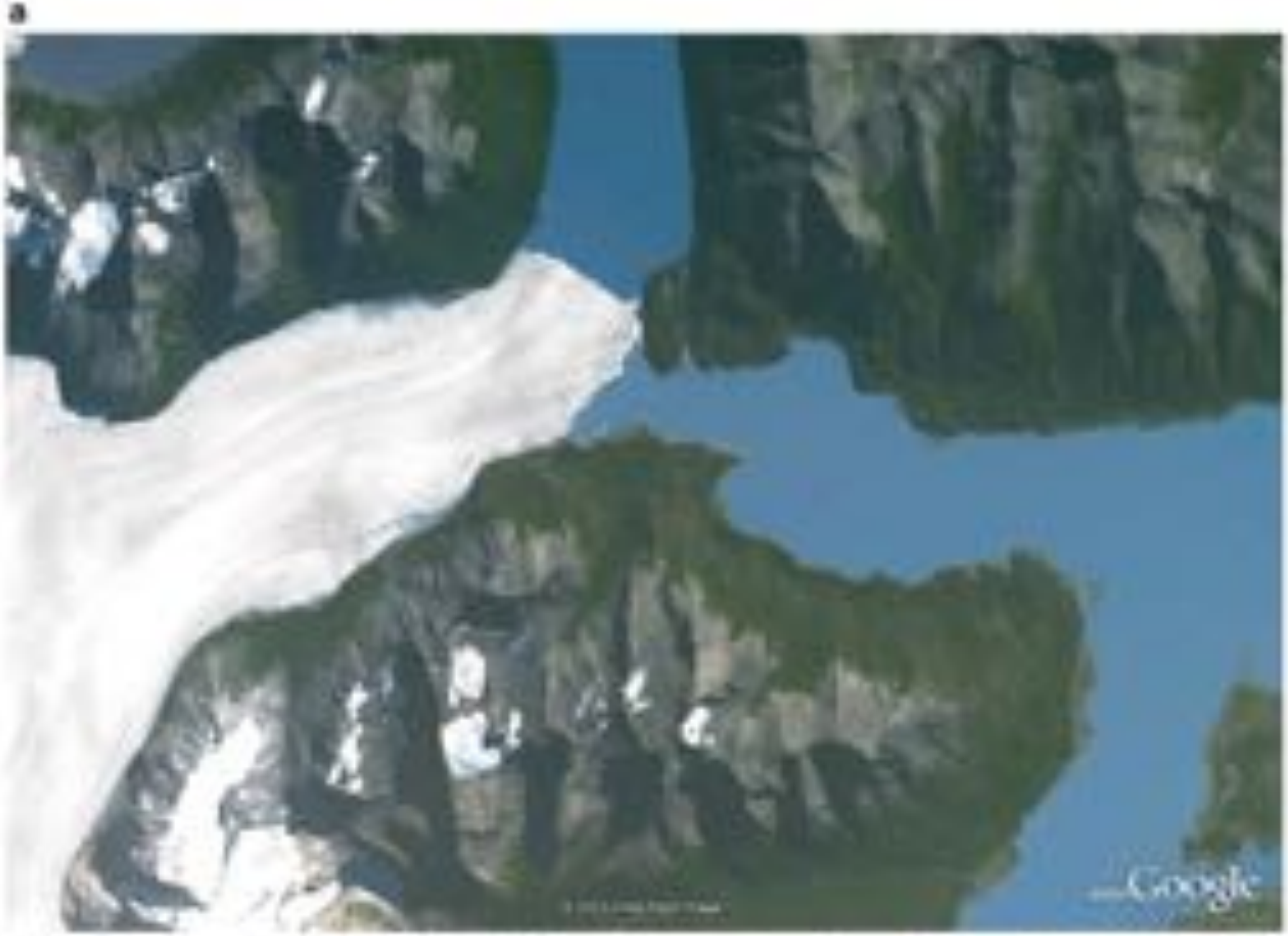

Fig. 13.5 (a) The famous Perito Moreno Glacier in southern Patagonia (Argentina) at 50°28'S and 73°03'W with a tongue nearly 5 km wide. The glacier oscillates within several years and closes the eastern section of Lago Argentino. As a consequence, lake water is stored up to about 20 m higher than in the northern part, and the glacial tongue may float and break. From time to time, the southern lake bursts out. The satellite image shows a small barren bank along the lake on the right part of the image, which marks the maximum high water line without vegetation (Image credit: ©Google earth 2012). (b) Northern part of the tongue of the Perito Moreno Glacier calving into Lago Argentino (Image credit: D. [illegible])


b

Fig. 12.6 (**a**) San Quintin Glacier (southern Chile) calving into its terminal lake. (**b**, **c**) Glaciers from the Southern Patagonian Ice Field in Chile may reach the ocean in fjords, with steep fronts and sharp crevasses and calving icebergs. Scenes are several 100 m wide (Image credit: ©Google earth 2012)


b
Google

c

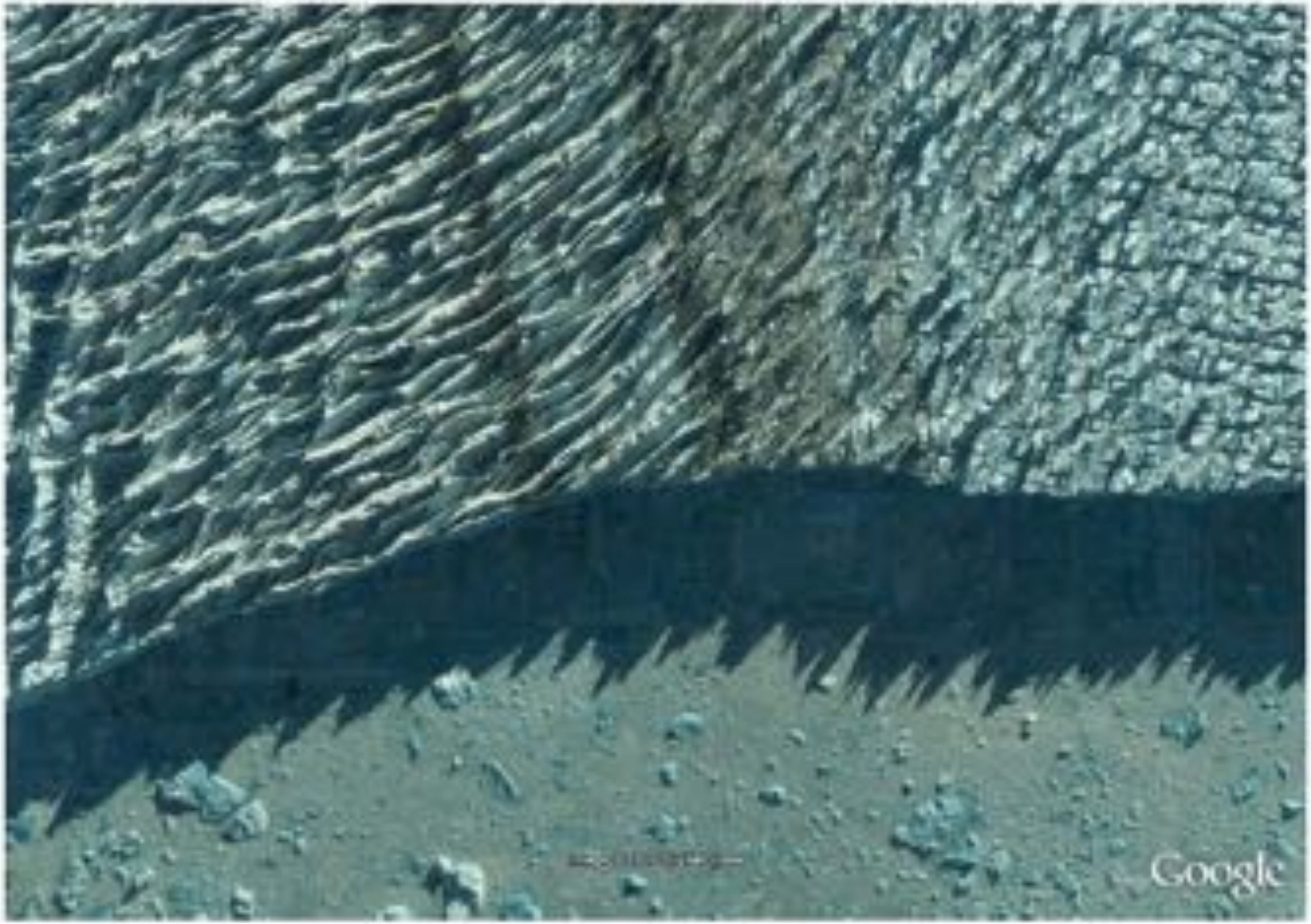


a
b
Google


a
Google


b
Google

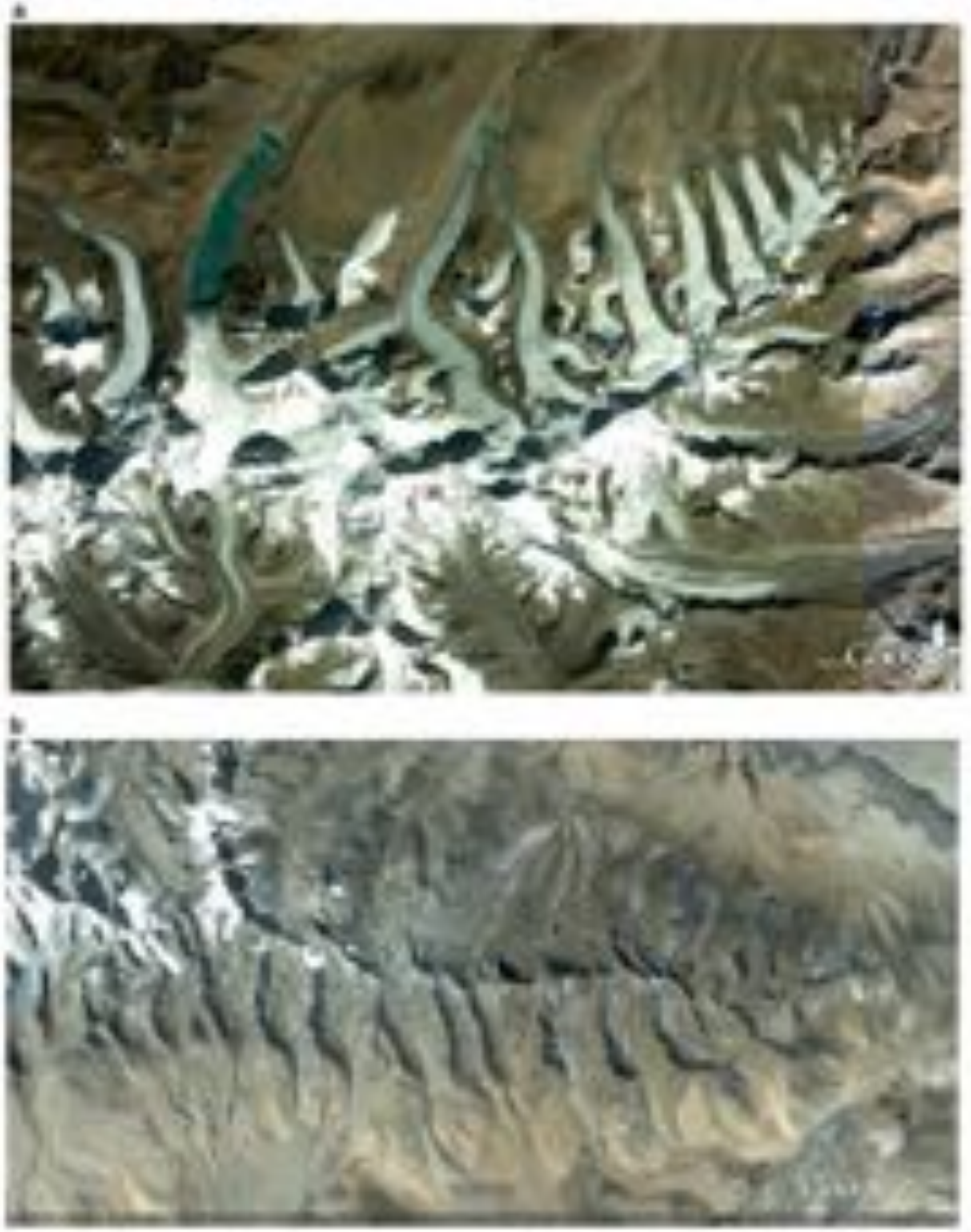
a
b

Fig. 12.15 A large boulder has protected the glacial ice beneath from radiation and melting and formed a "glacier table" in the European Alps (Image credit: D. Kuhlmann)

Fig. 12.16 Glaciers with medial moraine bands, documenting the confluence of a few or even many separated ice streams. (a) Example from the Himalayas, and (b) from eastern Greenland (Image credit: ©Google earth 2012)


b
Google

Fig. 12.17 (a, b) Two examples of Himalayan glaciers with a thick cover of surface moraines protecting the glacier ice. As a result, the glaciers end with thick tongues, which may also point to a period of glacier advance (Image credit: ©Google earth 2012)

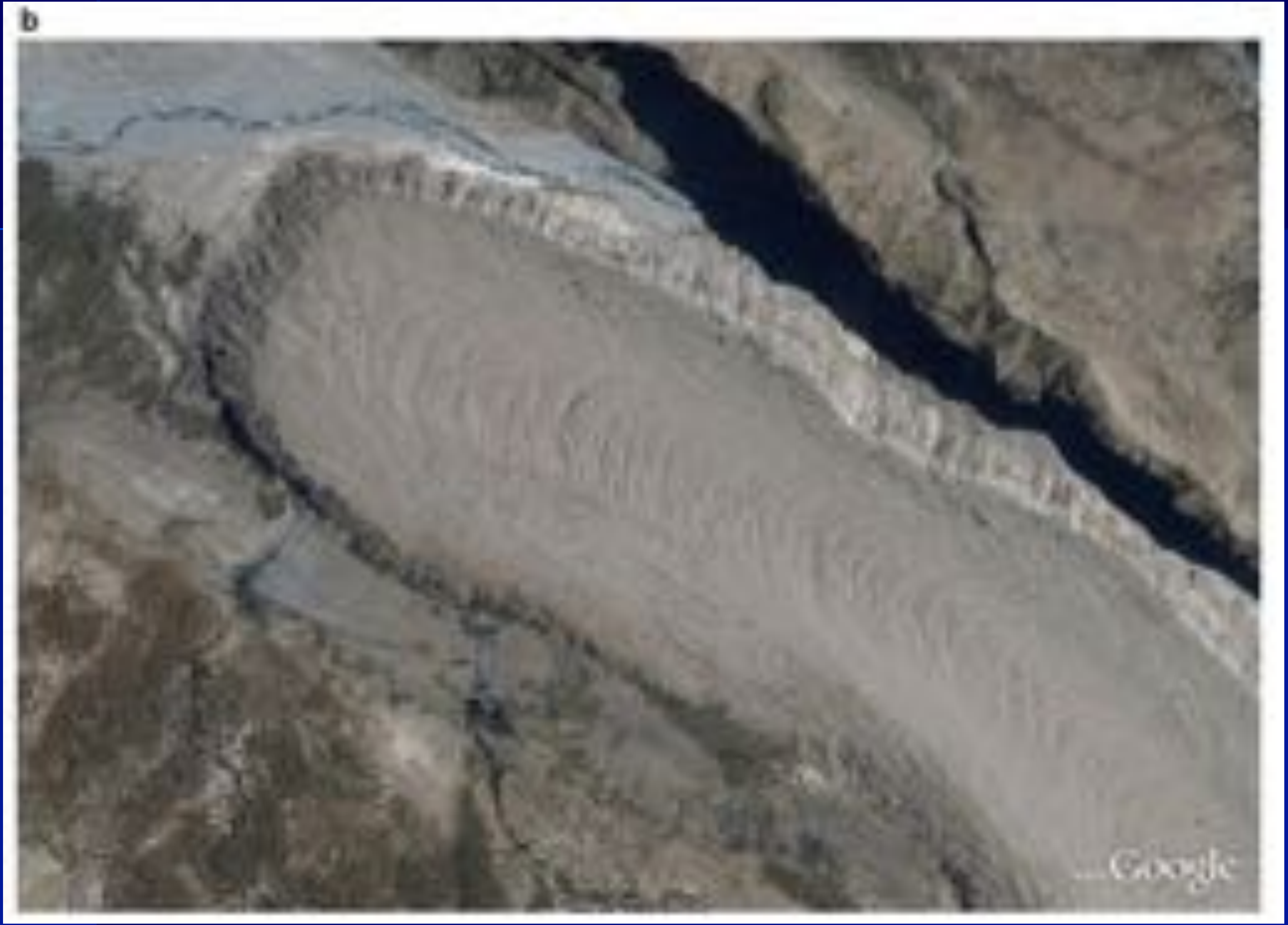
b
Google

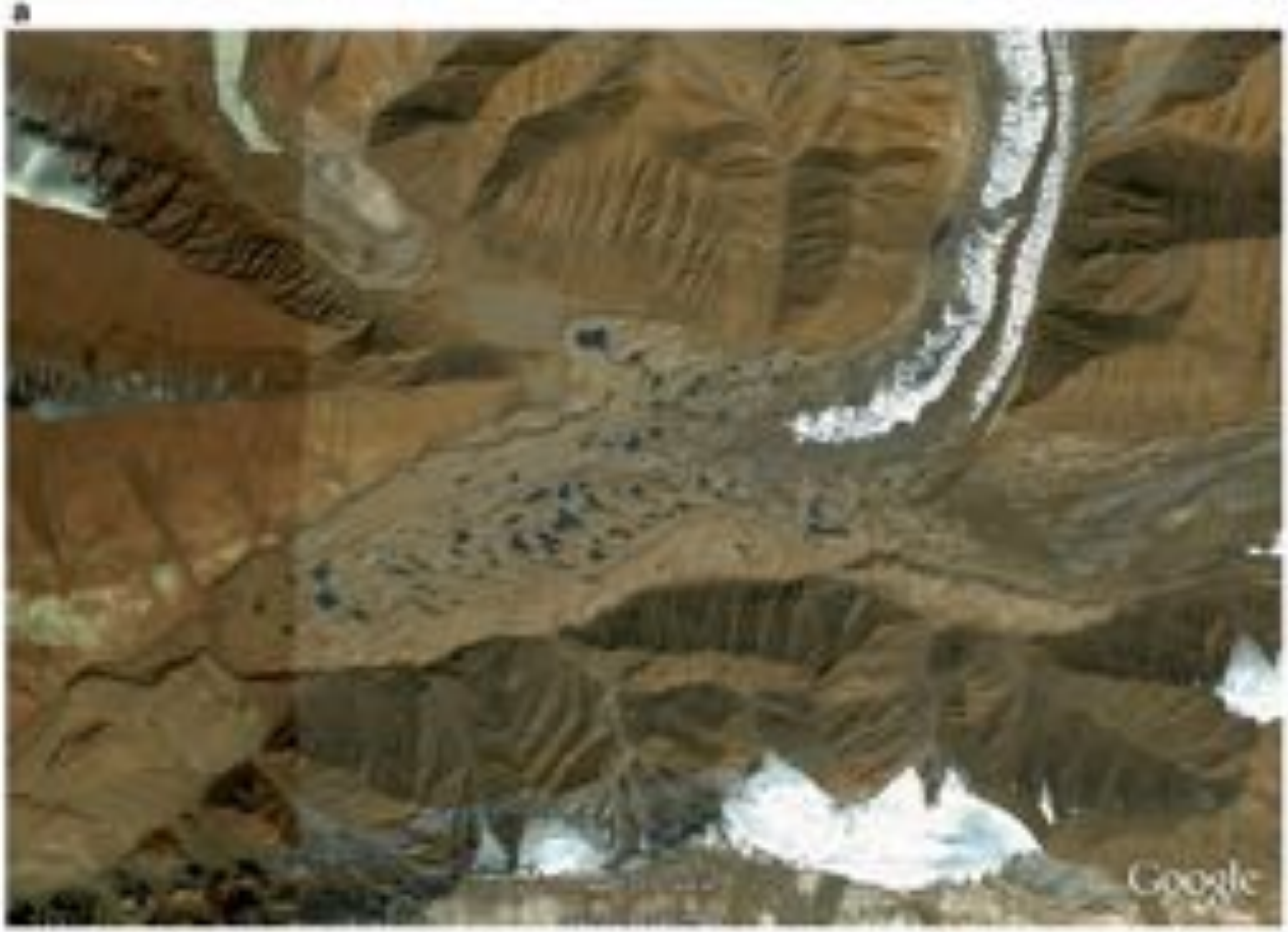

Fig. 12.18 (a, b) Southern Asian glaciers in the Himalayas, where the ice is almost entirely hidden under thick moraine material, but sinkhole-like depressions show that it still exists below the till (Image credit: ©Google earth 2012)

Fig. 12.59 (a) Large cirques in the southern Canadian Rocky Mountains (Image credit: D. Kalbitar). (b) A group of cirques in northern Iceland. The dark patches are lakes and document that the cirques were deepened by glacial erosion, now separated from the slopes of the valley by sills (Image credit: ©Google earth 2012)


b
Google


a


b
d


Google

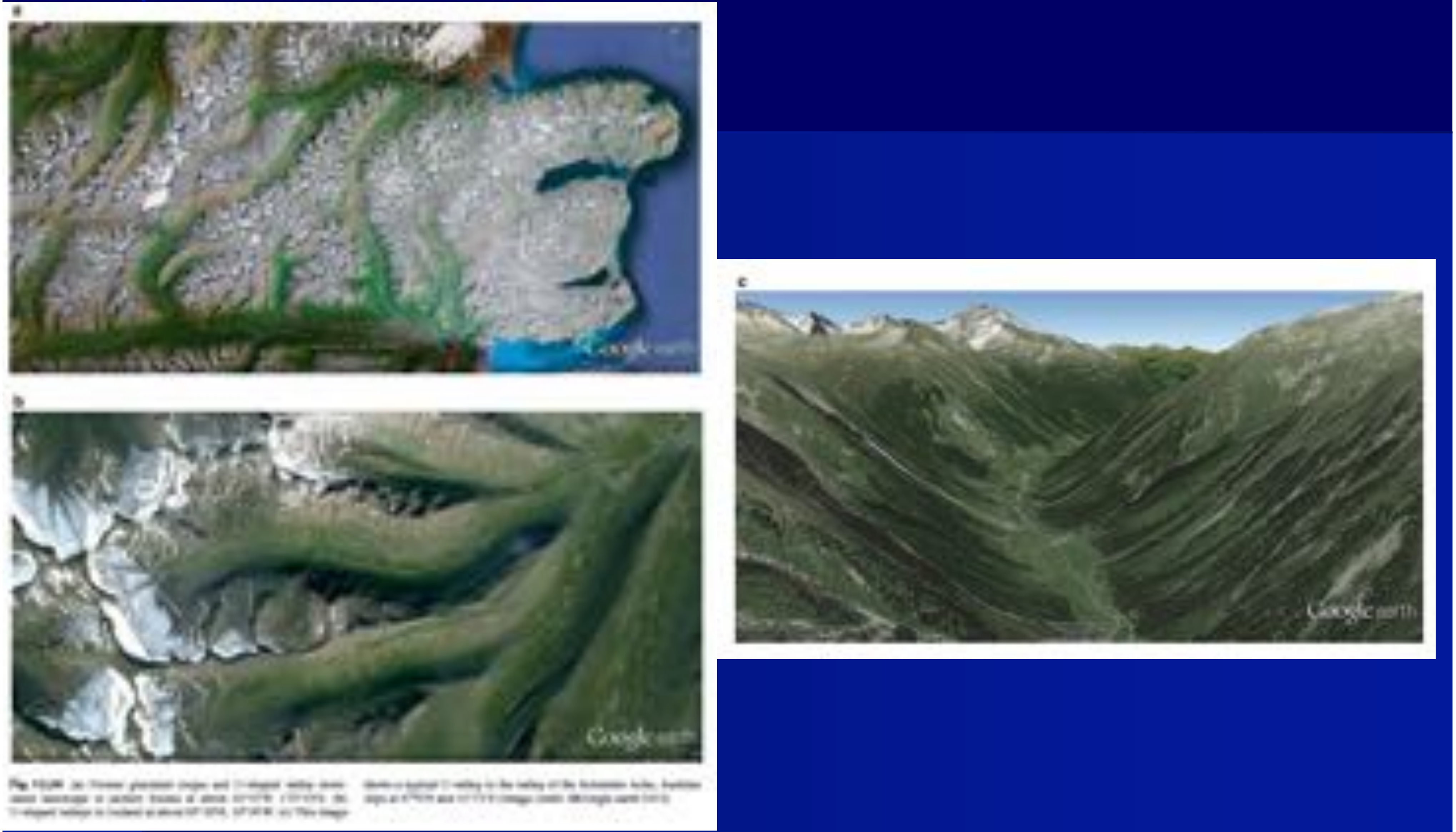
a
b
c
Google earth
Google earth
Google earth

Fig. 12.25 The "Finger Lakes" (up to 70 km long) are places of former glacier tongues during glacial periods that carved out these depressions into a flat landscape east of the Great Lakes of USA and Canada. The site is at about 42°41′N and 76°48′W. The glacial ice came from the north (Image credit: ©Google earth 2012)

Fig. 12.26 (a) Chaotic ground moraine particles (till) from a valley bottom in southern Switzerland. Most of the deposit has been washed away, but under large boulders columns or needles of the sediment may be preserved. They are called "earth pyramids" in the European Alps, although they mostly have the form of columns (Image credit: D. Kelletat). (b) Deformation of meltwater deposits by an advancing glacier east of Bariloche in western Argentina about 13,000 years ago at the end of the last glaciation. (c) Detail of (b) showing the small faults in the till strata documenting that the sediment was frozen during the last movement (Image credit: D. Kelletat)


b


c

Fig. 12.27 (a) Lakes, as well as lateral and terminal moraines, in front of glaciers in southernmost Tibet document a young glacier retreat at *28°15′N* and *86°17′E*. Scene is about 35 km wide. (b) Well preserved lateral and terminal moraines near *37°50′N* and *119°05′W* along the east side of California's Sierra Nevada recording the maximum extent of glaciers during the last glacial maximum advance and some late glacial re-advances. Scene is 20 km wide. (c, d) Terminal and lateral moraines from receding glaciers in the Himalayas at about *27°55′N* and *87°45′E* in (c), and *28°22′N* and *86°22′E* in (d). Lakes developed behind the wall of the terminal moraine by meltwater. (Image credit: ©Google earth 2012)

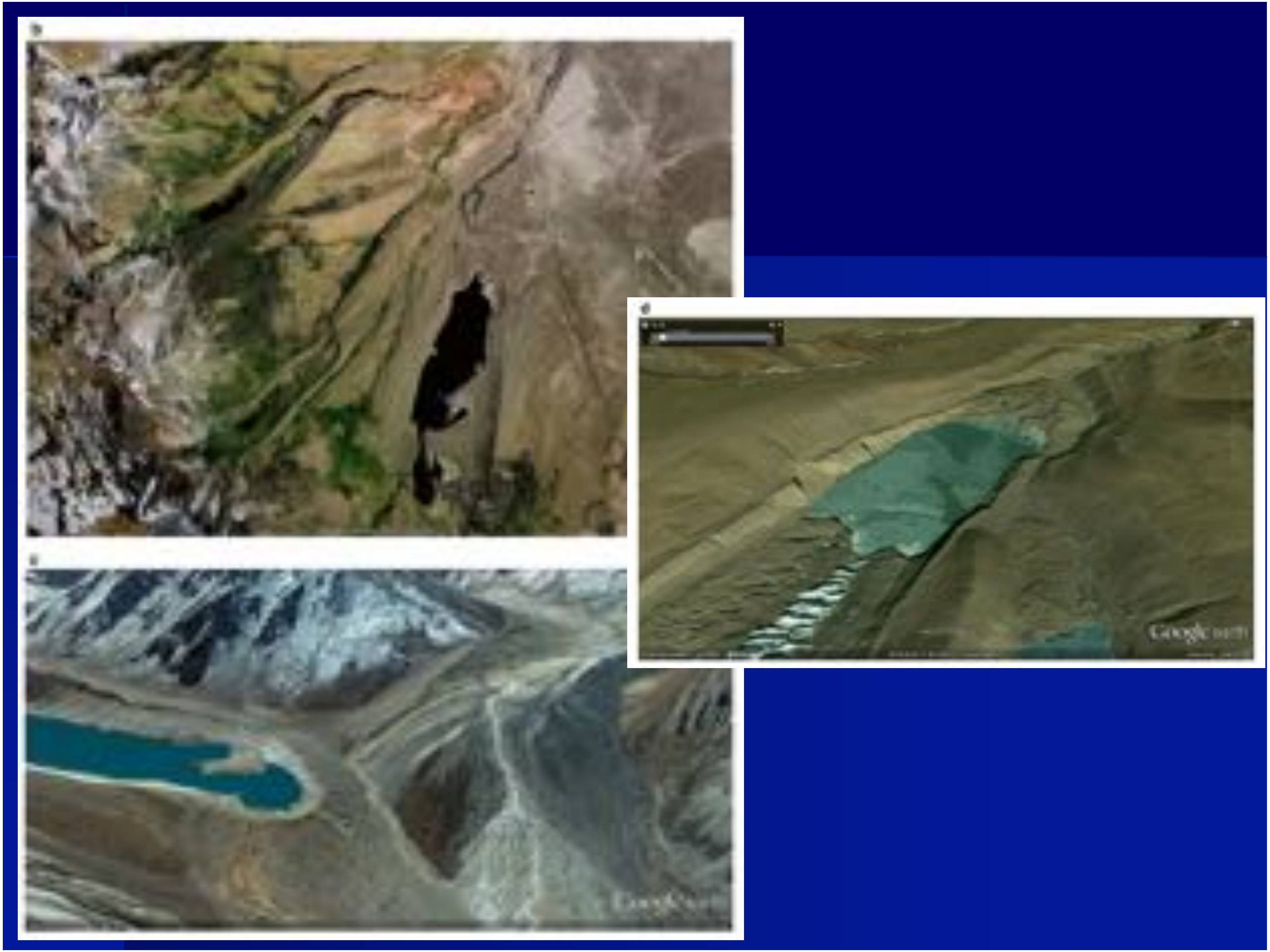
Google earth
Google earth

冰缘地貌


CANADA
RUSSIAN FEDERATION
Arctic Ocean
ICELAND
NORWAY
FINLAND
SWEDEN
Permafrost
Isolated
Sporadic
Discontinuous
Continuous

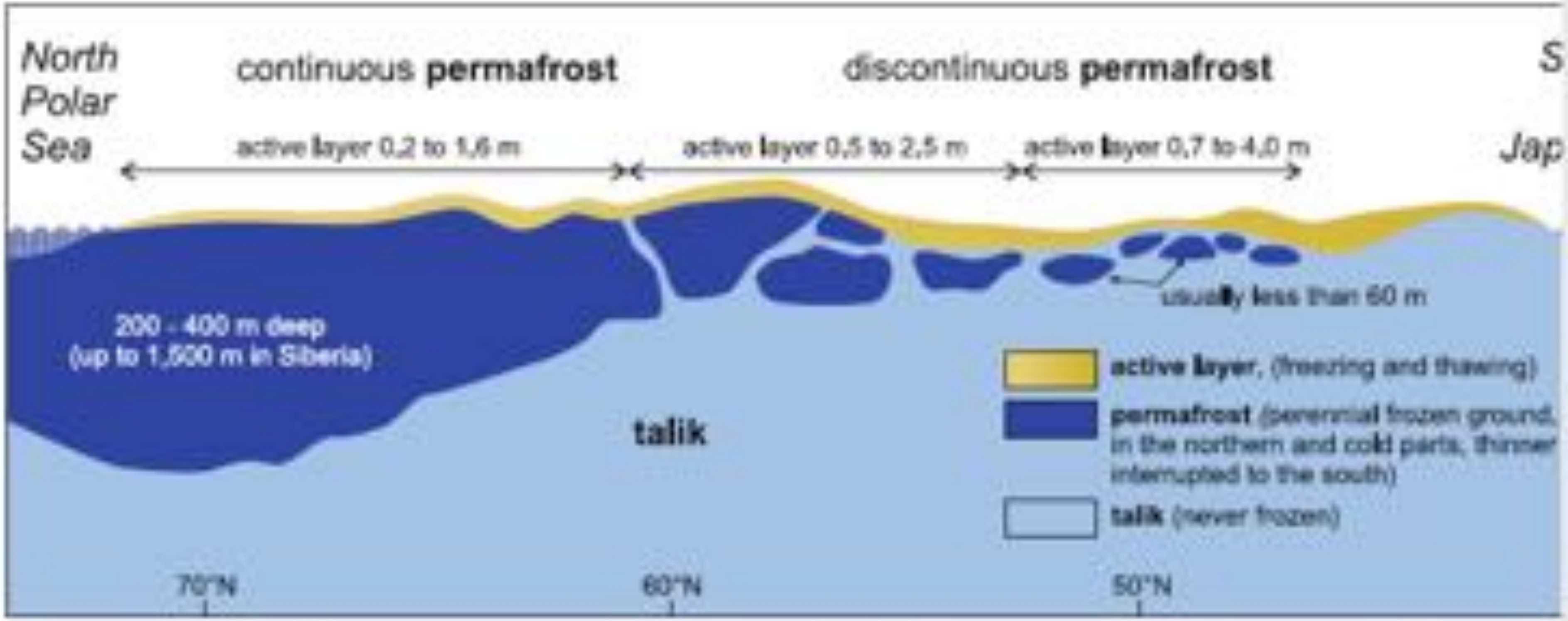

Fig. 13.2 A north–south section across the permafrost landscape in eastern Siberia (Russia). In the north, permafrost is several hundred meters deep and continuous. Towards lower latitudes, it is becomes thinner and shows gaps, whereas at even warmer latitudes it is separated into isolated patches and is only a few meters deep. As climate c affects permafrost from the surface, the thawing processes may ac ate permafrost decay in all latitudes (Image credit: A. Hager)

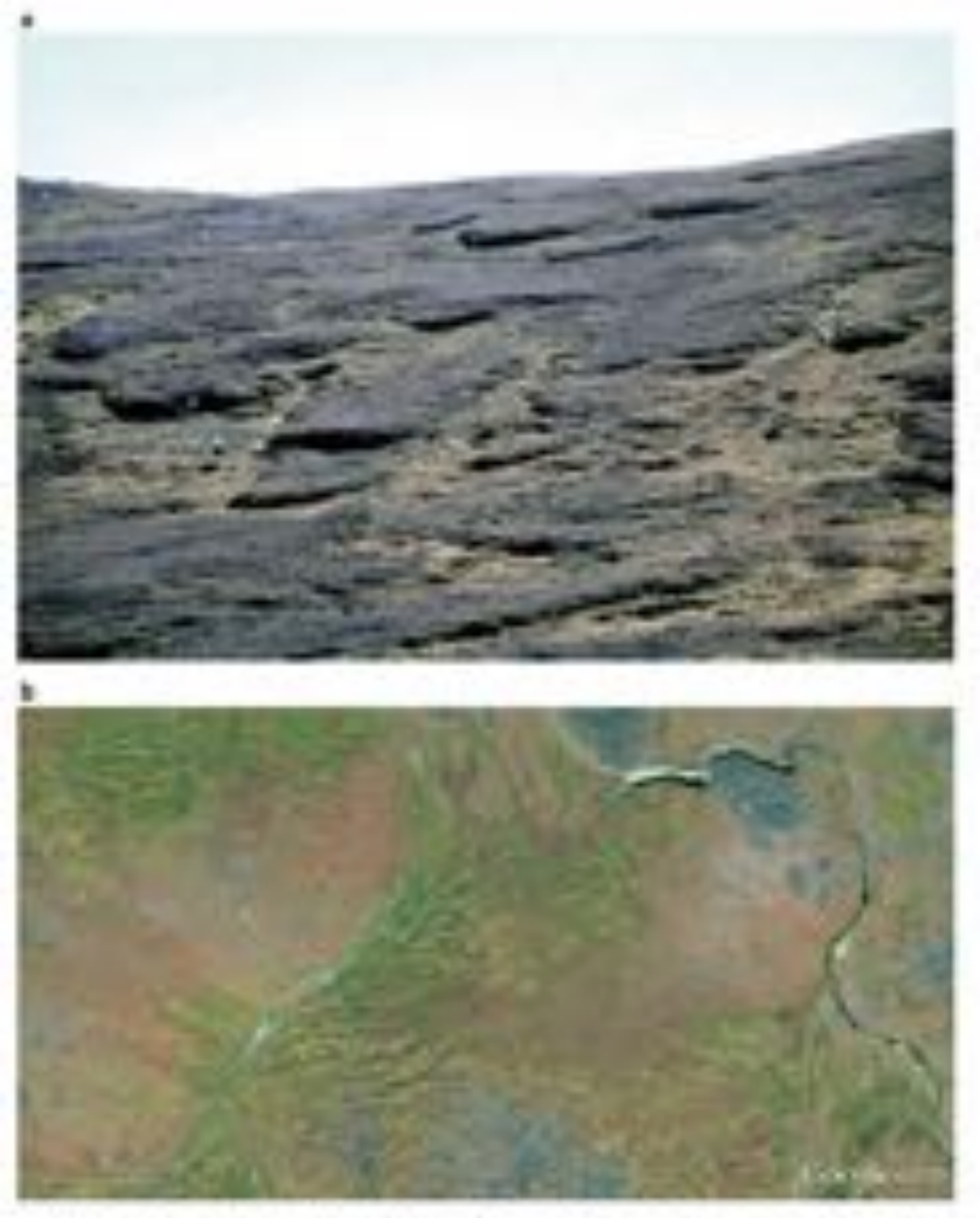
a
b

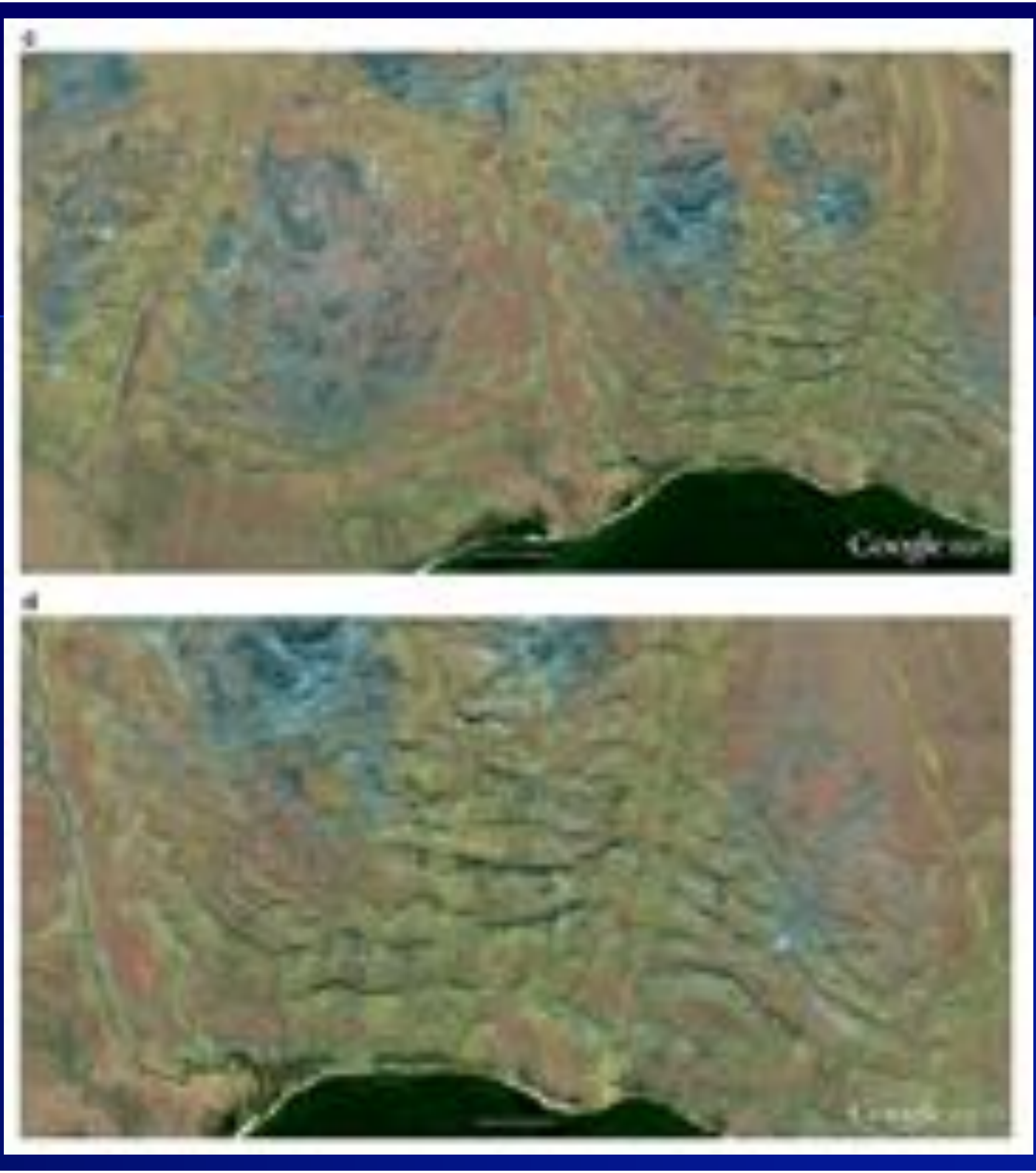
Google
Google


a

[illegible]


b

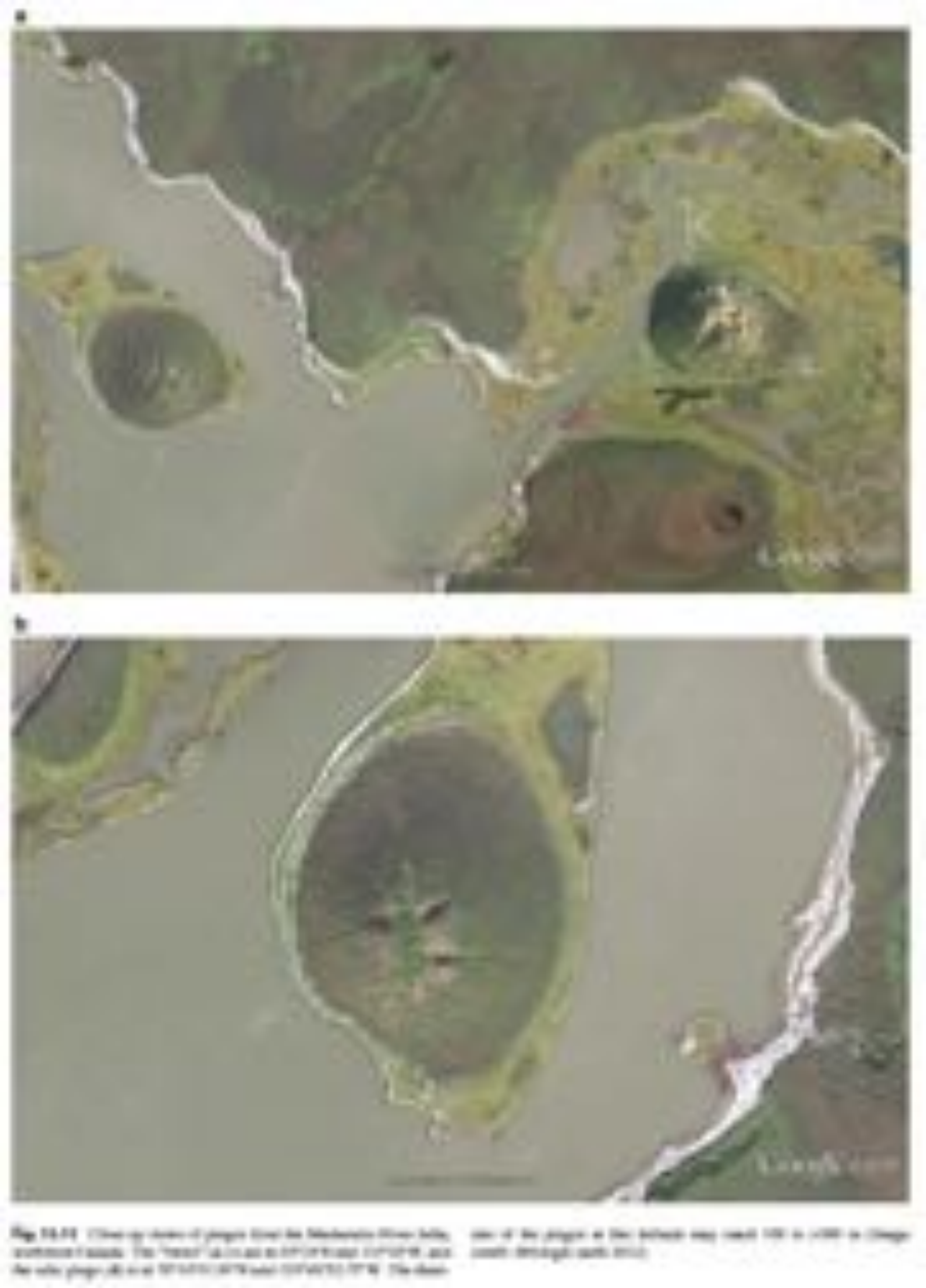


c
Google.com
d
Google.com

Fig. 13.15 With low temperatures (–25 to –40 °C) in winter, the frozen ground shrinks repeatedly and cracks open up in networks, which will be filled by meltwater in the warmer times of the year. The water travels deeper and opens the cracks farther in each thawing/freezing cycle. The cracks show more or less pure ice in the form of ice wedges and this kind of patterned ground is called "ice wedge polygons". The site is located in northern Alaska at *70°50'N* and *155°30'W* and the scene is about 5 km wide (Image credit: ©Google earth 2012)

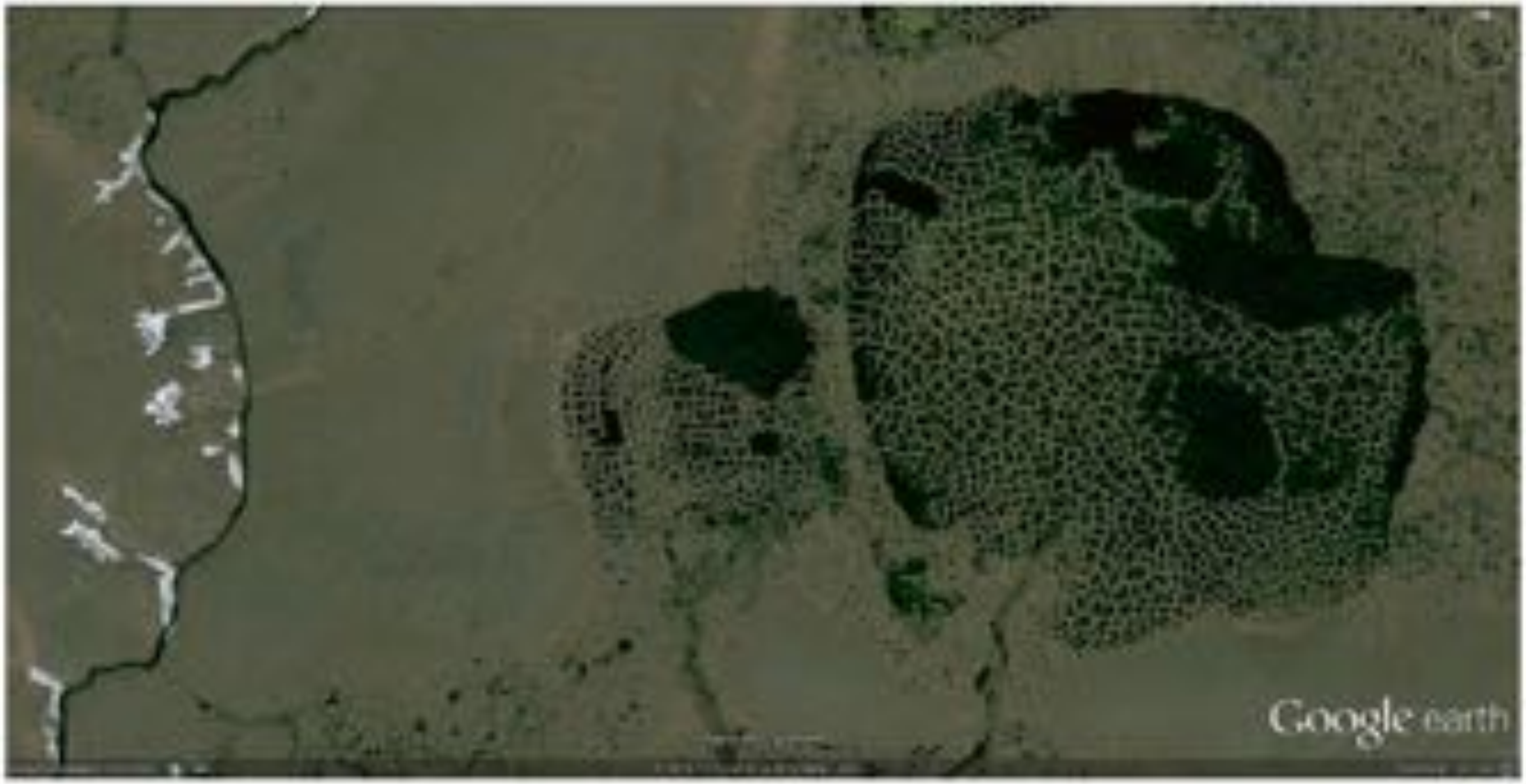

Fig. 13.16 Irregular network of patterned ground by ice wedge polygons in a shallow depression of northern Russia at *71°55′N* and *152°52′E*. Scene is 2.3 km wide (Image credit: ©Google earth 2012)

Fig. 13.17 (a) Ice wedge polygons in the permafrost of northern Alaska. Scene is 1 km wide at *70°55′27.57″N* and *155°19′35.19″W*. The overall pattern evidently is adapted by the sediment character and/or slight topography from the nearby river. Single polygons have diameters up to 40 m. (b) A 1.5 km wide scene at *70°22′22.48″N* and *151°03′41.51″W*. The pattern is irregular with a diameter of polygons of 15–35 m. We can identify dark lines within the elevated rims of the polygons which are melting ice wedges, whereas the elevation is the result of the pressure by actively freezing vertical fillings of fissures. As along each fissure a double low rim is formed, the polygons form a network of low-centered features that are filled by water in summer and frozen over winter. Freezing of the ponds also will exert pressure towards their outer rims and elevate the network lines, which may be under the influence of pressure from both sides (Image credit: ©Google earth 2012)


b
Google earth

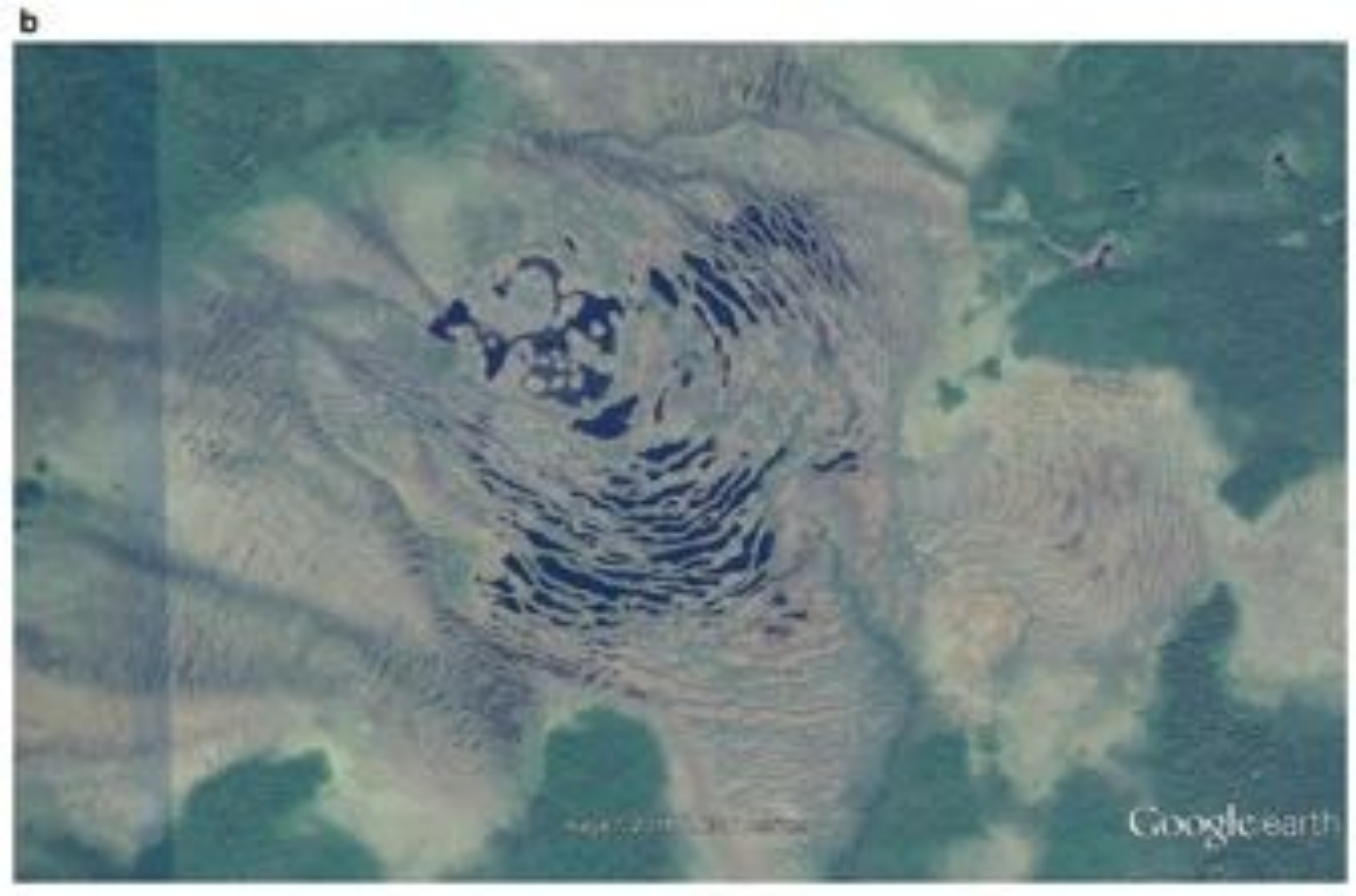
b
Google earth

Fig. 13.20 Two examples of recent thermokarst, which means thawing of permafrost. (a) Patches of the former permanently frozen ground are now collapsed by thawing, and new lakes with irregular but sharp contours (ice and debris cliffs) occur. Scene is 4 km wide, at 68°45'N, 161°11'E (b) Destruction of an older depression. Scene is 5.2 km wide at 69°38'N, 162°27'E. Both examples are from northern Siberia (Image credit: ©Google earth 2012)


b
Google earth

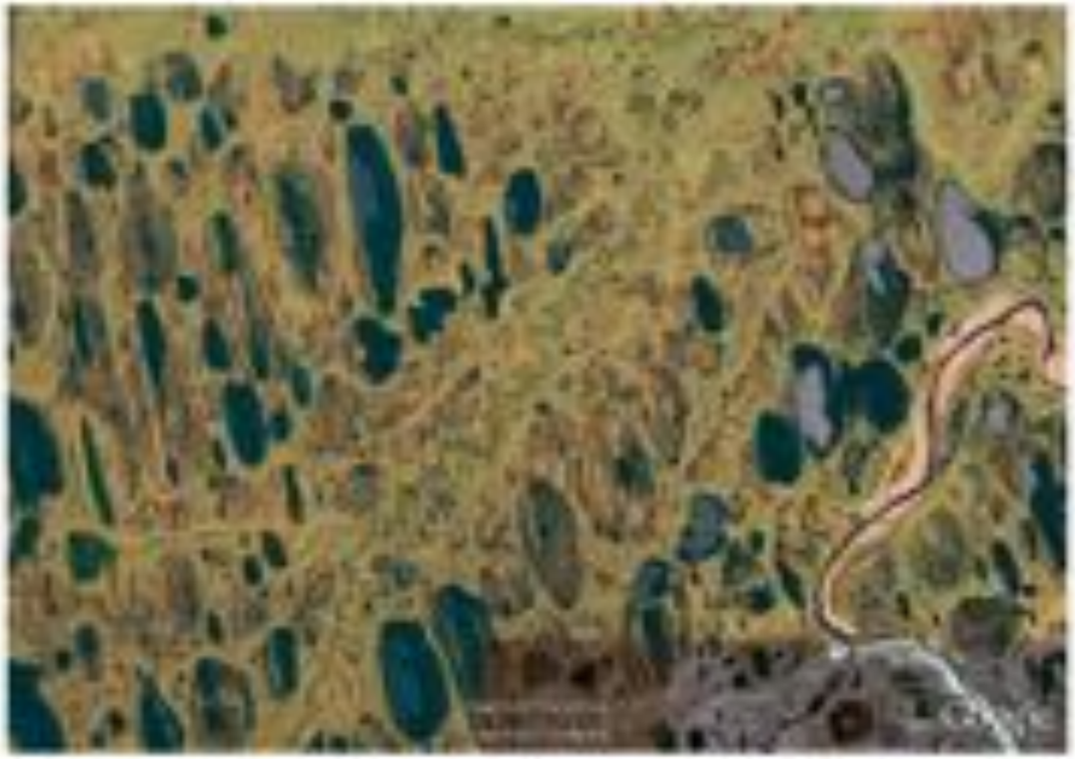

人工地貌

Fig. 14.2 In the northwestern parts of China, the loess landscape is transformed into terraces for crops and vegetables ([illegible]) (Image credit: ©Google earth 2012)

Fig. 14.3 Sand mining for construction purposes in southern Jordan at 31°01'N and 36°06'E. Image shows a 4.2 km wide section of the desert landscape (Image credit: ©Google earth 2012)

a

Fig. 14.6 (a) An open pit mining for Tertiary lignite in western Germany. The width of the pit is nearly 4 km with a depth of 120 m. The scene is at 50°52′N and 6°29′E. Partial refilling of the mine (the green terraces in the south) is now the action taken to minimize the consequences for the landscape. (b) Another lignite open pit mine in western Germany at 51°05′N and 6°7′E. The scene is 20 km wide. The partially refilled pit is 8 km wide and the hills of residual material is about 80 m high and about 1 km in diameter (Image credit: ©Google earth 2012)

[illegible]

Fig. 14.14 Modification of river runoff and sediment transport by reservoirs (dams indicated by arrows) around *47°05′N* and *119°57′W* along the Columbia River and the surrounding areas, USA (Image credit: ©Google earth 2012)


Google earth
海拔 76 米
视角海拔高度 5.54 公里


200 米
Image © 2017 DigitalGlobe
Google earth


Google earth